AD-A038 259 STANFORD RESEARCH INST MENLO PARK CALIF F/G 4/1
ICECAP '75--CHATANIKA RADAR RESULTS.(U)
MAY 76 P D PERREAULT, R R VONDRAK, T M WATT DNA001-74-C-0167
UNCLASSIFIED DNA-4086T NL

1 OF 2
AD A038259

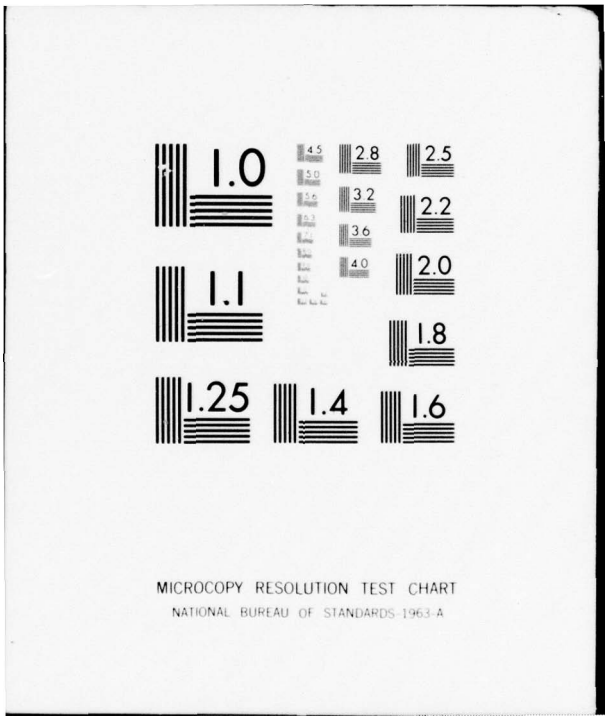
1.0
1.1
1.25
1.4
1.6
1.8
2.0
2.2
2.5
2.8
3.2
3.6
4.0
4.5
5.0
5.6
MICROCOPY RESOLUTION TEST CHART
NATIONAL BUREAU OF STANDARDS-1963-A

DNA 4086T

ICECAP '75--CHATANIKA RADAR RESULTS

HAES Report No. 43

Stanford Research Institute
333 Ravenswood Avenue
Menlo Park, California 94025

May 1976

Topical Report for Period February 1975—May 1976

CONTRACT No. DNA 001-74-C-0167

THIS WORK SPONSORED BY THE DEFENSE NUCLEAR AGENCY
UNDER SUBTASK L25AAXHX631-10.

Prepared for
Director
DEFENSE NUCLEAR AGENCY
Washington, D. C. 20305

Destroy this report when it is no longer needed. Do not return to sender.

UNCLASSIFIED

SECURITY CLASSIFICATION OF THIS PAGE *(When Data Entered)*

REPORT DOCUMENTATION PAGE

READ INSTRUCTIONS BEFORE COMPLETING FORM

1. REPORT NUMBER: DNA 4086T, HAES-43
2. GOVT ACCESSION NO.
3. RECIPIENT'S CATALOG NUMBER

4. TITLE *(and Subtitle)*: ICECAP '75--CHATANIKA RADAR RESULTS, HAES Report No. 43

5. TYPE OF REPORT & PERIOD COVERED: Topical Report, for Period Feb 75—May 76,

6. PERFORMING ORG. REPORT NUMBER: SRI Project 3118

7. AUTHOR(s): Paul D. Perreault, Richard R. Vondrak, Theodore M. Watt

8. CONTRACT OR GRANT NUMBER(s): DNA 001-74-C-0167

9. PERFORMING ORGANIZATION NAME AND ADDRESS:
Stanford Research Institute
333 Ravenswood Avenue
Menlo Park, California 94025

10. PROGRAM ELEMENT, PROJECT, TASK AREA & WORK UNIT NUMBERS: NWET Subtask L25AAXHX631-10

11. CONTROLLING OFFICE NAME AND ADDRESS:
Director
Defense Nuclear Agency
Washington, D.C. 20305

12. REPORT DATE: May 1976

13. NUMBER OF PAGES: 166

14. MONITORING AGENCY NAME & ADDRESS *(if different from Controlling Office)*: 162p.

15. SECURITY CLASS *(of this report)*: UNCLASSIFIED

15a. DECLASSIFICATION/DOWNGRADING SCHEDULE

16. DISTRIBUTION STATEMENT *(of this Report)*

Approved for public release; distribution unlimited.

17. DISTRIBUTION STATEMENT *(of the abstract entered in Block 20, if different from Report)*: DNA, DNA

18. SUPPLEMENTARY NOTES

This work sponsored by the Defense Nuclear Agency under Subtask L25AAXHX631-10.

19. KEY WORDS *(Continue on reverse side if necessary and identify by block number)*

Incoherent-scatter Radar	Ionospheric Current Density
Auroral Ionosphere	Height-integrated Conductivities
Electron Density	Joule Heating
Ion Velocity	Particle Energy Deposition
Ionospheric Electric Fields	E-region Neutral Winds

20. ABSTRACT *(Continue on reverse side if necessary and identify by block number)*

Results of the Chatanika DNA 617 Radar support coverage of the ICECAP '75 operation are presented, along with magnetometer, riometer, all-sky-camera, and boresite television data gathered to give a more complete picture of ionospheric processes.

Eight instrumented rockets were launched during the period 26 February through 12 March 1975 as part of the ICECAP '75 program. Two daytime →OVER

DD FORM 1 JAN 73 1473 EDITION OF 1 NOV 65 IS OBSOLETE

UNCLASSIFIED

SECURITY CLASSIFICATION OF THIS PAGE *(When Data Entered)*

332 500

4B

20. ABSTRACT (Continued)

launches--Astrobee D probes on 26 February and 1 March 1975--took place during periods of relatively quiet geomagnetic activity when peak energy deposition, due to precipitating electrons, was of order 0.1 ergs/cm^2-s or less. Maximum E-layer electron densities were less than 10^5 cm^3.

A twilight launch on 6 March (at 0343 UT) also occurred during relatively quiet geomagnetic conditions. E-layer electron densities of less than 10^5 cm^3 and electric field strengths of less than 5 mV/m resulted in low rates of joule dissipation and energy deposition.

The four evening launches (6, 10, 11, and 12 March) occurred during periods of moderate to high geomagnetic activity. Total energy deposition rates ranged from 2 to as high as 50 ergs/cm^2-s and were associated with high electron precipitation and electric field strengths.

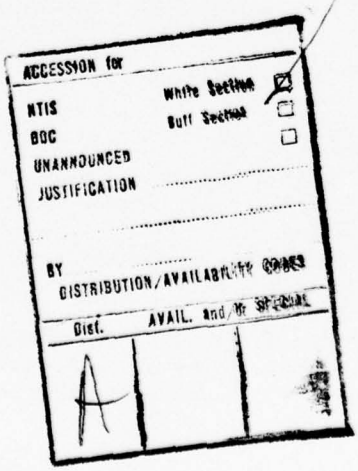

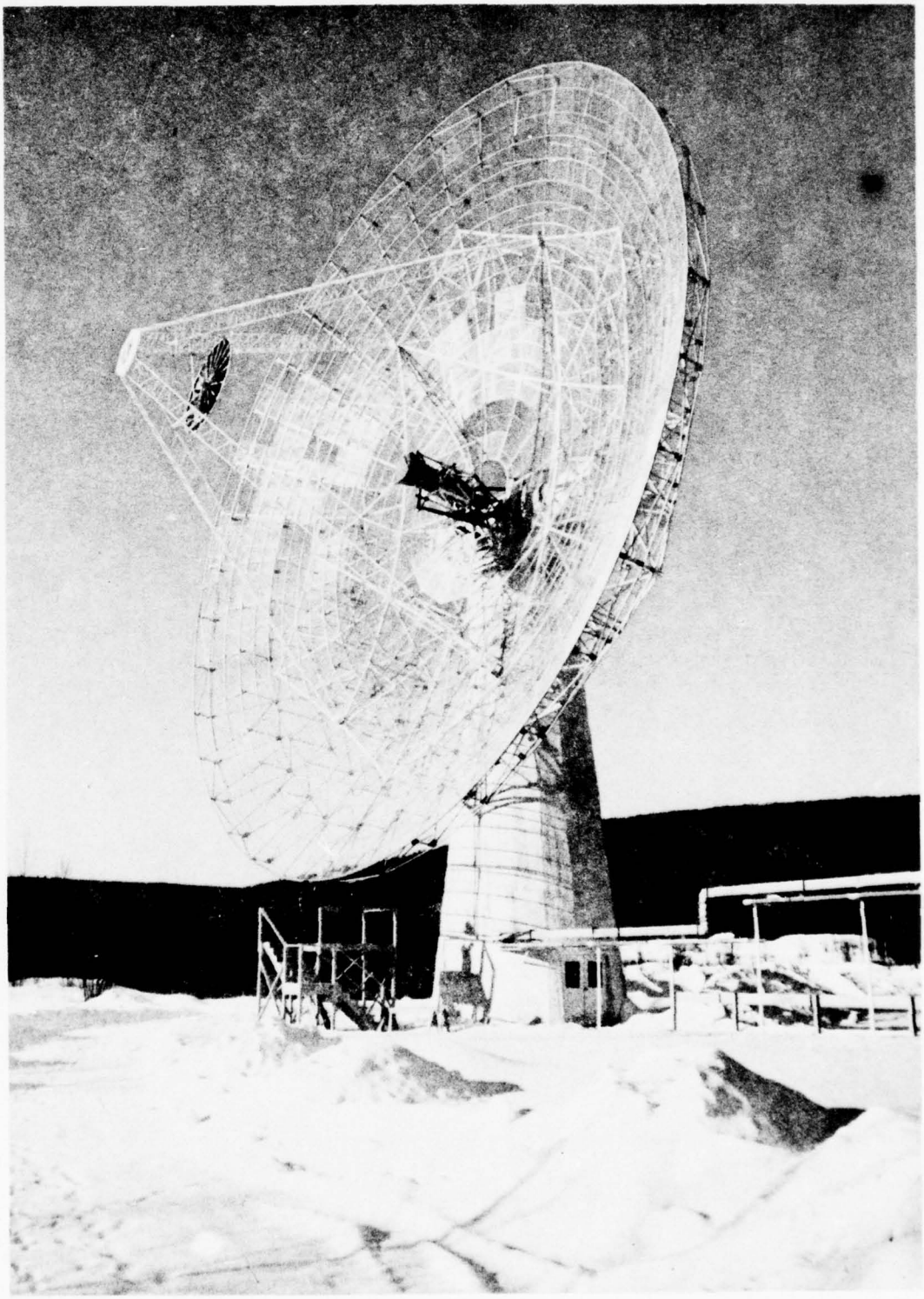

FRONTISPIECE PHOTOGRAPH OF THE CHATANIKA RADAR

PREFACE

Appreciation and thanks for their valuable and untiring efforts in the operation and maintenance of the radar during the chilly Alaskan winter go to the Chatanika field site personnel: J. Kelly, H. Burch, and R. Love.

The large volume of data collected during the ICECAP support runs was massaged into final form with the able assistance of M. McCready, B. Phillips, T. Rubin, and B. White.

Our thanks go to Dr. M. Baron and Mr. J. Spencer for their critical reading of this manuscript, and to Mr. D. Evelyn of D.N.A. for his support and encouragement during this effort.

Data used in connection with this report were obtained from the Geophysical Institute at Fairbanks, Alaska, from WDC-A for Solar Terrestrial Physics (Geomagnetism), and from Space Data Corporation, Phoenix, Arizona.

CONTENTS

ILLUSTRATIONS

TABLES

I INTRODUCTION

ICECAP is an auroral measurements program to acquire geophysical data required for the formulation and testing of models and predictive computer codes. The models and codes describe atmospheric ionization, excitation, and optical emissions in the (aurorally) disturbed ionosphere. These codes are needed to assess and evaluate the operation of critical DoD radar and optical systems in nuclear disturbed environments. Auroral disturbances studied in ICECAP are similar to nuclear disturbances in that both are characterized by dramatic optical effects, magnetic disturbances, and enhanced plasma densities resulting from the interaction of energetic particles with the atmospheric constituents.

The general objectives of ICECAP are as follows:

(1) Provide measurements of chemical and emission processes occurring in the disturbed atmosphere.

(2) Uncover unsuspected chemical or interactive processes leading to important infrared radiations.

(3) Provide experimental data against which models and computer codes can be compared and evaluated.

(4) Provide data that can be used to update and improve theoretical models and predictive computer codes.

The specific objectives of ICECAP '75 were to execute a coordinated field-measurement program to investigate ionization and excitation mechanisms and dominating chemistry leading to both short- and long-wavelength infrared (SWIR and LWIR) emissions. Measurements were to be made under both aurorally active and quiet conditions. Eight instrumented rockets were launched between 26 February and 12 March, two during daytime conditions, one at twilight, and five at night.

A large array of ground-based instruments monitored the auroral ionospheric conditions as part of the ICECAP '75 program. The primary objectives of the ground-based support measurements were to monitor auroral ionospheric conditions to determine optimum launch times, and to provide correlative and background data to complement the rocket measurements. Ground-based and rocket-borne sensors made simultaneous measurements of emissions, ionization, ionization sources, heating by particles and electric fields, ion and neutral composition, and neutral, ion, and electron temperatures.

The Chatanika incoherent-scatter radar was operated in support of ICECAP '75 during every rocket launch.* The purpose of the radar operations was as follows:

(1) Provide background measurements on the state of the ionosphere before and after each launch (e.g., electron density, conductivities, electric field, neutral wind, and current density).

(2) Provide estimates of energy inputs to the atmosphere from both joule heating and particle precipitation before, during, and after rocket launches.

(3) Provide correlated, real-time measurements of ionospheric electron densities, electric fields, and energy spectra of auroral electrons during the rocket flights.

(4) Enable cross-calibration of parameters measured by the radar with the same parameters measured by other rocket and ground-based techniques.

---

*The radar did not provide usable data during the rocket flight on 4 March 1975.

This report presents the results of the Chatanika radar operations during ICECAP '75. As an aid in comparing the radar (and rocket) measurements with geophysical conditions, the report also presents magnetometer, riometer, all-sky-camera, and boresite TV data. The incoherent-scatter radar results are also compared with available auroral-clutter maps obtained with the DNA 609 phased-array radar located at Homer, Alaska, when the Homer data were available.

II INSTRUMENTATION AND LOCATION

The DNA 617 incoherent-scatter radar and associated data-analysis techniques have been described in a number of reports.[1-4]* The parameters of the radar system are shown in Table 1.

Table 1

PARAMETERS OF THE CHATANIKA AURORAL-ZONE INCOHERENT-SCATTER RADAR

Parameter	*Adjustment* Range	Normal Operation
Transmit frequency	1280-1300 MHz	1290 MHz
Transmit power (peak)	0-5 MW	3-4 MW
Duty cycle (maximum)	3%	2.7%
Transmit polarization		*Right-hand circular*
Receive polarization		Left-hand circular
Antenna diameter		27 m
Antenna aperture		180 m^2
Antenna beamwidth (full-width half-power)		0.6°
Antenna gain		47.1 dB
System noise temperature		190° K
Pulse length	10-500 μs	67 and 320 μs (alternate interpulse periods)
Receiver video bandwidth	4-200 kHz	50 kHz
Receiver IF bandwidth	≤10 MHz	50 kHz

*References are listed at the end of the report.

The radar uses an on-line XDS 930 computer to preprocess, format, and record the data. The computer also drives real-time data displays for experiment management by the radar operator. The same computer is used off-line to reduce the recorded radar data and obtain the measured parameters of electron density, electron and ion temperature, and plasma drift. Another XDS 930, available in Menlo Park, is also used for analysis of the radar data.

The geographic and geomagnetic coordinates of the Chatanika incoherent-scatter radar are given in Table 2. Figure 1 is a map of Alaska showing the location of the Chatanika and Homer (DNA 609) radars.

Table 2

COORDINATES OF CHATANIKA INCOHERENT-SCATTER RADAR

Geographic Coordinates		Dipole Geomagnetic Coordinates		Magnetic Field	
Latitude	Longitude	Latitude	Longitude	Dip Angle	Declination
65.103° N	145.451° W	64.918° N	103.338° W	76.92°	28.77° E

The Chatanika radar site is about 3 km southeast of the Poker Flat rocket range, from which the ICECAP rockets were launched. The map of the Fairbanks vicinity (Figure 2) shows the location of the Chatanika radar with respect to Poker Flat, Ester Dome (optical observations), and other scientific instrumentation.

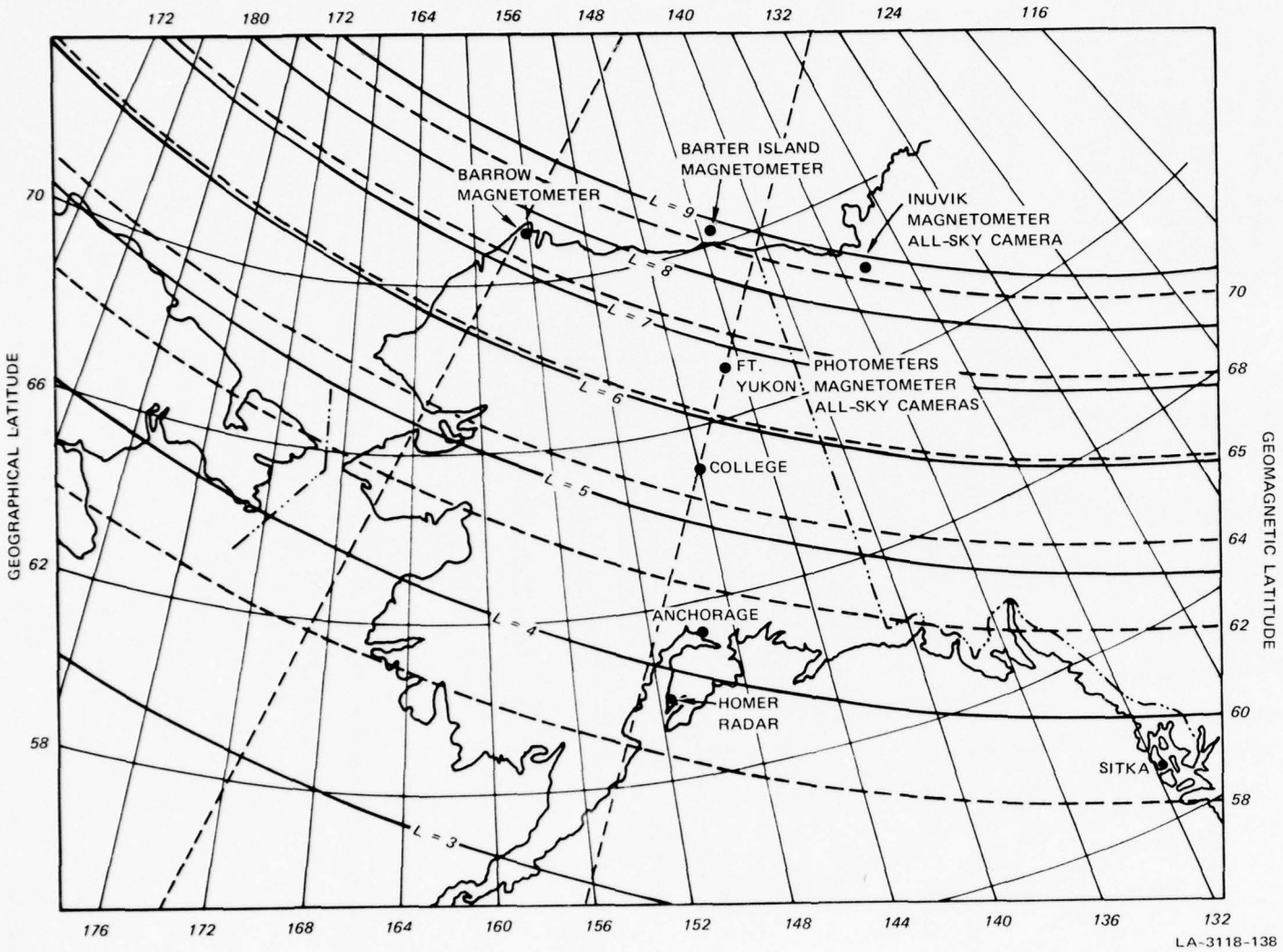

FIGURE 1 MAP OF ALASKA SHOWING MAGNETIC ASPECT ANGLES FOR THE HOMER RADAR AND MAGNETIC L-SHELLS

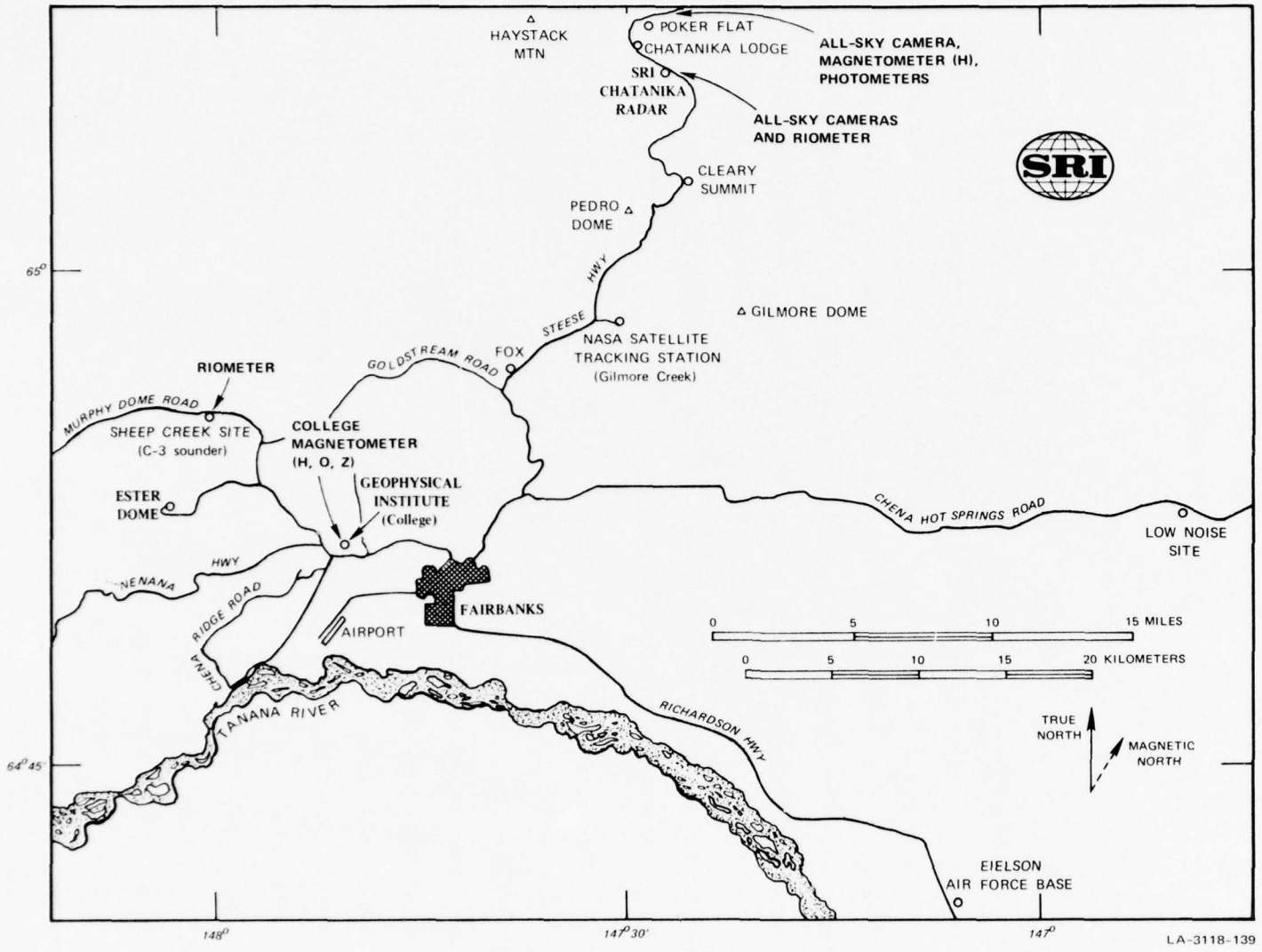

FIGURE 2 MAP OF FAIRBANKS, ALASKA VICINITY SHOWING LOCATIONS OF CHATANIKA RADAR AND OTHER SCIENTIFIC INSTRUMENTATION

III MEASUREMENT THEORY

A. General

Using the incoherent-scatter technique, the Chatanika radar can obtain a great deal of information about the ionospheric plasma and the forces and processes acting upon it. Table 3 summarizes the radar-derived quantities obtained during the various ICECAP '75 experiments. Not all of these quantities were available for each rocket experiment. For example, on 26 February the radar antenna was operated in a single-position mode, and consequently no information was obtained on vector quantities. In other cases, electron densities were so low that minimum time resolutions had to be increased to much greater than 5 s in order to obtain a reasonable signal-to-noise ratio (SNR).

The data presented in this report are derived from both radar and collateral sources. Section V describes measurements made during each ICECAP experiment. For each experiment a subsection entitled Background Measurements presents radar measurement data characterized by resolution times of 5 to 10 minutes and extending over periods typically exceeding an hour. Radar data included in this category are parameters 1 through 7 in Table 3. Collateral data are also presented in those subsections; i.e., magnetometer and riometer records and various optical measurements (all-sky camera, satellite photos, and boresight television). For each experiment, a subsection entitled Correlated Measurements presents measurements of the horizontal separation between the radar beam and the rocket, along with finely resolved measurements of electron density and energy spectra of auroral electrons (Parameter 8 in Table 3).

Table 3

QUANTITIES MEASURED BY THE CHATANIKA RADAR

No.	Parameter	Altitude Region (km)	Range Resolution (km)	Typical Time Resolution	References
1	Electron density	>60	10	≥5 s	1-6
2	Conductivities	Height-integrated ~90 to ~150	60	≥5 s	7, 8, 10
3	Electric field	>170	60	~6 min	7, 8
4	Neutral wind	Height-averaged ~90 to ~150	60	~6 min	7-9
5	Current density	Height-integrated ~90 to ~150	10	~6 min	7, 8, 10
6	Energy deposited by auroral electrons	Height-integrated ~90 to ~150	60	≥5 s	11, 12
7	Joule heating	Height-integrated ~90 to ~150	60	~6 min	7, 9
8	Energy spectra of auroral electrons	60 to 150	10	≥5 s	13

Notes: Parameters 6 and 7 are usually considered together in the subsections entitled Energy Deposition.
Parameters 6, 7, and 8 are usually deleted under sunlit conditions.

The basis for this format is convenience and uniformity. The rationale of the division is that since the interesting part of a rocket flight occupies much less than 5 minutes or so, only those measurements with very short resolution times can provide detailed correlations with time-varying rocket measurements.

It is instructive to note the limitation on the determination of Parameters 6 and 8 in Table 3. Each of these parameters is deduced on the assumption that ionization takes place entirely as a result of precipitation of energetic particles. During nightime or at very low ($\lesssim$90 km) altitudes, this may be a reasonable assumption, but where an appreciable flux of EUV is present it is probably a poor assumption. A precise determination of electron production due to solar photons is very difficult,[14] and it has not been attempted in this report. Under all conditions of solar illumination at altitudes above ~90 km, there is surely some contribution to electron production due to solar photons. Accordingly, with one exception we have deleted calculations of Parameters 6 and 8 in Table 3 for all daytime experiments. Since Parameter 7 is considered in summation with Parameter 6, it has also been deleted under the same circumstances. An exception to this rule is made in the case of the D-region experiment on 26 February, where the emphasis of the experiment was on altitudes below 100 km.

In general, the quantities obtained by the radar during ICECAP '75 have been derived according to well documented methods, as indicated in Table 3. However, a few of the techniques used have been just recently implemented, and deserve some discussion at this point. In addition, radar data are sometimes contaminated by echoes from the rocket. Removal of the contaminated data is time consuming and may not always be required, but the presence of possible contamination should be recognized.

B. D- and E-Region Electron Density

In Ref. 6 an analysis was conducted into the special problems associated with making radar measurements of electron densities at low altitudes. Figure 3, taken from Ref. 6, illustrates the types of errors

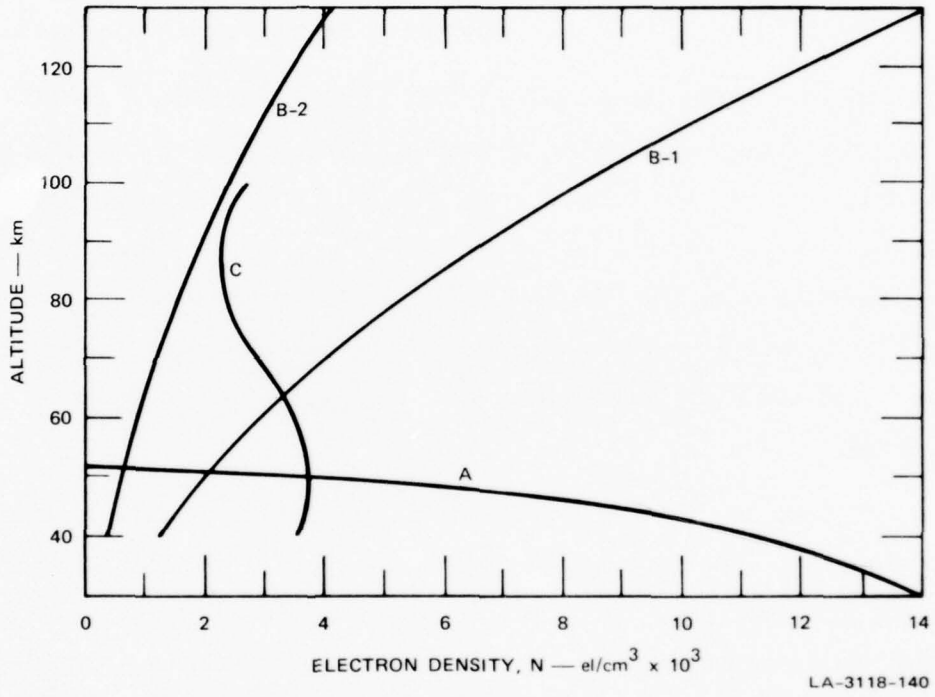

FIGURE 3 LOW-ALTITUDE ACCURACY LIMITS OF CHATANIKA RADAR. Curve A: Ground-clutter signal for 70° elevation, a 50-μs transmitted pulsewidth, and averaged over 360° of azimuth. Curves B-1 and B-2: Altitude profile of the standard deviation of statistical fluctuations for a 1- and 10-minute integration, respectively. Curve C: Altitude profile of minimum computable electron density based on Debye-length considerations.

analyzed there. For purposes of the ICECAP '75 experiment, the significance of the error sources is as follows.

Ground clutter (Curve A) imposes an absolute minimum altitude of about 55 km for any ionospheric measurements, and for certain antenna positions, ground-clutter returns may cause interference at altitudes as high as 60 km.

Statistical noise limits (Curves B-1 and B-2) vary as the square of range and as the inverse square root of integration time. For one-minute integrations, the rms value of statistical uncertainty in the D- and E-regions is as large as 10^4 el/cm^3.

Debye-length considerations establish an absolute lower detectability limit of about 2 to 4 x 10^3 el/cm^3 in the D- and E-regions (Curve C).

It should also be noted that for large values of Debye length, measurement accuracy is improved by making a correction to raw data based on electron and ion temperature. A technique for making radar measurements of electron and ion temperature at E-region altitudes is nearly developed,[15] but the technique was not in use during the ICECAP '75 experiments. During ICECAP '75, D- and E-region temperatures were obtained from a model atmosphere,[16] and the model values were used for making the appropriate density corrections.

Temperature corrections to measured density values based on model temperatures are somewhat time-consuming and are not routinely performed, and under most conditions this omission is justified. Figure 4, obtained from Ref. 6, illustrates the errors present before the appropriate corrections have been made. In the figure, the error is expressed as the ratio of true density N to uncorrected density N′, and the ratio N/N′ is plotted as a function of the ratio N'/T_e, where T_e is electron temperature. For expected electron temperatures of <300° K in the D region, it can be seen that a correction becomes necessary only when raw (uncorrected) densities dip as low as 3 to 4 x 10^4/cm^3.

C. Recombination Coefficient

The determination of some quantities, such as Parameters 6 and 8 in Table 3, requires a model of effective recombination coefficient as a function of altitude. This quantity is defined by the relationship

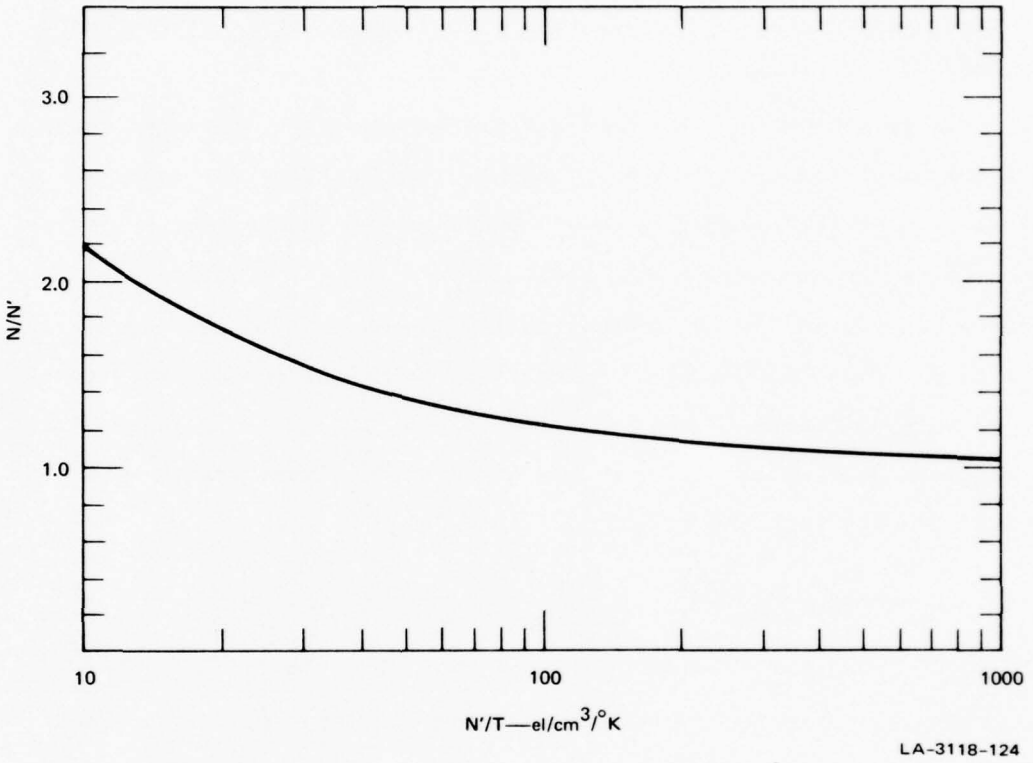

FIGURE 4 RELATIONSHIP BETWEEN RAW DENSITY AND TEMPERATURE-CORRECTED DENSITY FOR THE CHATANIKA RADAR. N' is Raw Density, N is Temperature-Corrected Density, and T is Plasma Temperature.

$Q = \alpha N^2$, where Q is production rate, N is electron density, and α is effective recombination coefficient.

The effective recombination coefficient has been studied over a range of altitudes and by a variety of methods.[17,18] For purposes of simplicity and convenience, and in consideration of the limited scope of this report, a height-independent value of 3×10^{-7} cm^3/s has been adopted for calculations of Parameter 8, while for Parameter 6 a simple, height-dependent model[12] has been used. If it is later determined that greater accuracy is required in the deduced values of the α-dependent parameters, improved models of α can be employed, at the cost of greater complexity and effort.

D. Radar Measurement of Differential Energy Distribution of Incident Auroral Electrons

Recently a technique has been devised by which the Chatanika radar measurements of ionospheric density can be used to infer the energy distribution of the incoming auroral electrons.[13] When an auroral electron strikes the atmosphere, the altitude profile of ionization that it produces depends on the electron's initial energy. If the incident electrons have a distribution of energies f(E), the total ionization production rate Q at any altitude is the sum of the production rates for each energy. The altitude profile of Q can be obtained from the radar measurements of electron density n by the relation

$$Q = \alpha n^2$$

where α is the effective recombination coefficient and we have assumed transport-free equilibrium.

A computer technique has been devised for obtaining f(E) from the ionization profile, and is referred to as UNTANGLE. The starting point of the UNTANGLE process is the conversion of the electron density profile into a production-rate profile. This production-rate profile is then deconvolved by successive fitting to a library of production-rate profiles for monoenergetic electrons. It is assumed that the incoming angular distribution is field-aligned, although similar results are obtained if the incoming angular distribution is assumed to be isotropic over the downward hemisphere. The program starts at the lowest altitude at which there is detectable ionization, determines the flux and energy of incident particles necessary to produce the measured ionization, subtracts from the measured profile the ionization produced at all altitudes by the monoenergetic flux, and then steps up in altitude (down in energy) until the energy range 1 to 30 keV is covered. A more complete description

of the UNTANGLE technique and its application is given elsewhere.[19] The distributions presented in this ICECAP '75 report are based on a preliminary version of UNTANGLE that has greatest accuracy between 3 and 16 keV. Refinement of the technique and a detailed evaluation of its precision are currently in progress.

E. Contamination of Radar Data by Rocket Echoes

During the flight of a rocket, radar data are contaminated by echoes from the vehicle and the rocket exhaust. The problem is not confined to situations in which the rocket is in the main lobe of the radar antenna. Analysis of radar records indicates that substantial contamination can occur even when the antenna gain in the direction of the spurious echo is over 40 dB below boresight gain.

Data contamination can affect any of the various outputs of the radar. The most common form in which contamination appears, however, is as extraneous enhancements of electron density. At any instant of time, a rocket echo will appear as an enhancement at an equivalent altitude given approximately by $H_{eq} = R \sin \theta$, where R is the range from the radar to the rocket and θ is the elevation angle of the radar antenna. The equivalent altitude of the extraneous enhancement is therefore, in general, not the same as the rocket altitude.

Although a rocket echo is sharply confined in range, the contamination extends over a significant interval in altitude. The range-resolution limitation of the radar causes a smearing in altitude. Further smearing occurs because of rocket range variations during a finite integration time. The altitude interval of contaminated data is given approximately as the interval H_a to H_b, defined as

$$H_a = \left(R_a - \Delta R\right) \sin \theta \qquad (1)$$

$$H_b = \left(R_b + \Delta R\right) \sin \theta \qquad (2)$$

where R_a and R_b are the radar-to-rocket ranges at the beginning and ending, respectively, of the integration period, and ΔR is the range resolution of the radar. It follows that data contamination from rocket echoes can be reduced by minimizing the integration periods during the flight of a rocket.

The reality of this effect is demonstrated by radar measurements made during the rocket flight of 26 February 1975. Figure 5 illustrates five successive density profiles obtained during the ascent of the rocket. During each of the profiles obtained from 20-s integrations, the rocket was well outside the main beam of the radar antenna. The quantities H_a and H_b corresponding to each of the profiles have also been listed. It can be seen that the observed enhancements agree closely with the predicted altitudes. In Profile 1, contamination is absent above 83 km altitude, and the portion of the profile above 90 km is real. For the other profiles, it is not possible to separate the rocket contribution from the ionospheric contribution.

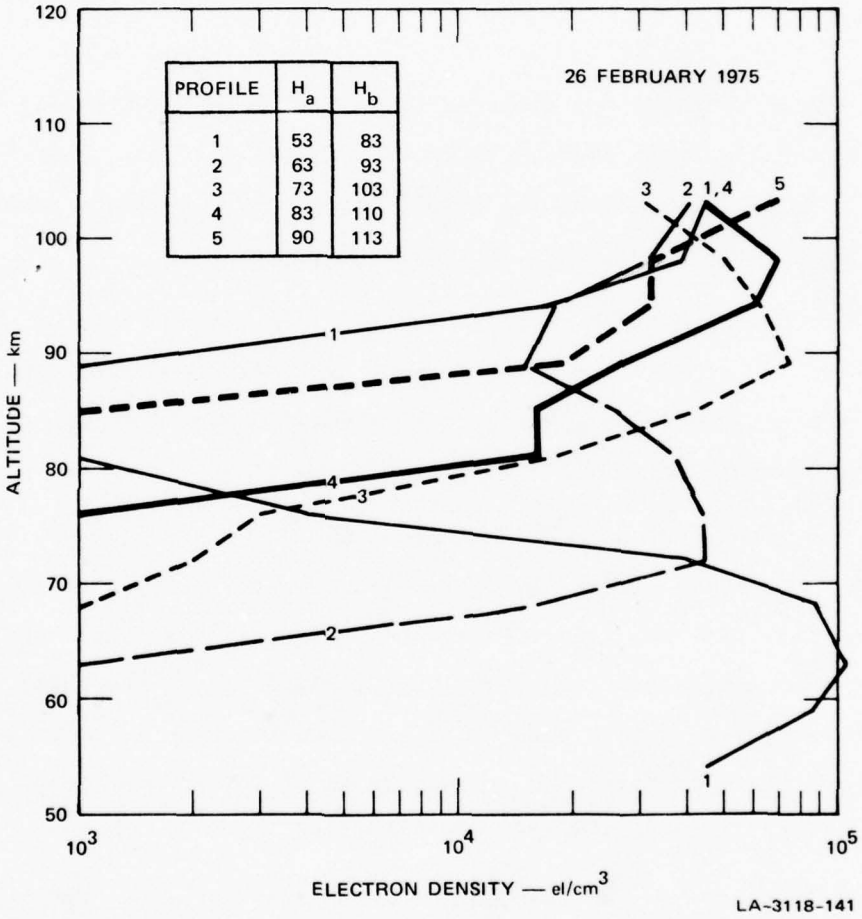

FIGURE 5 SUCCESSIVE MEASUREMENTS OF ELECTRON-DENSITY PROFILES MADE WITH THE CHATANIKA RADAR DURING THE UPLEG OF THE ROCKET FLIGHT ON 26 FEBRUARY 1975, ILLUSTRATING THE CONTAMINATING EFFECT OF ROCKET ECHOES

IV OPERATIONAL SUMMARY

A total of eight instrumented rockets were launched during the period 26 February through 12 March 1975 as part of the ICECAP '75 program.* Table 4 summarizes the ICECAP '75 rockets, payload, auroral and solar conditions, and Chatanika radar operating modes.

The Chatanika radar operated successfully during seven of the eight launches. On 4 March the radar transmitter failed and was inoperative from 0645 UT to 0823 UT. Thus, no coordinated radar data are available for the launch at 0739 UT.

During the various ICECAP missions the radar was operated in a variety of antenna modes. During the 26 February mission the radar antenna direction was fixed; therefore no vector information was obtained. During the missions on 1 March, 4 March, and 6 March, the radar antenna was operated either in a three-position azimuth or in an azimuth-scan mode, and yielded unambiguous measurements of vector quantities such as electric fields, currents, and neutral winds.

On 10 March the radar antenna was operated in a two-position azimuth mode. Under the assumption that plasma velocity parallel to the geomagnetic field was small, these measurements yielded the same vector quantities obtainable with a three-position operating mode. For a 6-minute period during the rocket flight, the antenna was pointed manually so the radar beam would intersect the rocket trajectory.

---

*Rocket timing and trajectory data were provided by Space Data Corporation, Phoenix, Arizona.

Table 4

ICECAP '75 OPERATIONS SUMMARY

Date	Launch Time (UT)	Vehicle	Payload Experiment	Auroral Conditions	Solar Zenith Angle (deg)	Radar Operating Mode
2/26/75	2250:00.027	Astrobee D IC503.22-1	Gerdian Condenser	Quiet	74.3	Azimuth 309.5°, Elevation 76.5°
3/01/75	0100:00.020	Astrobee D IC503.14-3	OH	Quiet	80.0	Azimuth Scan, Elevation 65°
3/04/75	0739:30.025	Nike Javelin IC506.14-2	OH	Quiet	116.4	Three-position Azimuth, Elevation 60°
3/06/75	0343:00.028	Nike Hydac IC507.11-1A	LWIR	Quiet	93.5	Azimuth Scan, Elevation 65°
3/06/75	0616:30.020	Nike Hydac IC507.11-3	LWIR	Moderately disturbed	109.0	Azimuth Scan, Elevation 65°
3/10/75	0912:20.040	Nike Hydac IC507.11-2A	LWIR	Disturbed	118.6	Two-position Azimuth, Elevation 60° except fixed at nominal rocket intercept 0914-0920 UT
3/11/75	0633:09.040	Nike Javelin IC511.21-1A	E-Fields	Disturbed	108.8	Two-Position Azimuth, Elevation 60°
3/12/75	0748:10.035	Sergeant Hydac IC519.07-18	Multi	Disturbed	114.1	Azimuth Scan, Elevation 65°, Azimuth 29°, Elevation Scan

On 11 March, during the launch window, the radar was being operated in a six-position azimuth mode in connection with an independent experiment. For a 40-minute period that included the rocket flight, the ongoing experiment was interrupted and the radar antenna was operated in a two-position azimuth mode to provide closely coordinated vector measurements.

On 12 March, for several hours before the launch, the radar was operated in an azimuth-scan mode in order to measure ionospheric transport, electron density, and neutral winds. Approximately two minutes before launch, the operational mode of the radar antenna was changed to an elevation scan in the magnetic meridian, thus yielding information on latitudinal variation of auroral ionozation.

In the following sections we will present the Chatanika radar measurements made in support of the ICECAP '75 experiments. Data from collateral sources are also included to the extent available.

V MEASUREMENT RESULTS

A. 26 February 1975--Astrobee D

1. General

An Astrobee D rocket (IC 503.22-1) carrying a Gerdian condenser was launched from Poker Flat at 2250:00 UT on 26 February. The rocket reached an apogee of 103.3 km at about 160 s after launch and was above 60 km altitude for about 190 s. The experiment took place under daytime conditions, with a solar zenith angle of 74.3° at launch.

During the period 2225 UT to 2350 UT, the Chatanika radar was operated in support of the rocket experiment. The antenna remained fixed at 209.5° azimuth and 76.5° elevation--that is, directed up the geomagnetic field line. The transmitter used a 67-μs density-data pulse, yielding 10 km range resolution, and a 20-s integration interval was used.

2. Background Measurements

Ionospheric and geomagnetic background conditions were quiet for this experiment. Although optical measurements are not available because of solar illumination, other observations indicate no significant auroral or geomagnetic activity.

Geomagnetic conditions during this experiment are illustrated by Figure 6, which presents H-component magnetograms from four stations distributed in latitude but in the same local time sector. It can be seen that geomagnetic conditions were very quiet during this experiment.

Absorption conditions in the D-region were also quiet during the experiment, as indicated by Figure 7, which illustrates riometer

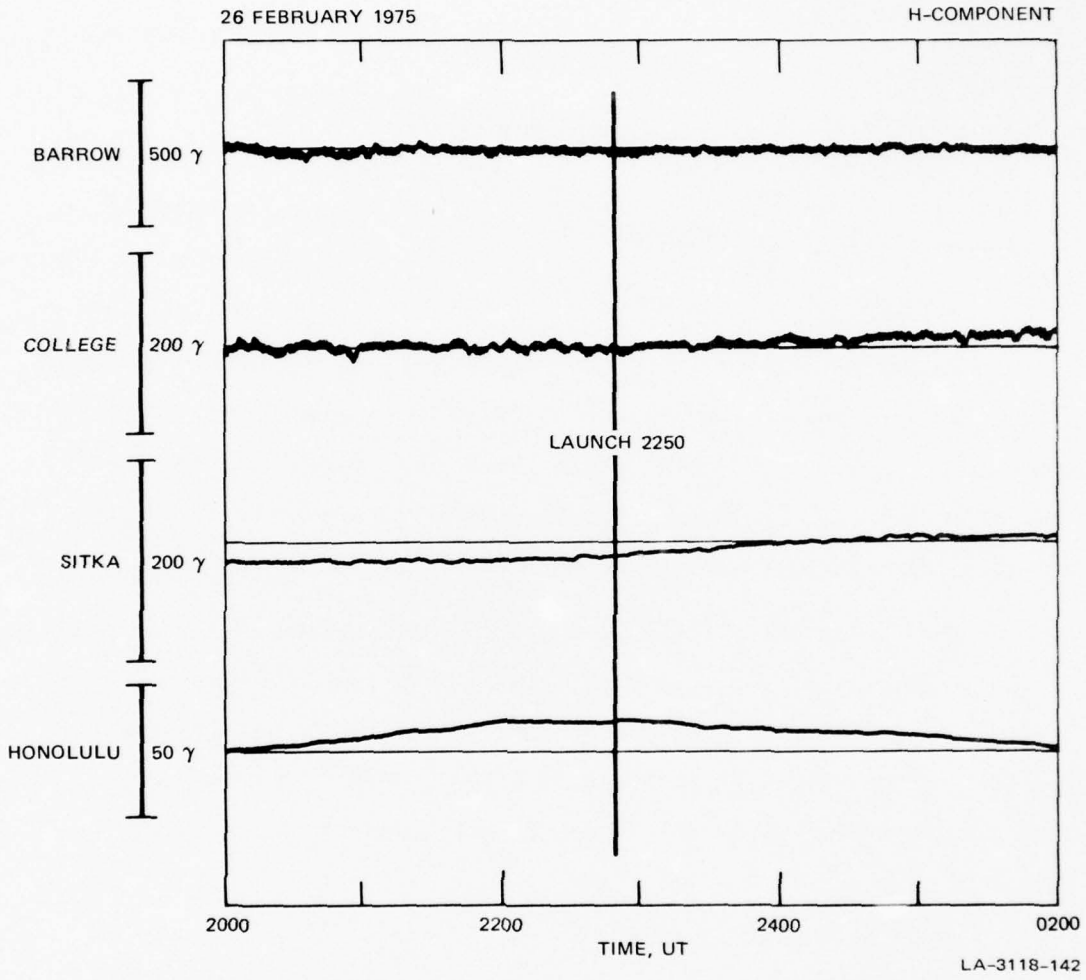

FIGURE 6 H-COMPONENT MAGNETOGRAMS ON 26 FEBRUARY 1975 FROM FOUR STATIONS DISTRIBUTED IN LATITUDE BUT IN THE SAME LOCAL TIME SECTOR AS THE ROCKET TRAJECTORY

records from the College site for both the period of the experiment on 26 February and a similar period on 9 March, a quiet reference day. The spikes on the record for 26 February are associated with radio interference.

Background electron densities in the ionosphere are presented in Figure 8, which illustrates density contours obtained from radar measurements integrated over 5-minute intervals for a 90-minute period

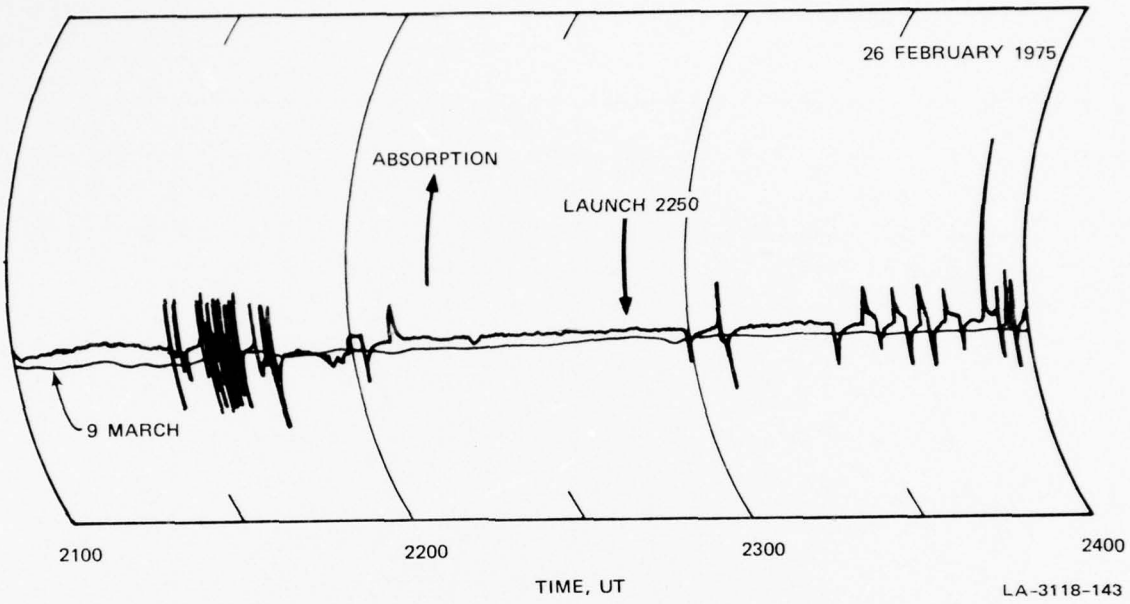

FIGURE 7 COLLEGE RIOMETER RECORD FOR 26 FEBRUARY 1975. The record for 9 March 1975 is representative of a quiet day.

encompassing the rocket experiment. Measurable electron densities exist down to about 85 km altitude and were temporally smooth throughout the period of interest.

Since the radar antenna was operated in a single position throughout this experiment, no vector quantities were measured. We thus have, for this experiment, no information on electric fields, current densities, neutral winds or joule heating.

3. Correlated Measurements

a. Separation Between Rocket and Radar Beam

The rocket launch occurred at 2250:00 UT, 50 minutes after local noon. At the time of this writing, the trajectory information available to us from Space Data Corporation (SDC TM-B65A) appears to be unreliable for times earlier than about 89 to 90 s after launch. For

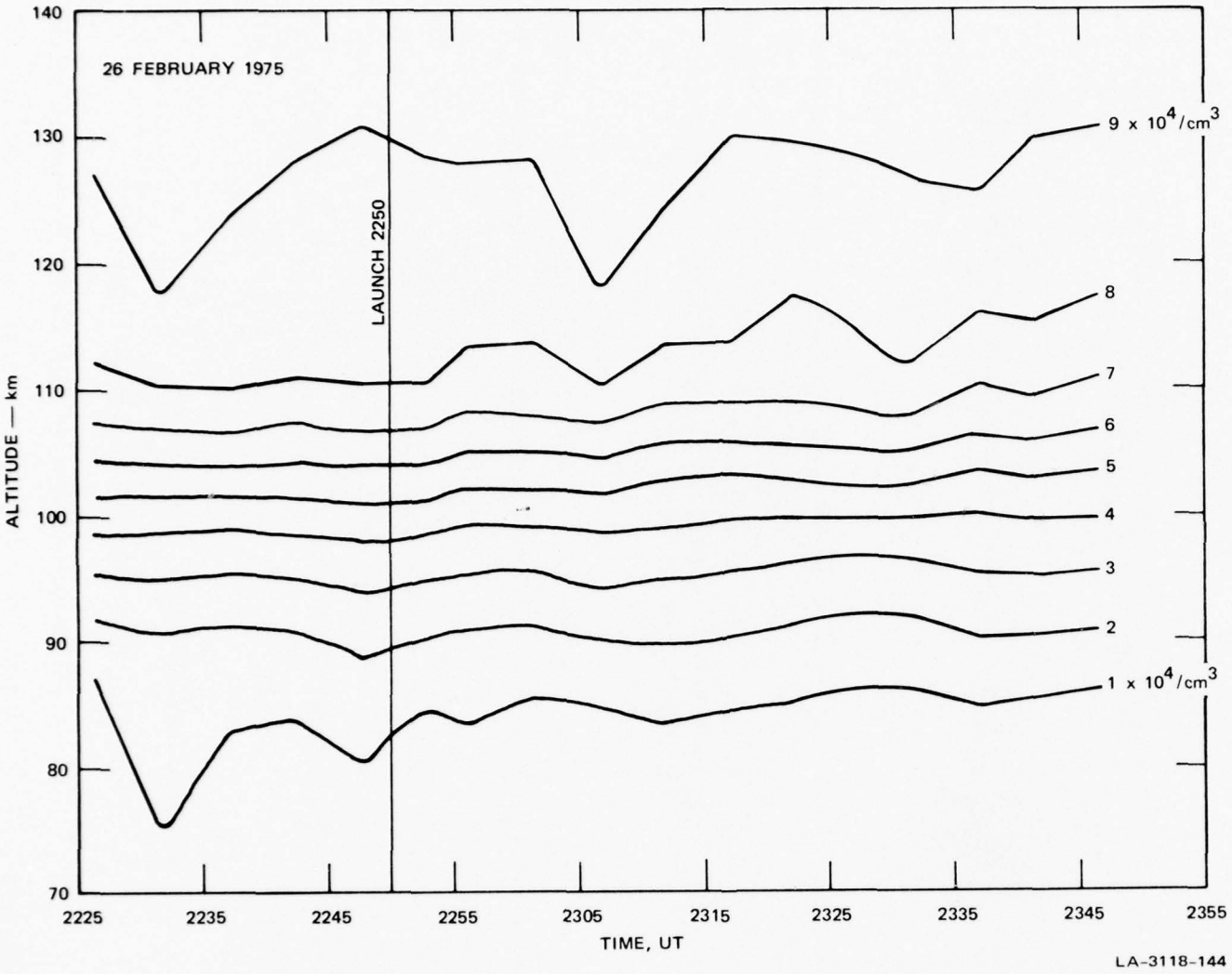

FIGURE 8 BACKGROUND CONTOURS (5-Minute Averages) OF ELECTRON DENSITY FOR THE EXPERIMENT ON 26 FEBRUARY 1975

times later than 80 s after launch, we have calculated the total horizontal separation and the latitudinal component of the horizontal separation between the rocket and the radar beam. Figure 9 illustrates the results of these calculations. Figure 9 shows that some obvious uncertainties exist in the computations at flight times less than 90 s. Nevertheless, it can be seen that horizontal separations of 40 to 60 km exist between the radar and rocket measurements during the time of D- and E-region measurements. It is obvious that the rocket was well outside the main beam of the radar at all times.

Although the rocket was never in the main beam of the radar, its presence in the sidelobes caused a significant effect on radar measurements of electron density.

b. Electron Density

Figure 10 illustrates, in solid lines, contour plots of temperature-corrected electron density during the immediate period surrounding the rocket flight. Superimposed on the contours is the equivalent altitude of the rocket during the flight, as interpreted by the Chatanika radar.

It can be seen that echoes from the vicinity of the rocket have introduced artifacts in the data that appear as density enhancements. The effect is very pronounced on the upleg of the flight and there is little or no effect during the downleg. As our best estimate of actual densities we have drawn fine dashed lines through the artificial enhancements connecting the undisturbed portions of the contours.

With the most obvious errors thus removed, we may consider the meaning of the electron-density contours. In particular, it is instructive to consider the reality of the apparent oscillations in the contours, especially following the rocket flight. We first note that

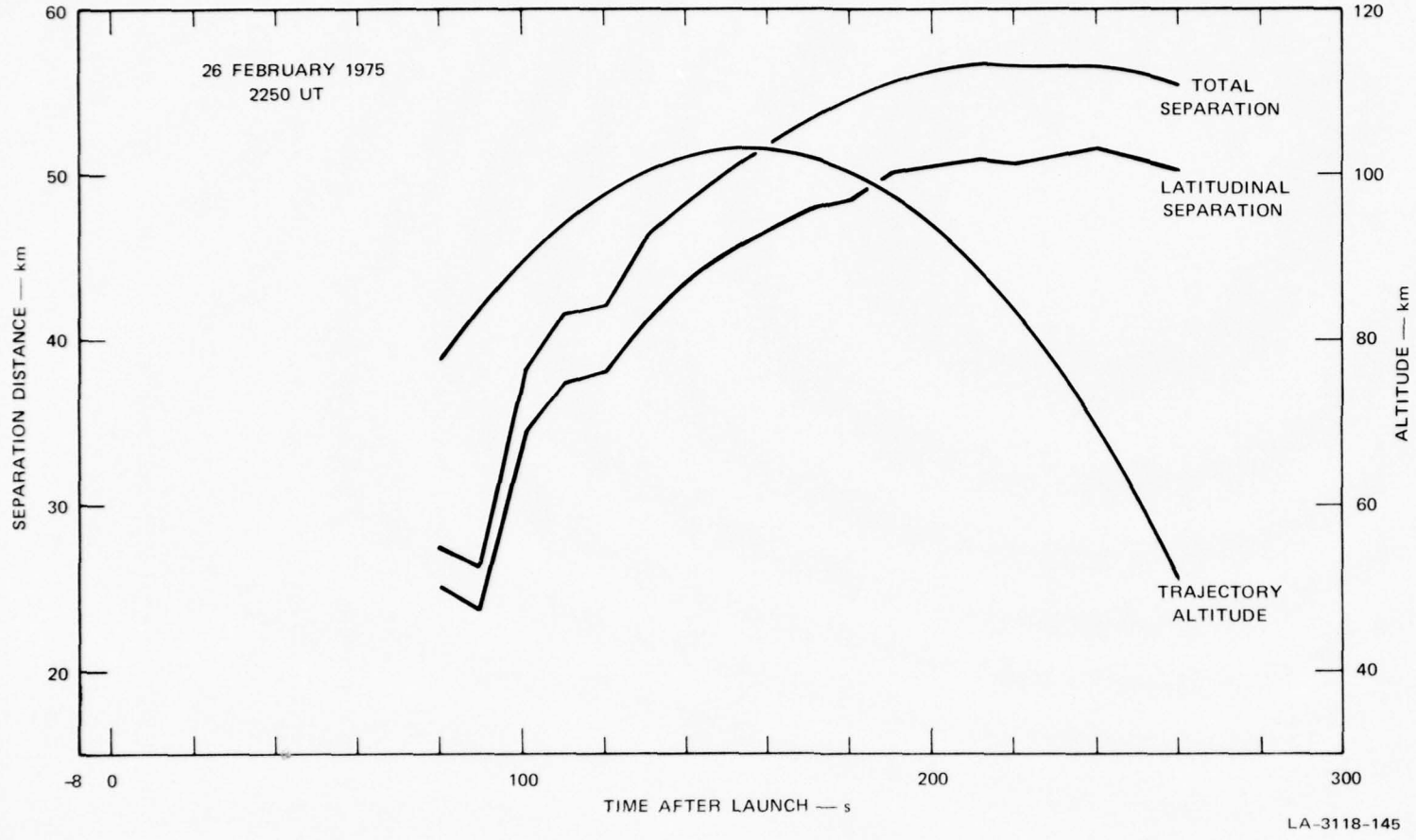

FIGURE 9 TRAJECTORY ALTITUDE OF THE ROCKET AND HORIZONTAL SEPARATION DISTANCE BETWEEN THE RADAR BEAM AND THE ROCKET FOR THE FLIGHT OF 2250 UT, 26 FEBRUARY 1975

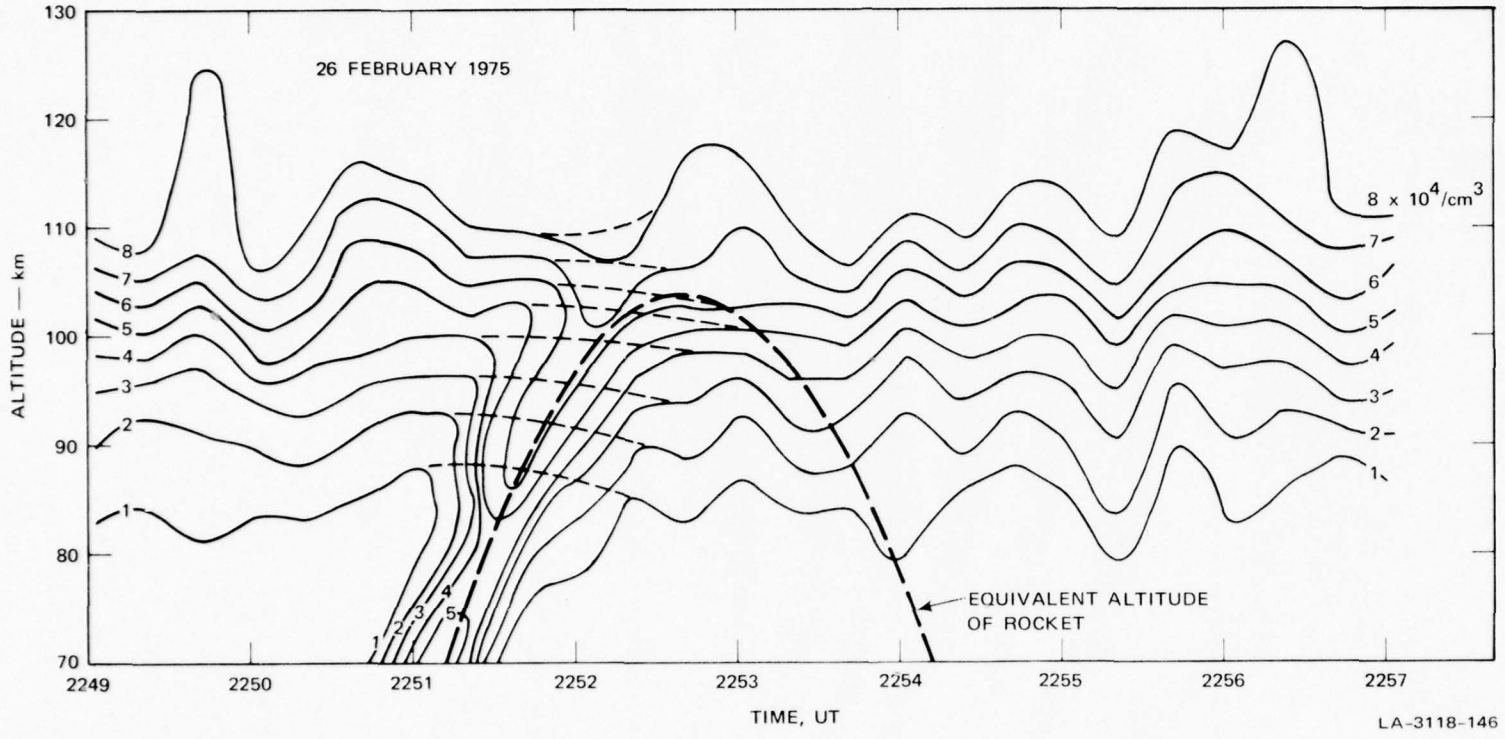

FIGURE 10 CONTOURS OF ELECTRON DENSITY AND THE EQUIVALENT ALTITUDE OF THE ROCKET DURING THE FLIGHT OF 2250 UT, 26 FEBRUARY 1975. The dashed lines represent estimates of the contours that would have been obtained in the absence of contamination from rocket echoes.

calculated density is proportional to the quantity $R^2(S - N)/N$, where R is range, S is measured signal power at range R, and N is measured noise power. At small values of SNR, such as were obtained here, any systematic fluctuations in apparent density could be due to correlated fluctuations in noise power. We have checked this possibility and have found no correlation during this period between noise power fluctuations and the apparent density fluctuations.

The second point considered is the statistical uncertainty of the density measurements. The measurement data on which these contour plots are based were obtained with 20-s integrations and averaged over 13.5 km in range. It can be shown that under these conditions the statistical uncertainty in altitude associated with any contour is of the order of ±3 km. Thus, the fluctuations are real.

c. Energy Deposited by Auroral Electrons

With the use of the corrected contours shown in Figure 10 it is possible to reconstitute an altitude profile of electron density appropriate to the time period 2249 UT to 2257 UT. Such an altitude profile is illustrated in Figure 11.

In Ref. 6 a study was performed of effective recombination coefficient in the D-region and lower E-region under PCA conditions. Seasonal dependence, if any, was not determined, but a definite dependence on solar zenith angle was found. Using the results of that study, we have obtained an altitude profile of effective recombination for a solar zenith angle of 74.3°, and that profile has also been plotted in Figure 11.

The data presented in Ref. 6 were obtained under ionizing and seasonal conditions quite different than those existing on 26 February. Nevertheless, if we ignore the possible significance of such differences and assume that the plotted profile is appropriate for the present

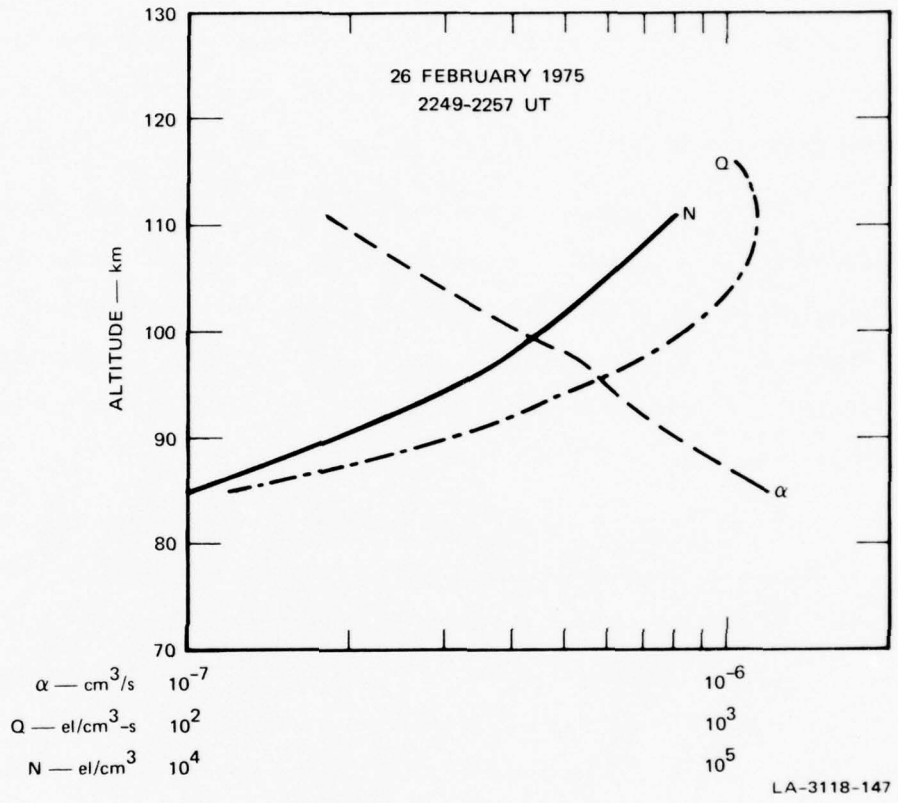

FIGURE 11 ALTITUDE PROFILES OF ELECTRON DENSITY, N, EFFECTIVE RECOMBINATION COEFFICIENT, α, AND ELECTRON PRODUCTION RATE, Q, APPROPRIATE TO THE ROCKET FLIGHT AT 2250 UT, 26 FEBRUARY 1975. Details are given in the text.

conditions, we can obtain an estimated altitude profile of electron production rate.

If we use the definition of effective recombination coefficient $\alpha = Q/N^2$, where Q is electron production rate and N is electron density, it is a simple matter to derive a profile of electron production rate. Figure 11 illustrates a profile of Q obtained in this manner.

The profile of Q thus obtained necessarily refers to the total production rate--including the effects of both solar EUV and energetic particles. If we assume that these are the only significant sources of electron production present, the production due to energetic

particles can be obtained by subtracting the estimated production due to solar EUV. We have not performed such a calculation, but Thrane[14] has studied the problem and outlined the solution.

Using the typical results obtained by Thrane, it appears, without performing any detailed calculation, that solar EUV production represents a very small (≤10%) contribution to the total production shown in Figure 11. As a first-order approximation, then, it appears that the profile of production shown in Figure 11 is due almost entirely to energetic particles.

If we further assume that auroral electrons are the only significant source of corpuscular ionization, we can estimate the energy deposited by the incoming auroral electrons. Assuming 35 eV per ion pair of production, a graphical integration of the curve labeled Q in Figure 11 yields an estimate of 0.103 ergs/cm^2-s deposited between 85 and 110 km altitude. Since observed production is negligible below 85 km during this period, and since 110 km corresponds approximately to the penetration altitude of 5-keV electrons, we may conclude that the total energy flux of electrons with energies >5 keV is about 0.103 erg/cm^2-s.

4. Summary

An Astrobee D rocket with a Gerdian condenser was launched from Poker Flat at 2250 UT into a quiet, sunlit ionosphere. The rocket reached an apogee of 103 km. During this experiment the radar was operated in a single-position mode; thus, no vector measurements were obtained.

During the flight of the rocket, temporally smooth electron densities were observed at altitudes as low as 80 km. In addition, radar data were contaminated by rocket echoes during the upleg of the flight, and corrected densities were obtained by subtracting the effects of the rocket echoes from the total radar signals. Horizontal separation between

the radar beam and the rocket varied from 30 to 60 km during the D- and E-region portions of the flight.

B. 1 March 1975--Astrobee D

1. General

An Astrobee D rocket (IC 503.14-3) carrying an OH payload was launched from Poker Flat at 0100:00 UT on 1 March (1500 LT on 28 February). The rocket reached an apogee of 106.9 km at 157 s after launch. The experiment took place under late afternoon sunlight, with a solar zenith angle of 80° at launch.

During the period 0041 UT to 0158 UT, the Chatanika radar was operated in support of the rocket experiment. During the entire period the antenna was operated in a continuous azimuth scan mode at a fixed elevation of 65°. The azimuth scan consisted of slewing the antenna alternately clockwise and counterclockwise through 360° at a rate of approximately 1°/s. The transmitter used a 67-μs data pulse for density measurements, yielding 10 km range resolution, and a 15-s integration interval was used. Because of the use of azimuth scan mode, the minimum resolution time for vector measurements was about 6 minutes.

2. Background Measurements

a. Geomagnetic Conditions

Geomagnetic conditions were only slightly disturbed during the experiment. Figure 12 illustrates geomagnetic H-component records from four observatories, distributed in latitude but in about the same local time sector, for a six-hour period centered at the launch time. It can be seen that during the flight of the rocket, variations in the local (College) H-component were less than 40 γ, but generally increasing.

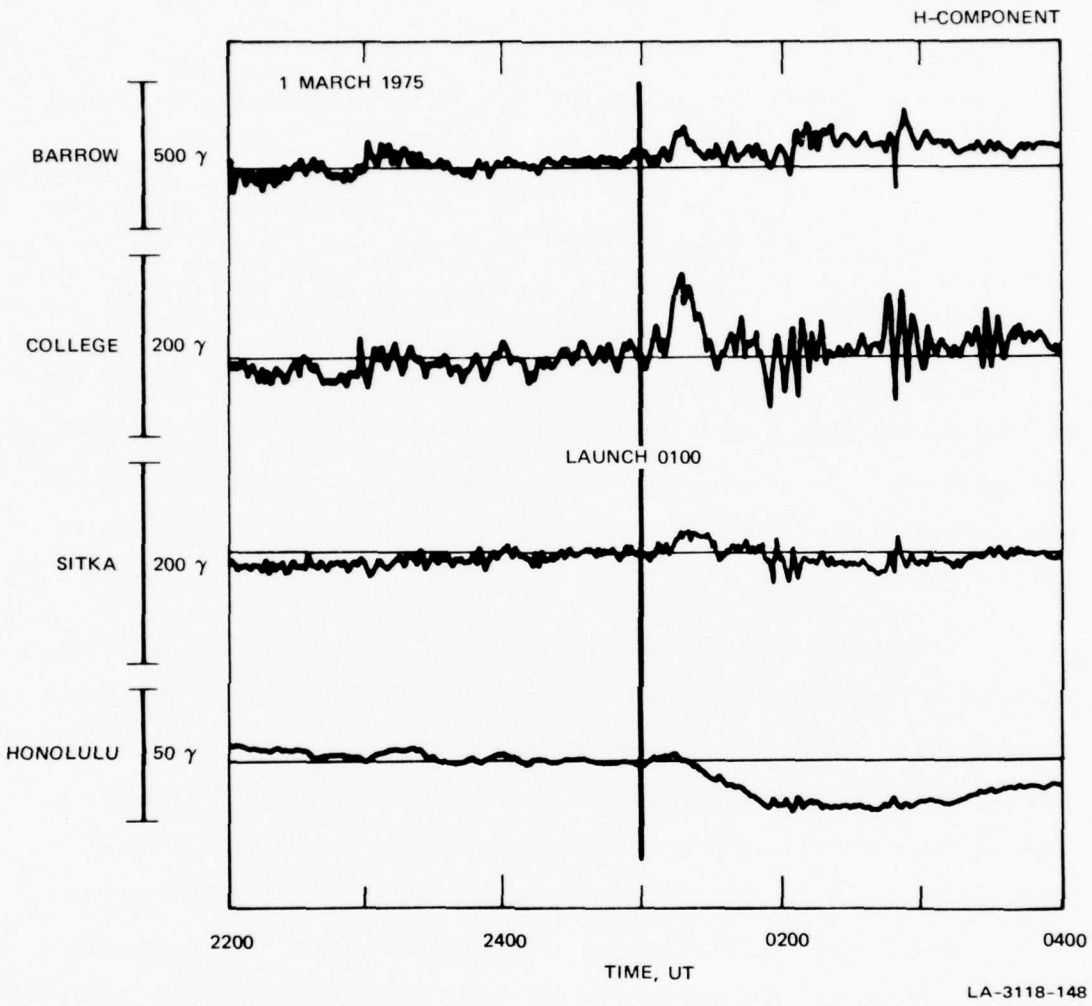

FIGURE 12 H-COMPONENT MAGNETOGRAMS ON 1 MARCH 1975 FROM FOUR STATIONS DISTRIBUTED IN LATITUDE BUT IN THE SAME LOCAL TIME SECTOR AS THE ROCKET TRAJECTORY

b. Auroral Conditions

Since the experiment took place under daylight conditions, optical measurements of any possible auroral activity were precluded.

c. Absorption

Riometer measurements from College also indicate moderate conditions. It can be seen in Figure 13 that there is a modest level of

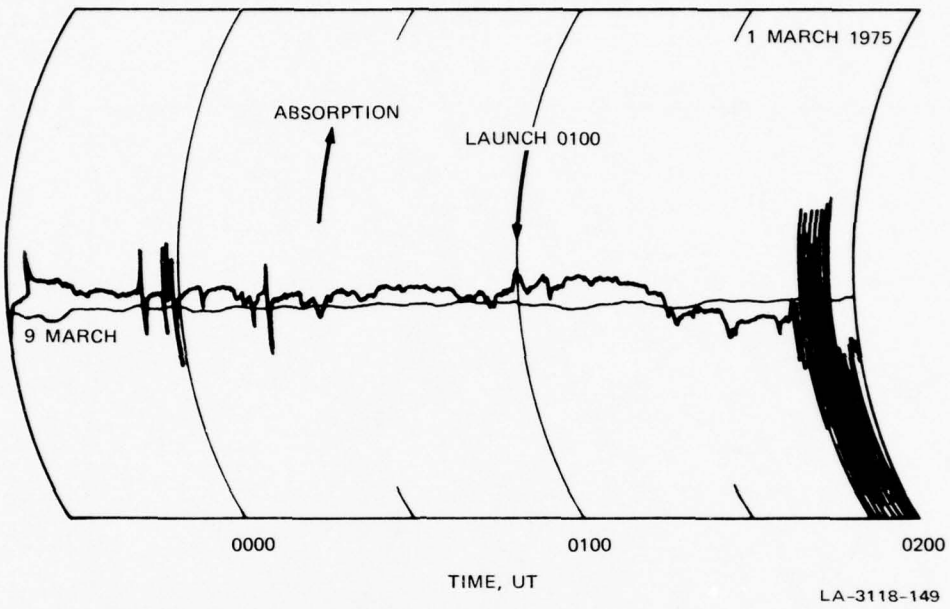

FIGURE 13 COLLEGE RIOMETER RECORD FOR 1 MARCH 1975. The record for 9 March 1975 is representative of a quiet day.

relatively constant absorption during the flight of the rocket. It can also be seen that at about 0125 UT the absorption level diminishes rapidly.

d. Electron Density

Ionospheric densities were moderately quiet during the experiment. Figure 14 is a radar-derived contour plot of ionospheric electron density during the period 0041 UT to 0158 UT. The contours are obtained from nominal 6-minute integrations, each representing an average over a 360° azimuth sweep of the antenna. It can be seen that a small E-layer begins to form at least as early as 0041 UT, achieves its maximum density of about $1 \times 10^5/cm^3$ at about 0110 UT, and disappears by 0120 UT. The decrease in density is consistent with the decrease in absorption shown to occur at about 0120 UT in Figure 13.

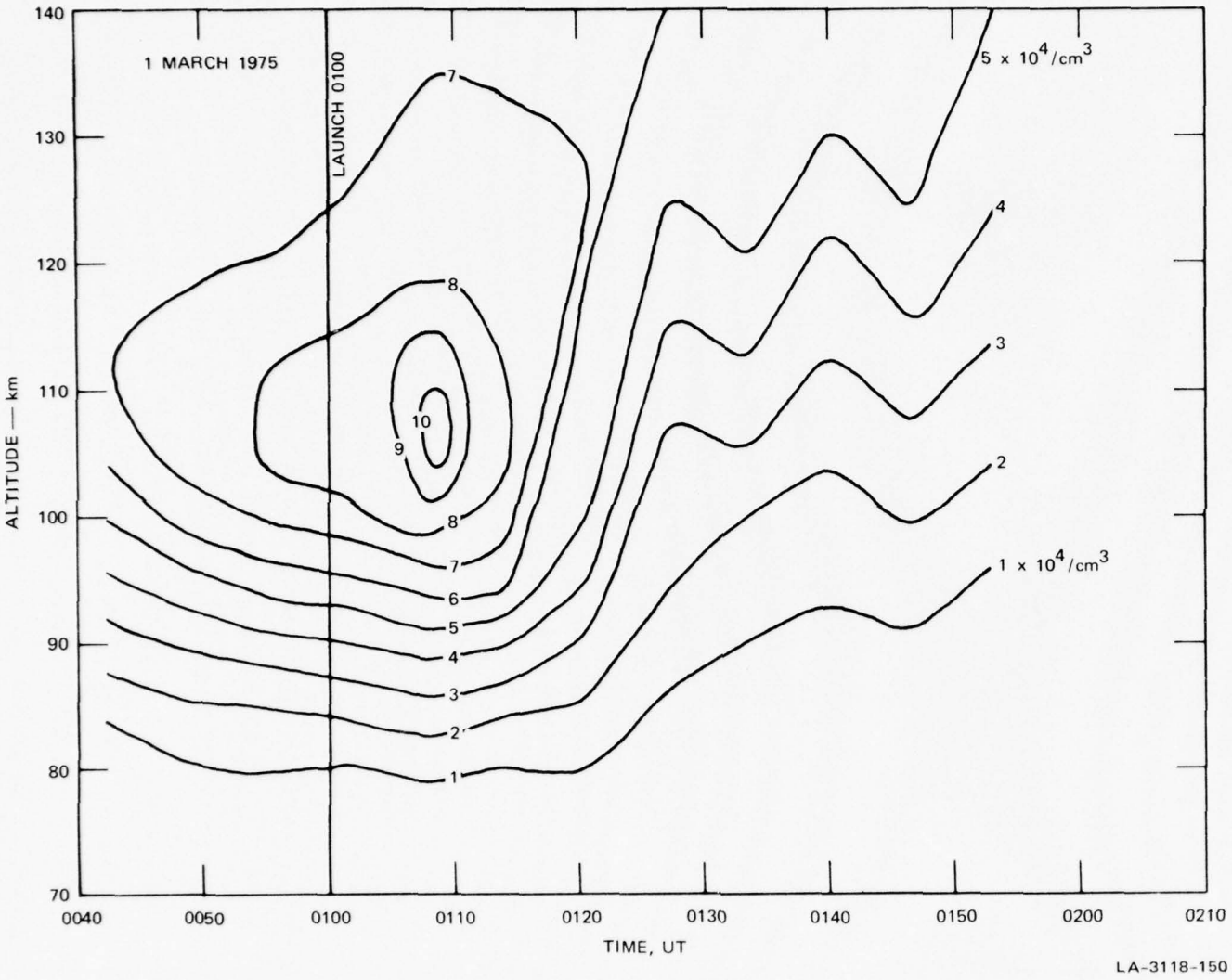

FIGURE 14 BACKGROUND CONTOURS (6-Minute Averages) OF ELECTRON DENSITY FOR THE EXPERIMENT ON 1 MARCH 1975

e. Height-Integrated Conductivities

The Hall and Pedersen conductivities discussed in this report are all height-integrated, as described in earlier ICECAP reports. Figure 15 contains plots of these conductivities based on 1-minute averages, for the period of the radar experiment. The vertical dashed

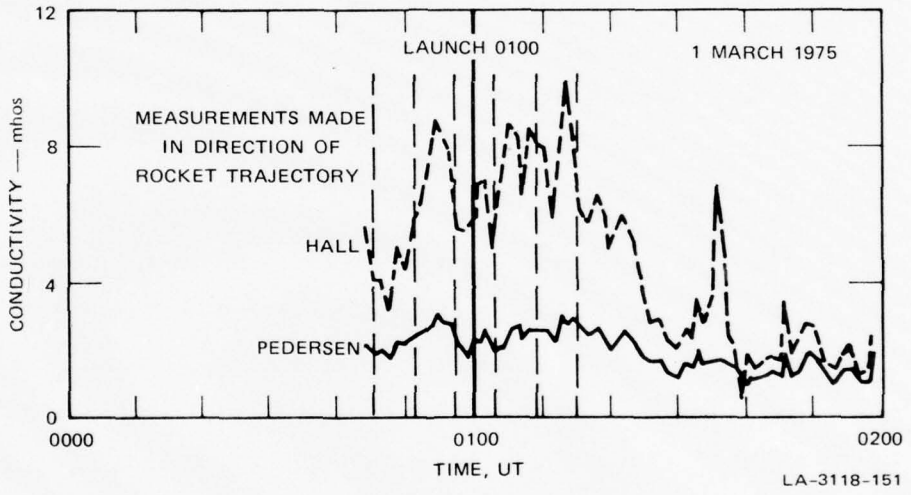

FIGURE 15 HEIGHT-INTEGRATED CONDUCTIVITIES FOR THE EXPERIMENT ON 1 MARCH 1975. Vertical dashed lines represent times near launch when the radar beam was pointed in the azimuthal direction of the rocket trajectory.

lines on the figure indicate the times during the rocket flight when the radar antenna was pointing in the azimuth direction of the rocket trajectory. Temporal variations in the conductivities indicate changes (both temporal and spatial) in the primary electron energy spectrum, as observed by the radar. Furthermore, the Hall conductivity tends to be more sensitive to density variations below about 125 km altitude, while the Pedersen conductivity tends to be more sensitive to density variations above 125 km. Specifically, a change in the peak energy of energetic electrons would manifest itself as a change in the Hall-to-Pedersen conductivity ratio.

It can be seen that, beginning about 0115 UT, both Hall and Pedersen conductivities decrease systematically. The changes indicate diminishment in the flux of energetic electrons after about 0115 UT. The reduction in total flux of energetic electrons is, of course, consistent with the decrease in electron density shown in Figure 14 to occur after about 0120 UT. Height-integrated conductivities were measured once in the direction of the rocket during its flight. The measurements, occurring near apogee of the rocket (0103 to 0104 UT), yielded values of 1.9 and 5.0 mhos for the Pedersen and Hall components, respectively.

f. Electric Field

The Chatanika radar-derived electric field is calculated from the estimates of average ion velocity between 182 km and 236 km altitude. Since the vector estimates are obtained from component measurements made at different times and at different locations in space, the resulting electric field represents averages over a time of about 6 minutes, and over a volume having about 88 km horizontal radius and a vertical extent of 54 km.

The electric field morphology for the period of the experiment is shown in Figure 16. During the flight of the rocket, a small electric field was present over Chatanika, having a northward component of about 5 mV/meter and an eastward component of about 3 mV/meter. The magnitude of the field increased beginning about 0115 UT, well after the experiment was completed.

g. Neutral Wind

Height-averaged neutral-wind estimates are presented in Figure 17 as geomagnetic north-south and east-west components, each based on 6-minute integrations. During the entire flight of the rocket there

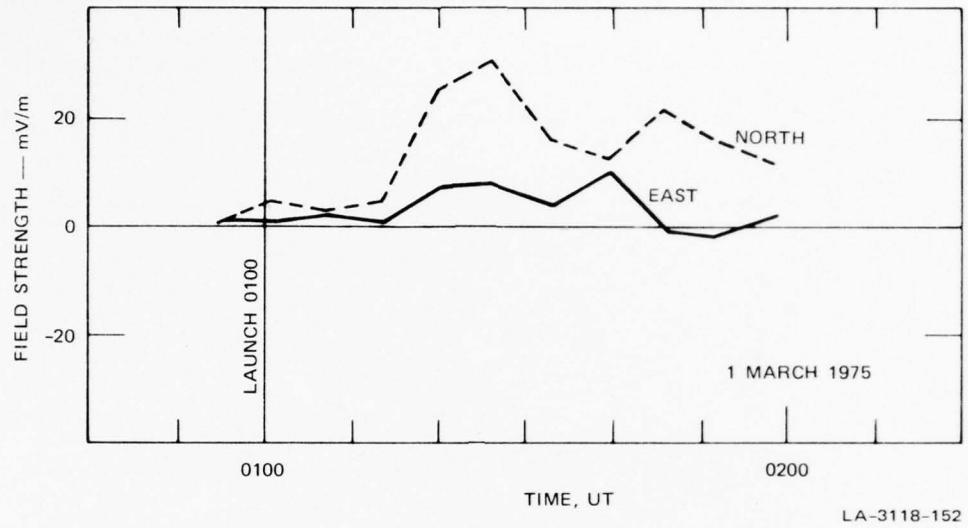

FIGURE 16 ELECTRIC FIELD FOR THE EXPERIMENT ON 1 MARCH 1975

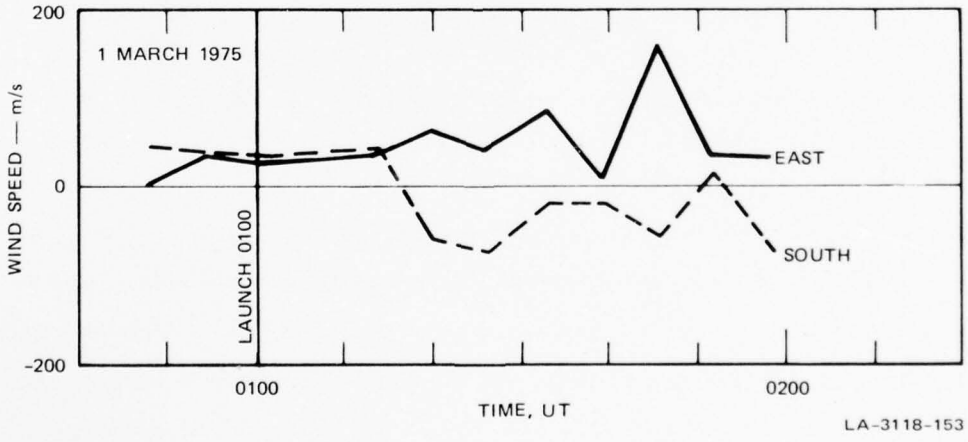

FIGURE 17 HEIGHT-AVERAGED E-REGION NEUTRAL WIND FOR THE EXPERIMENT ON 1 MARCH 1975

was a small, steady neutral wind, having components of about 50 m/s northward and 80 m/s eastward. At about 0115 UT, well after the rocket flight had terminated, both components of wind velocity changed and exhibited large variations through the end of the radar experiment.

h. Height-Integrated Current Density

Six-minute averages of height-integrated current density during the period of the radar experiment are presented in Figure 18.

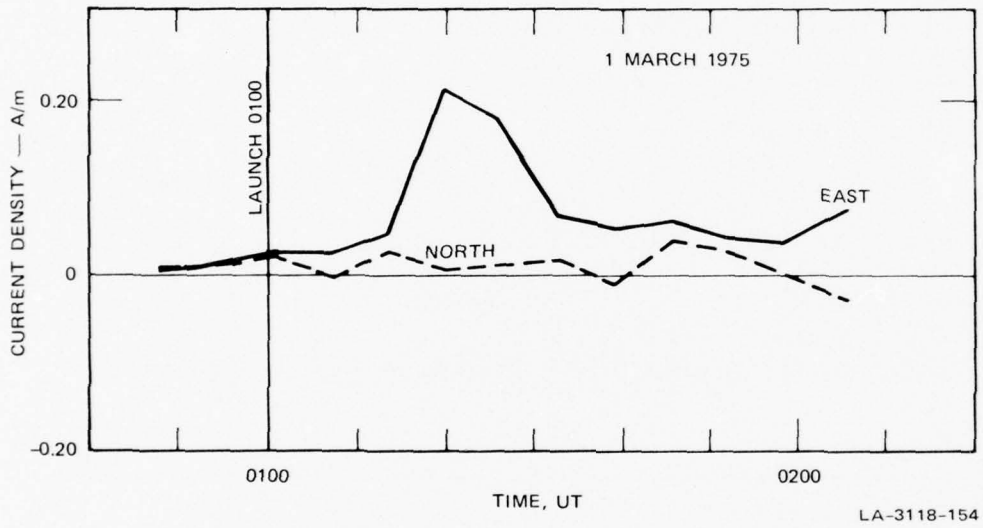

FIGURE 18 HEIGHT-INTEGRATED CURRENT DENSITY FOR THE EXPERIMENT ON 1 MARCH 1975

During the flight of the rocket, total current density was low and apparently stable, having an eastward component of about 40 mA/m and a northward component of about 20 mA/m. Throughout the period of the radar experiment, the northward component remained small, varying between zero and about 5 mA/m. Beginning at about 0106 UT, the eastward component increased to about 200 mA/m and thereafter maintained an average value of perhaps 60 mA/m. The polarities of both components remained essentially unchanged during the radar experiment.

3. Correlated Measurements

a. Separation Between Rocket and Radar Beam

During the rocket experiment the radar antenna was scanned continuously in azimuth. This mode of operation provided high-quality vector information.

Figure 19 illustrates a plan view of the situation during the ionospheric passage of the rocket. The ground track of the rocket is shown with various times after the launch given as a parameter. Corresponding to each of the designated times the figure shows the geographic location at which the radar beam intersects the altitude plane containing the rocket. The instantaneous positions of the rocket and the radar beam intersection point are connected by lines, the length of which are indicative of the horizontal separation distance and direction between the end points. It can be seen that, because of the scanning of the radar antenna, horizontal separation distance varies widely during the flight of the rocket. Figure 20 illustrates horizontal separation distance as a function of time after launch. It can be seen that, for the rocket in the altitude range 80 to 102 km, horizontal separation distance varies from 10 to 60 km.

b. Electron Density

Figure 21 illustrates contour plots of radar-derived electron density obtained during the experiment along with a plot of the equivalent altitude of the rocket. The contours were prepared by drawing smooth curves through the data points, which were obtained at 15-s intervals. As noted already, the antenna scanned continuously in azimuth at about 1°/s throughout the experiment, and the azimuth direction as a function of time is noted along the top of the figure. The rocket azimuth (21.5°) is also noted.

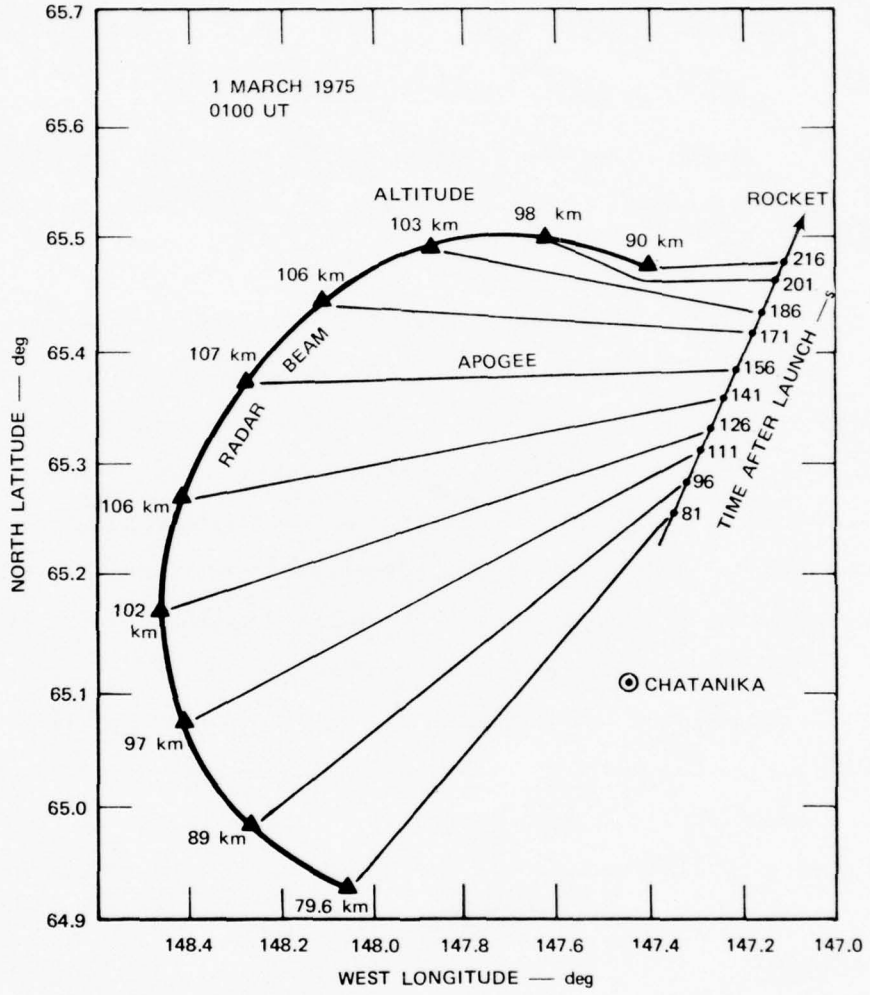

FIGURE 19 GEOGRAPHICAL RELATIONSHIPS BETWEEN THE ROCKET TRAJECTORY AND THE RADAR BEAM DURING THE FLIGHT OF 0100 UT, 1 MARCH 1975

Considerable structure can be seen in the density contours. Although temporal and spatial variations in ionization cannot be unambiguously separated from these data, there is little doubt that significant spatial variations are present.

It does not appear that any significant rocket-induced contamination is present in the data.

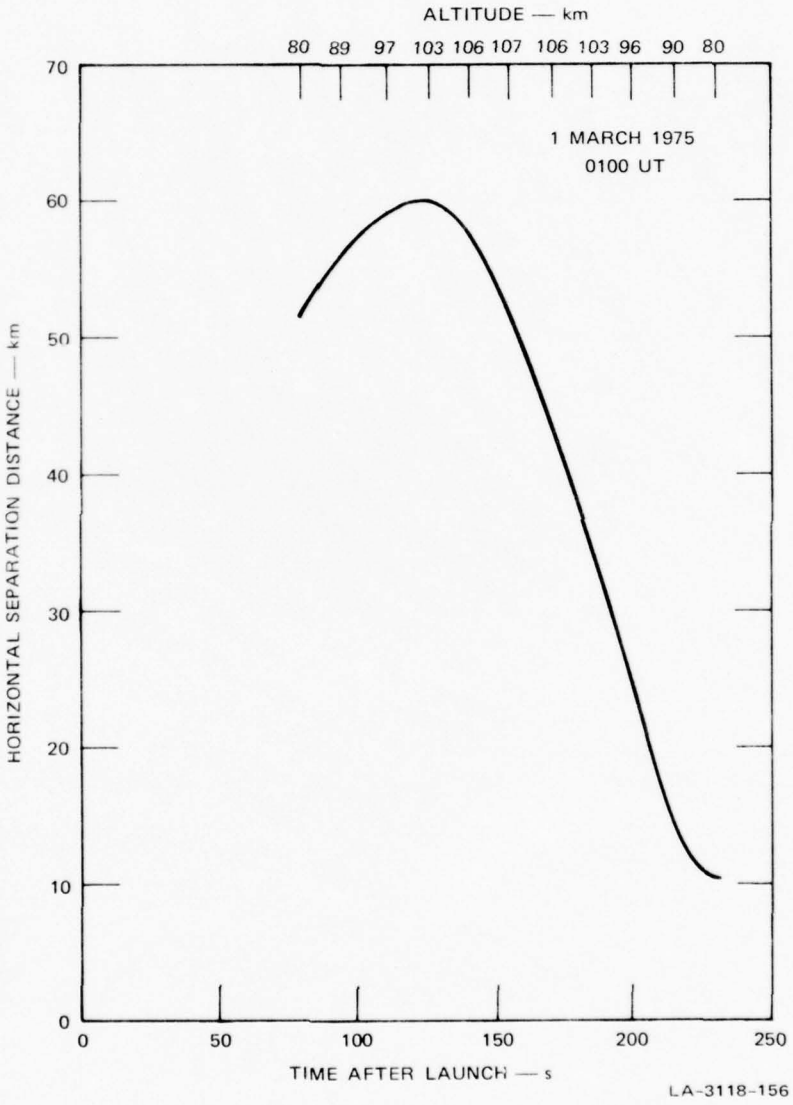

FIGURE 20 HORIZONTAL SEPARATION DISTANCE BETWEEN THE RADAR BEAM AND THE ROCKET DURING THE FLIGHT OF 0100 UT, 1 MARCH 1975

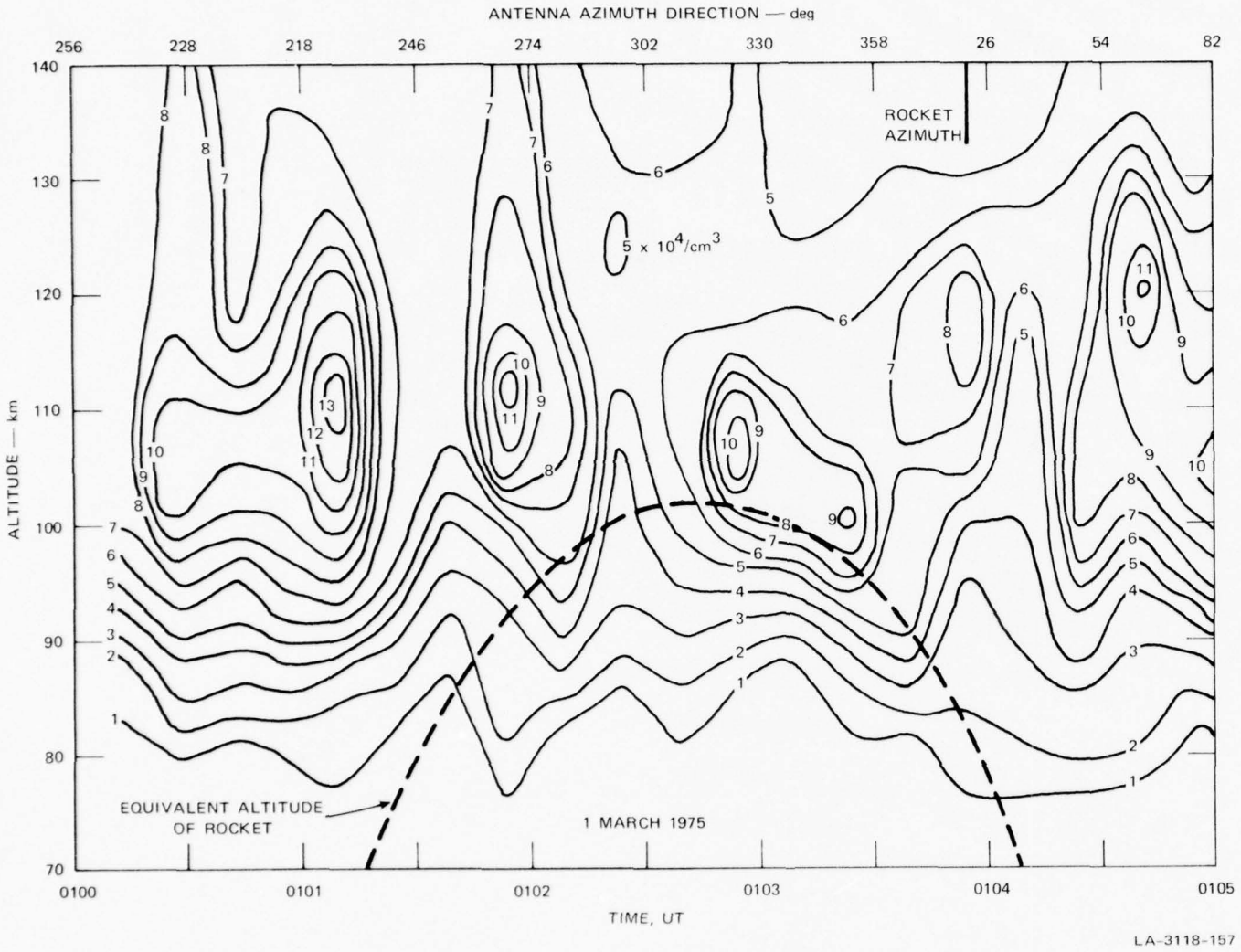

FIGURE 21 CONTOURS OF ELECTRON DENSITY AND THE EQUIVALENT ALTITUDE OF THE ROCKET DURING THE FLIGHT OF 0100 UT, 1 MARCH 1975

4. Summary

An Astrobee D rocket with an OH payload was launched from Poker Flat at 0100 UT on 1 March into a quiet, sunlit ionosphere. The rocket reached an apogee of 106.9 km at 0102:37 UT and the flight terminated at 0105:11 UT. During the flight of the rocket an auroral E-layer was present, characterized by a peak density of about 10^5 el/cm^3 at 108 km altitude and measurable densities (>10^4 el/cm^3) as low as 80 km altitude. In spite of the presence of auroral ionization, conditions were moderately quiet during the flight, as indicated by measurement of electron density, D-region absorption, and geomagnetic variations.

Radar measurements in support of the rocket experiment were made from 0041 UT through 0158 UT. During the entire period, the radar antenna was operated in an azimuth-scan mode, yielding both density data and various vector quantities. During the flight of the rocket, densities exhibited a great deal of structure, and from radar measurements alone it is impossible to separate unambiguously temporal and spatial variations. All radar measurements that were averaged over all antenna positions indicate quiet, steady conditions during the rocket flight.

Most measurements exhibited increasing structure beginning around 0115 to 0120 UT. Between this time and the end of the measurements at 0158 UT, D- and E-region electron densities decreased, electric fields increased in magnitude and exhibited temporal variations, height-integrated conductivities decreased, height-integrated current densities increased, and neutral winds exhibited increasing variability. Systematic variations in direction of the various vector quantities were not observed during the period of the radar experiment. In sum, conditions during the rocket flight were quiet, with a nominal amount of particle precipitation present.

C. 4 March 1975--Nike Javelin

1. General

A Nike-Javelin rocket (IC 506.14-2) carrying an OH payload was launched from Poker Flat at 0739:30 UT on 4 March. The rocket reached an apogee of 100 km at 165 s after launch. The experiment took place under nighttime conditions, with a solar zenith angle of 116.4° at launch.

From about 0530 UT through 1100 UT the Chatanika radar was dedicated to supporting the rocket experiment. During this period the radar antenna was operated sequentially in three azimuth positions--6.5°, 51.5°, and 209°. The transmitter used a 67-μs data pulse for density measurements, and a 15-s integration period was used.

Unfortunately, the radar transmitter malfunctioned sometime between 0620 UT and 0640 UT and it was not restored to normal operation until 0823 UT. As a result of this circumstance, no meaningful correlations can be made between radar and rocket-borne measurements.

2. Background Measurements

a. Geomagnetic, Auroral, and Absorption Conditions

Geomagnetic and auroral conditions were quiet during the rocket experiment. The Chatanika all-sky films indicate no visible aurora during the flight. Figure 22, showing the H-component of magnetometer records at four locations, and Figure 23, showing the College riometer records, both indicate that quiet conditions existed during the rocket experiment.

b. Electron Density

Figure 24 presents four vertical profiles of electron density obtained from radar measurements. Each profile represents about

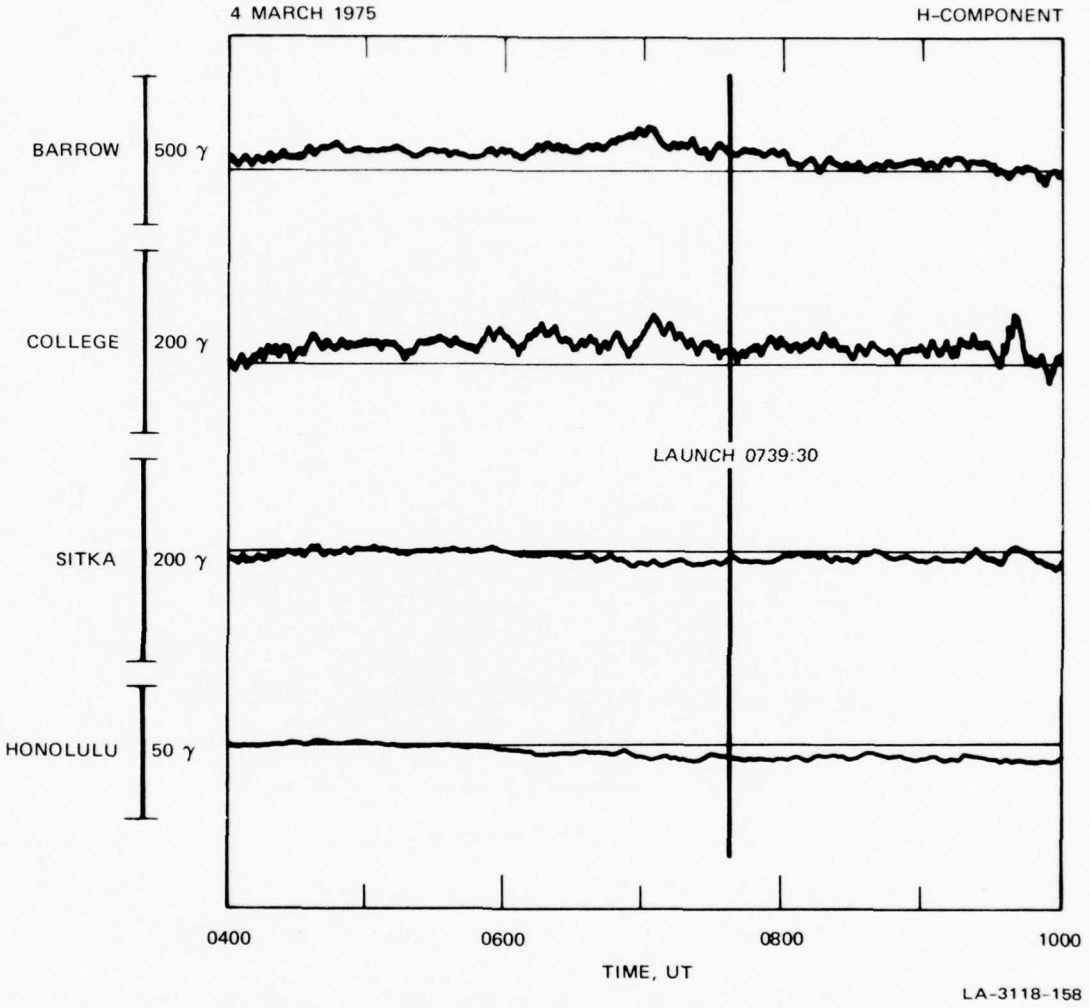

FIGURE 22 H-COMPONENT MAGNETOGRAMS ON 4 MARCH 1975 FROM FOUR STATIONS DISTRIBUTED IN LATITUDE BUT IN THE SAME LOCAL TIME SECTOR AS THE ROCKET TRAJECTORY

12 minutes of integration centered at the time indicated, and is an average over the three azimuth positions of the antenna. The profiles centered at 0556 UT and 0614 UT depict conditions just prior to the radar malfunction, and the profiles centered at 0832 UT and 0851 UT depict conditions just after the radar was restored to operation.

It is apparent that a definite E-layer was present around 0600 UT, having a density peak of 7 to 8 $\times 10^4$ el/cm^3 occurring at about

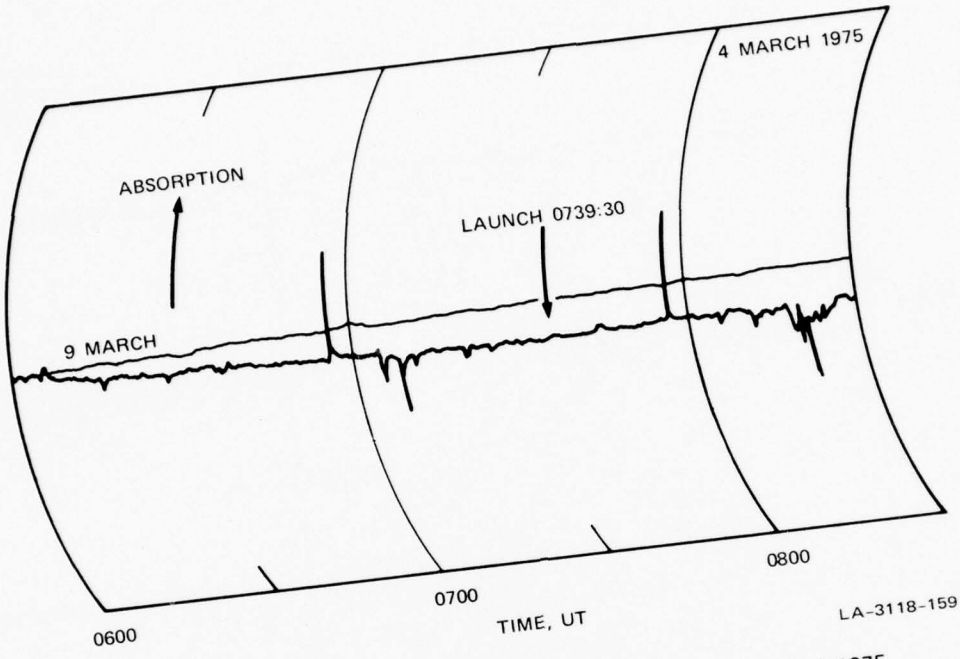

FIGURE 23 COLLEGE RIOMETER RECORD FOR 4 MARCH 1975

100 km altitude. Measurable ionization also existed as low as 80 km altitude during this time. The successive profiles suggest that E-layer ionization was decreasing at this time. Solar zenith angle at 0600 UT was 108°; thus, the observed layer cannot be due to solar EUV.

By the time radar operation was restored near 0830 UT the enhanced ionization in the D- and E-region had disappeared, leaving no measurable ionization below about 100 km altitude.

Comparison of the 0556 and 0614 UT profiles suggests a slight diminishing trend in density of the E-layer in the time frame 0550 to 0620 UT. Comparison of the 0832 and 0851 UT profiles indicates a temporal increase in electron densities above 100-km altitude but with only a tenuous E-layer present. Solar zenith angle at 0830 UT was about 118°; thus, the observed increase is not due to solar EUV.

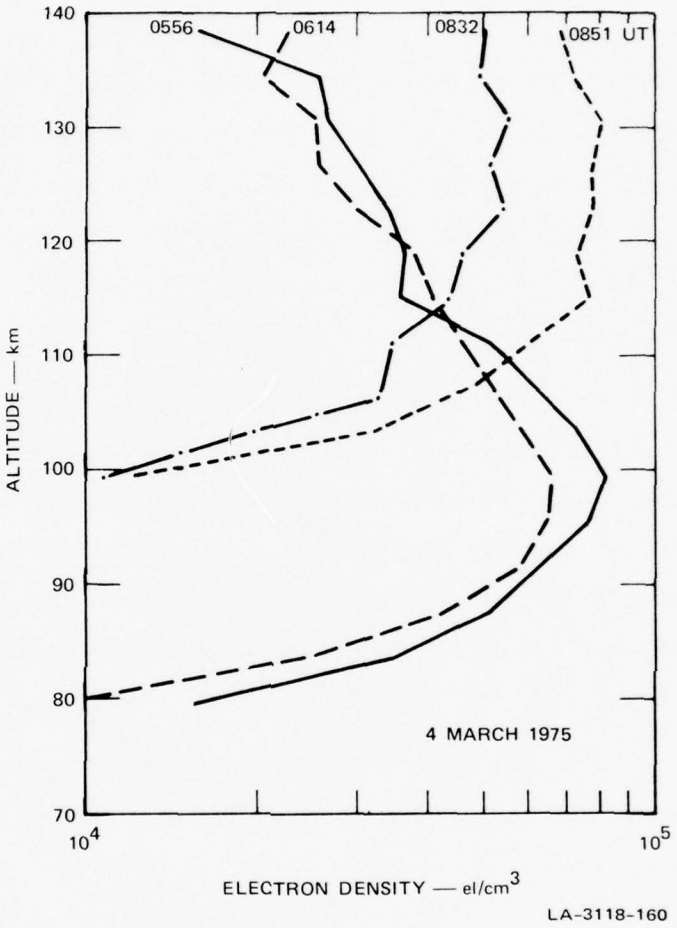

FIGURE 24 TWO PAIRS OF ALTITUDE PROFILES OF ELECTRON DENSITY OBTAINED JUST BEFORE AND JUST AFTER THE PERIOD OF RADAR MALFUNCTION 0620-TO-0823 UT, 4 MARCH 1975

c. Radar Vector Measurements

Since the radar was inoperative for two hours during the center of the launch window, no measurements were obtained during this time period.

D. 6 March 1975--Nike Hydac

1. General

On 6 March, two rockets were launched from Poker Flat as a part of the ICECAP program. The first launch occurred at 0343:00 UT and

consisted of a Nike-Hydac rocket (IC 507.11-1A) carrying a liquid-helium-cooled radiometer experiment. The main purpose of the experiment was the measurement of LWIR emission profiles of CO_2, NO, and O_3 at twilight. Solar zenith angle was 93.5° at the time of launch. The rocket reached an apogee of 132 km at 193 s after launch, and was above 70 km altitude from 0344:13 to 0348:02 UT.

The second launch occurred at 0616:30 UT and also consisted of a Nike-Hydac rocket (IC 507.11-3) carrying a liquid-helium-cooled radiometer experiment. The main purpose of the second experiment was the measurement of LWIR emission profiles of CO_2, NO, and O_3 under quiet night conditions. Solar zenith angle was 109° at the time of the second launch. The rocket reached an apogee of 154 km at 195 s after launch and was above 70 km altitude from 0617:35 to 0622:02 UT.

During the period 0331 to 0711 UT, the Chatanika radar was operated in support of the ICECAP program. During this entire period, the radar antenna was scanned continuously in azimuth, at a rate of one full scan every 6 minutes, while the elevation angle was held fixed at 65°. The transmitter operated with a 67-μs track pulse (10 km range resolution) for density data, and a 320-μs data pulse (48-km range resolution) for spectrum measurements. A 15-s integration period was used.

It is convenient to consolidate the descriptions of both background conditions and vector-based measurements for the two rocket launches on 6 March. Correlated measurements involving time periods short compared with the durations of the rocket flights will be described separately for each of the two flights.

2. Background Measurements

a. Geomagnetic Conditions

The two launches on this evening took place during geomagnetic conditions that varied from quiet to moderately disturbed (see Figure 25). The first launch, at 0343 UT, occurred after a small enhancement

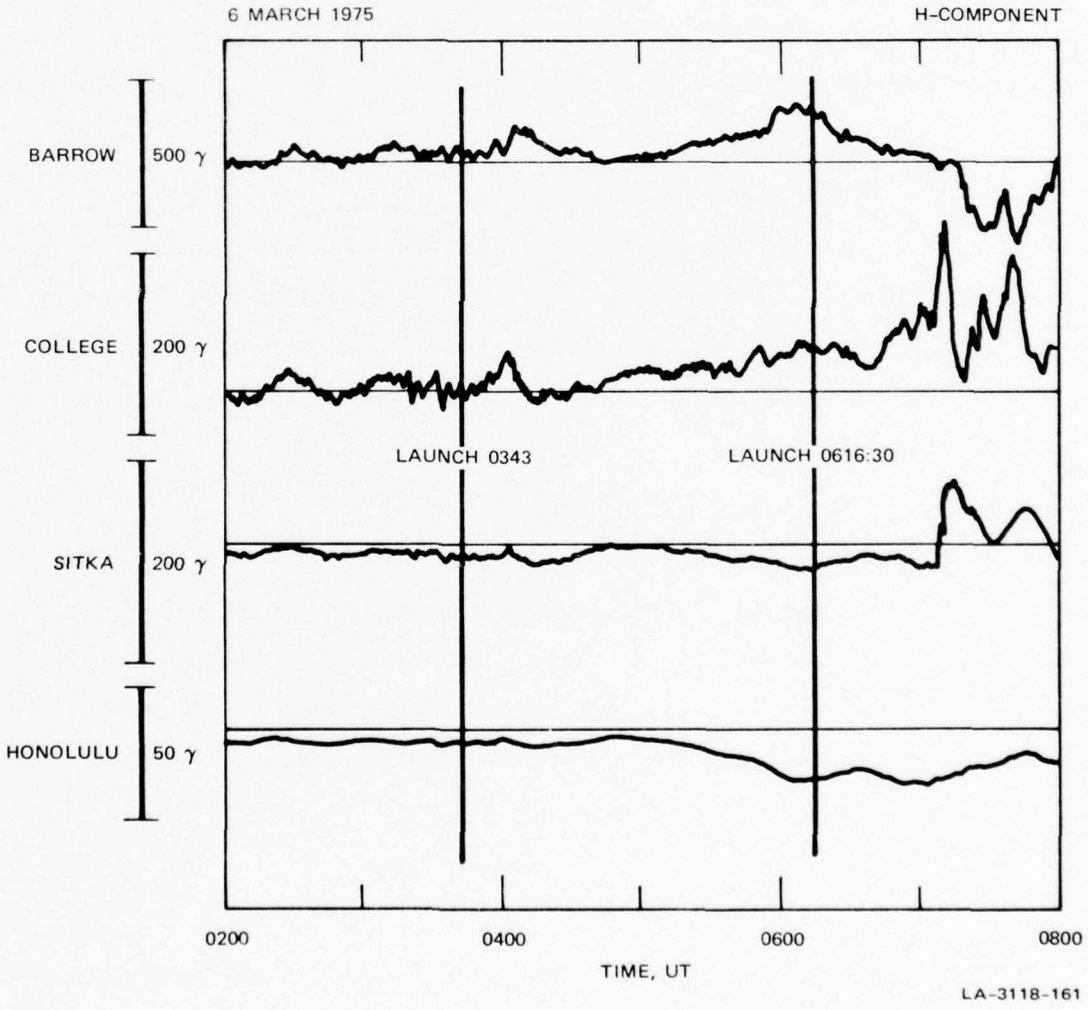

FIGURE 25 H-COMPONENT MAGNETOGRAMS ON 6 MARCH 1975 FROM FOUR STATIONS DISTRIBUTED IN LATITUDE BUT IN THE SAME LOCAL TIME SECTOR AS THE ROCKET TRAJECTORY

of the College H-component had subsided. The ring current was close to quiet levels, as seen in the Honolulu magnetogram.

However, by the time of the second launch (0616:30 UT) the eastward ionospheric current intensity had grown to a moderate level, resulting in the positive bays seen in the Barrow and College H-components. The effects of the ring current on the Honolulu and Sitka magnetogram can be seen until about 0705 UT, when a sharp enhancement of an eastward current system extended down to Sitka.

b. Auroral Conditions

Unfortunately at the time of launch the sky above the Chatanika all-sky camera was hazy and auroral observations were precluded. However, the Fort Yukon all-sky film (not shown) does show some faint auroral forms well poleward of Fort Yukon but none in the direction of Chatanika.

c. Absorption

Absorption measurements by the College riometer also indicate quiet to moderate disturbances. Figure 26 illustrates absorption measurements for the period 0230 to 0700 UT on 6 March. A similar measurement during the same time period on 9 March is superimposed as illustrative of very quiet conditions.

d. Electron Density

Background conditions may be described as moderately quiet during the period of the ICECAP experiment. Electron densities were fairly low during most of the period of radar operation, averaging less than $10^5/cm^3$ at E-region altitudes until after the second rocket experiment had terminated. Figure 27 illustrates contour plots of the logarithm

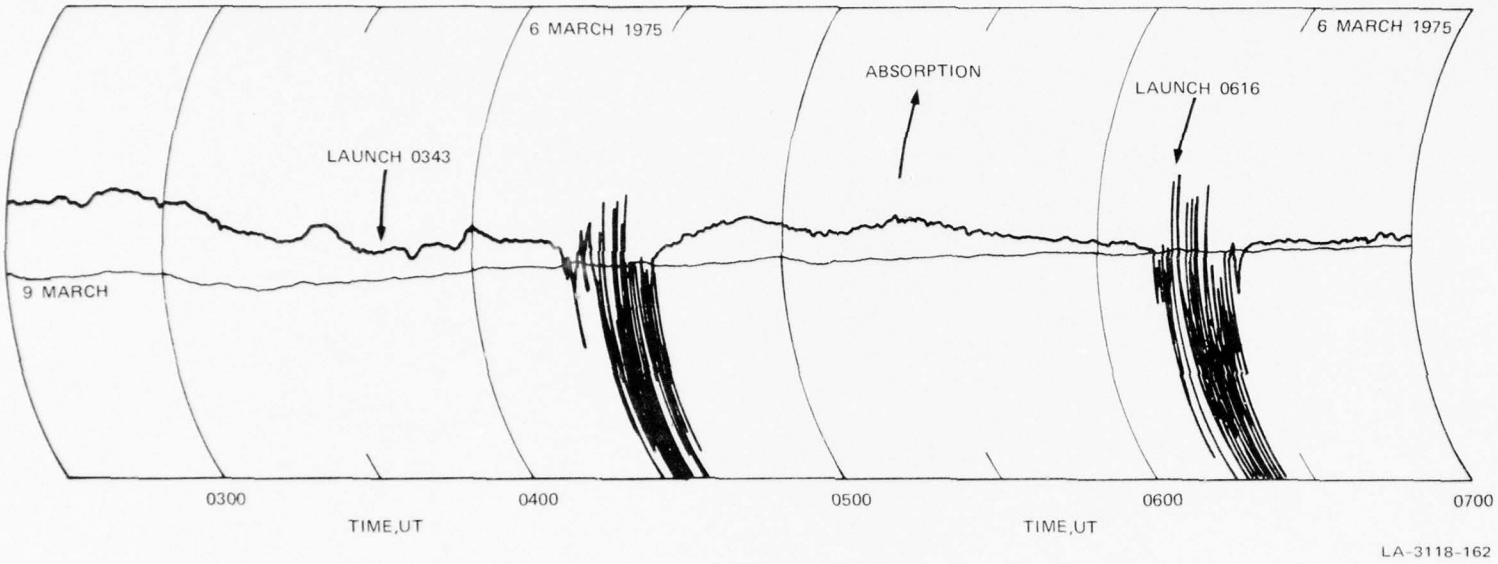

FIGURE 26 COLLEGE RIOMETER RECORD FOR 6 MARCH 1975. The record for 9 March 1975 is representative of a quiet day.

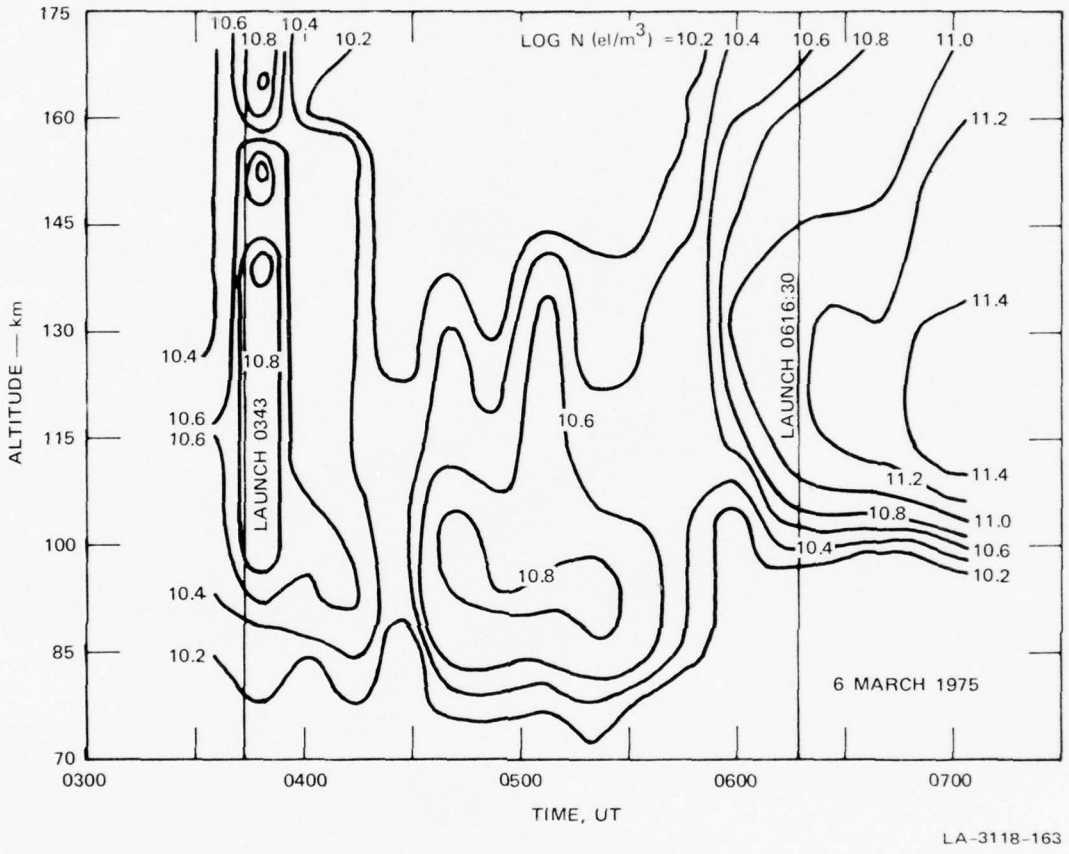

FIGURE 27 BACKGROUND CONTOURS (12-Minute Averages) OF ELECTRON DENSITY FOR THE EXPERIMENTS ON 6 MARCH 1975

of 12-minute averaged electron density in units of el/m^3. It can be seen that electron densities are indeed low over the period of interest. In addition, the amplitudes of density fluctuations relative to the average background values tend to be fairly large, a condition that is typical of low-SNR conditions.

Twelve-minute integrations (rather than the customary 6-minute integrations) were used in preparing the contours in Figure 27 in order to smooth out some of the relatively large fluctuations. Even with the smoothing thus employed, there can be seen a rapid buildup and decay of electron density centered near the time of the first rocket flight

(0343 to 0350 UT), and with an apparent duration of about 12 minutes. Peak densities of about $10^5/cm^3$ occurred during the first rocket flight, but by 0430 UT electron densities below 150 km altitude were no greater than $2 \times 10^4/cm^3$.

One can see at about 0550 UT the beginning buildup of densities in the E-region, associated with the auroral oval. By the time of the second rocket launch at 0616:30 UT, a tenuous but measureable E-layer was present, with a peak density of $>10^5/cm^3$ occurring near 130 km altitude. Following the second rocket flight, some increase in both flux and spectrum hardness can be inferred from the increase in peak electron density and the decrease in the altitude of peak density. Electron densities in the altitude range 80 to 100 km were low to moderate (1 to $4 \times 10^4/cm^3$) prior to about 0600 UT, and decreased rapidly to levels below $10^4/cm^3$ thereafter.

e. Height-Integrated Conductivities

As a result of the low electron densities present during this experiment the height-integrated conductivities are also quite low. Figure 28 illustrates the Hall and Pedersen conductivities observed during the period 0331 to 0711 UT. The conductivity measurements involved averages over one-minute time periods and 60° of azimuth scan; each data point can thus be associated with a fairly small region of space characterized by a certain direction from the radar. In particular, these spatially-resolved measurements permit us to describe conductivity values in the direction of the rocket trajectory (marked on Figure 28), as well as to investigate horizontal inhomogeneities in these parameters.

During the first rocket flight (0343-0349 UT) the Hall and Pedersen terms, measured in the direction of the flight path, were 2.15 and 0.63 mhos, respectively. For the rest of the period prior to 0600 UT

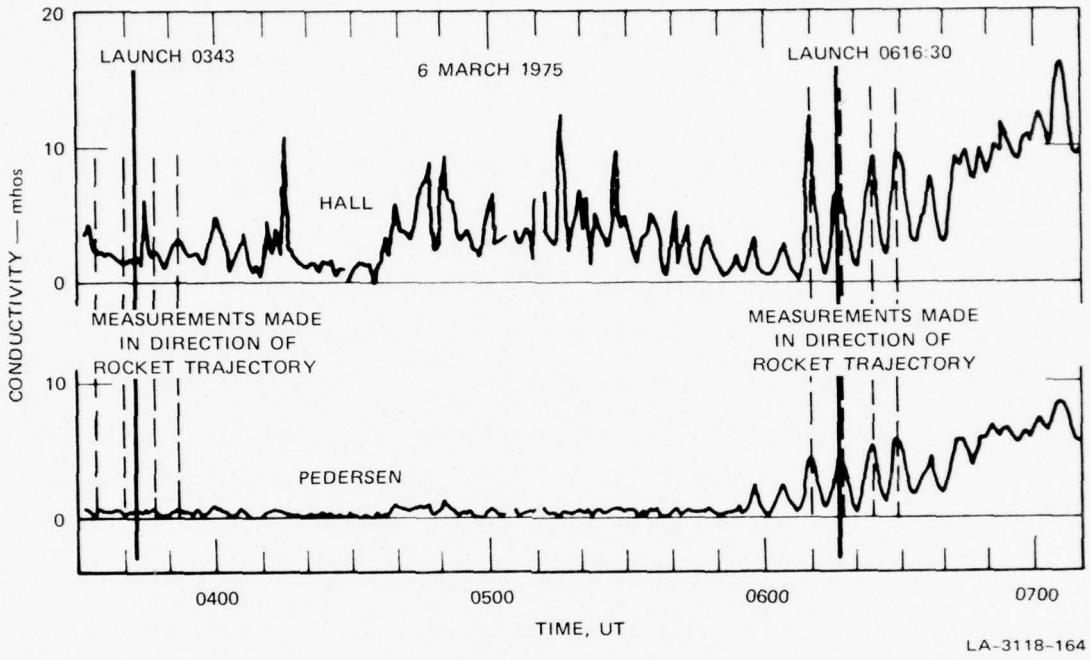

FIGURE 28 HEIGHT-INTEGRATED CONDUCTIVITIES FOR THE EXPERIMENTS ON 6 MARCH 1975. Vertical dashed lines represent times near each launch when the radar beam was pointed in the azimuthal direction of the rocket trajectory.

the Pedersen conductivity was less than 1.5 mhos, while the Hall component was less than 10 mhos. Both components began to increase at about 0600 UT as electron densities began to increase. During the second rocket flight the Hall and Pedersen components had increased to 6.6 and 4.2 mhos, respectively.

The conductivities show frequent oscillations with periods of about 6 minutes. These oscillations result from the modulating effect of large-scale horizontal gradients in electron density on measurements obtained with an azimuthally scanning antenna. For much of the period before 0600 UT, horizontal gradients were small and irregular. Beginning about 0600 UT, however, a marked inhomogeneity became evident as electron precipitation grew more intense in the north. During the second rocket flight the azimuthal asymmetry in the Hall conductivity was of the order of 6:1 due to this inhomogeneity.

It should be noted that large horizontal gradients in electron density are common occurrences near Chatanika, although such gradients are suppressed when the radar data have been averaged over a full azimuth scan or when observations are made using a fixed antenna position.

f. Electric Field

Ionospheric electric field estimates were obtained through radar measurements of ion velocity during the period 0331 to 0711 UT. Each electric field measurement involved an average of ion-velocity measurements over a complete azimuth scan of the antenna (about 6 minutes of time), and over the altitude range 171 to 272 km. The spatial region to which these measurements apply is thus a section of a cone with a major diameter of 230 km at 272 km altitude.

Figure 29 illustrates north-south and east-west components of the ionospheric electric field as measured by the radar. At the time of the first rocket launch, 0343 UT, the electric field strength was less than 5 mV/m and was directed entirely northward. Shortly after 0400 UT, the north-south component increased to about 20 mV/m, and from this time

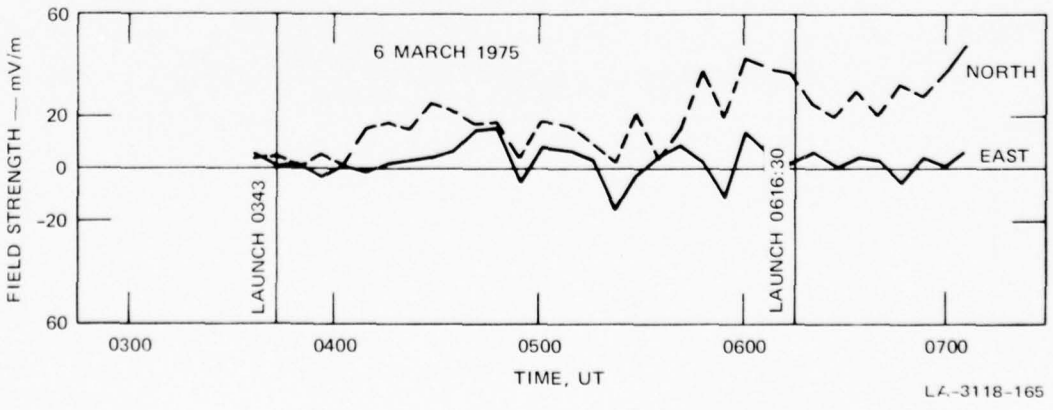

FIGURE 29 ELECTRIC FIELD FOR THE EXPERIMENTS ON 6 MARCH 1975

through the end of the experiment at 0711 UT, this component remained positive (northward-pointing), with values ranging as high as 42 mV/m. During the same time period, 0400 to 0711 UT, the east-west component oscillated from positive (eastward) to negative (westward) with amplitudes as large as 16 mV/m and no obvious pattern to the variations. The enhancements of the northward component of the electric field, on the other hand, seem to be associated with the enhancement of the eastward current system whose effects can be seen in the Barrow and College H-component magnetograms, as shown in Figure 25. At the time of the second launch at 0616:30 UT, the components of the electric field were 26 mV/m northward and less than 6 mV/m eastward.

g. Neutral Wind

Height-averaged (64 to 108 km) neutral-wind estimates are presented in Figure 30 as geomagnetic north-south and east-west components, each based on 6-minute integrations during the period 0331 to 0711 UT.

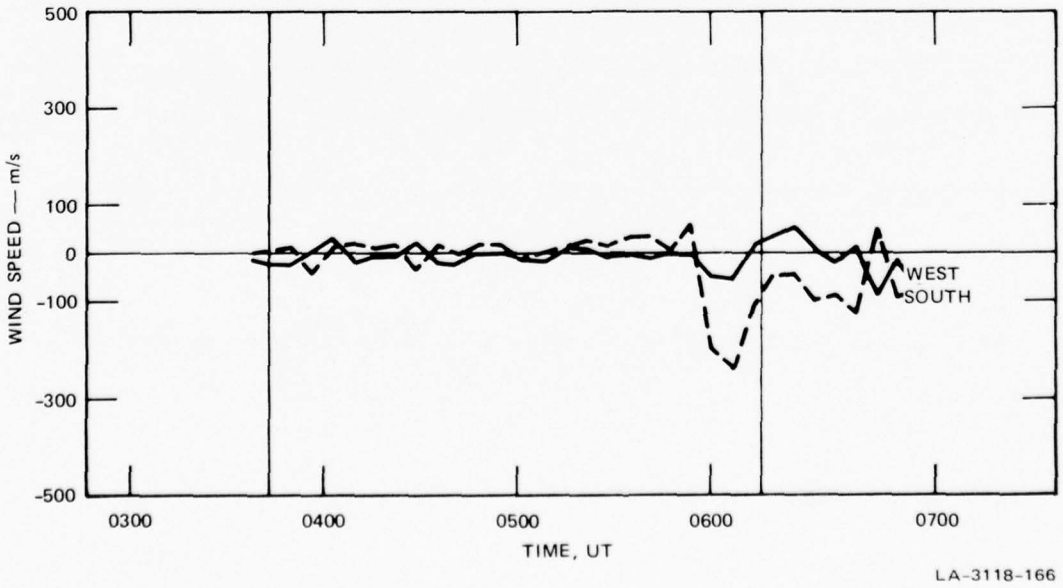

FIGURE 30 HEIGHT-AVERAGED E-REGION NEUTRAL WIND FOR THE EXPERIMENTS ON 6 MARCH 1975

Height-averaged neutral winds were generally small before about 0600 UT. During the first rocket flight the neutral wind was primarily westward-directed, with a magnitude of about 100 m/s. By 0355 UT, wind velocity had greatly diminished, and remained small (<25 m/s) until about 0545 UT.

Near 0600 UT, the neutral-wind velocity vector experienced a sharp enhancement and rotation. From a moderate northwesterly wind of about 7 m/s calculated at about 0545 UT, the neutral wind became strongly southwesterly (244 m/s) at 0607 UT. During the next 6-minute period it decreased in intensity (112 m/s) and rotated toward the south. During the second launch the wind dropped to a speed of about 60 m/s and rotated toward the southeast.

h. Height-Integrated Current Density

The height-integrated current was generally eastward during both launch periods (see Figure 31). During the first launch interval (0343 to 0349 UT) the current was very weak, having an intensity of 0.004 A/m. However, during the second launch period increasing electric fields and electron precipitation resulted in an eastward-directed current of 0.12 A/m.

i. Energy Deposition

During the first launch period (0343 to 0400 UT) the sum of the energy deposited by precipitating particles and by joule dissipation was less than 0.1 ergs/cm^2-s; thus, this period can be characterized as an almost undisturbed period (Figure 32).

In the interval between the launches the eastward electrojet intensified somewhat and particle precipitation increased. During the second launch interval the sum of the two heat sources reached

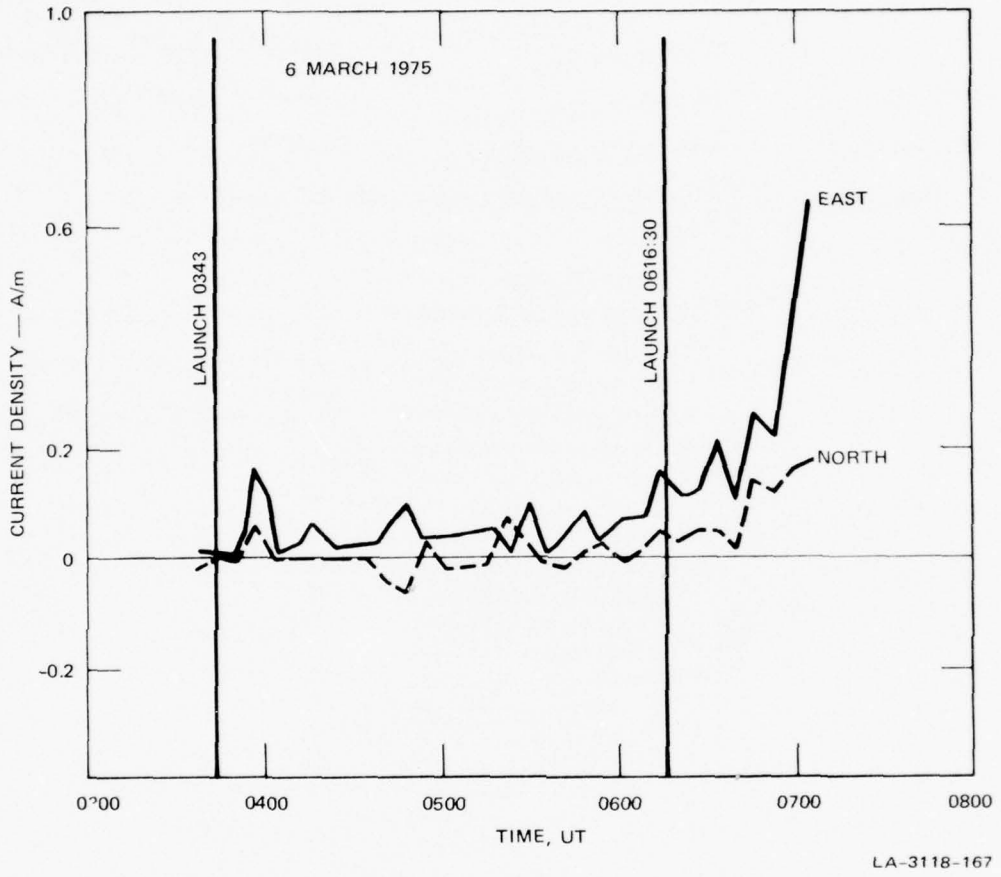

FIGURE 31 HEIGHT-INTEGRATED CURRENT DENSITY FOR THE EXPERIMENTS ON 6 MARCH 1975

2.2 ± 0.1 ergs/cm^2-s with the energy deposition rate due to electrons being about 35% less than that due to joule heating.

3. Correlated Measurements--0343 UT

a. Separation Between Rocket and Radar Beam

During the first rocket flight (0343 to 0350 UT) the radar operated continuously in an azimuth scan mode; thus, horizontal separation distance between the rocket and the radar beam depended on both the rocket trajectory and the scanning pattern of the radar antenna. Figures 33 and

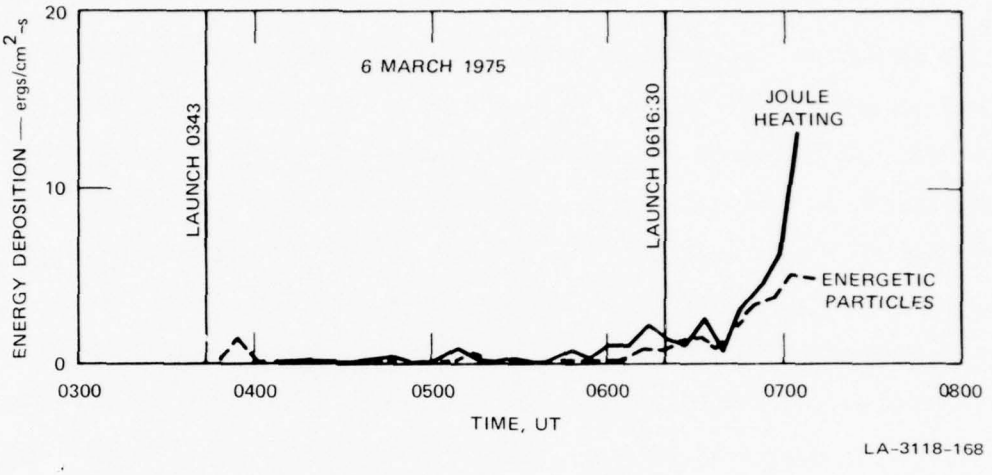

FIGURE 32 JOULE HEATING AND ENERGETIC PARTICLE CONTRIBUTIONS TO TOTAL ENERGY DEPOSITION FOR THE EXPERIMENTS ON 6 MARCH 1975

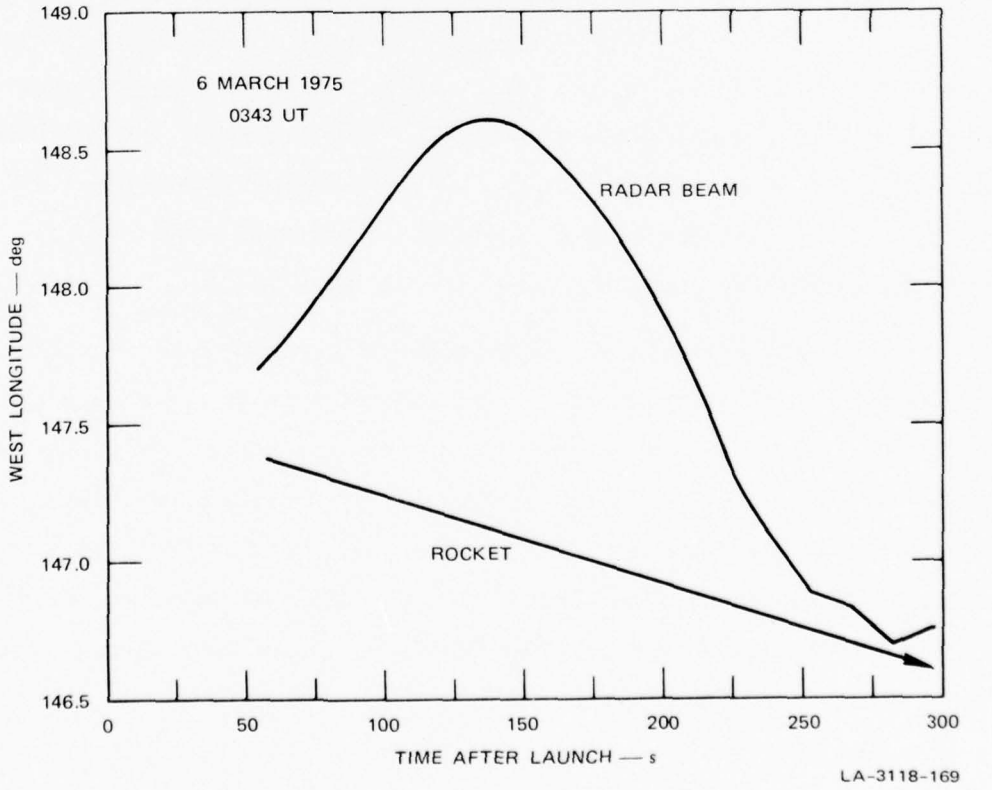

FIGURE 33 LONGITUDINAL SEPARATION BETWEEN THE RADAR BEAM AND THE ROCKET FOR THE FLIGHT OF 0343 UT, 6 MARCH 1975

34 illustrate the longitudinal and latitudinal positions, respectively, of the rocket and the intersection of the radar beam with the rocket altitude. The longitudinal and latitudinal separations can be combined, as in Figure 35, to yield total horizontal separation distance. Several altitudes of the rocket, at various times during the flight, are also indicated in Figure 35. It can be seen that a very small horizontal separation, about 10 km, occurs at about 245 s after launch (0347:05 UT), at an altitude of about 116 km. Correlation between radar and rocket measurements of density should thus be better at this time than at any other time during the flight.

b. Electron Density

Figure 36 illustrates contour plots of electron density obtained by the radar during the flight of the rocket. The data were obtained with 15-s integration periods, and reveal a generally low level of electron density ($<10^5/cm^3$) in the D- and E-regions during most of the flight. The contours exhibit rapid and apparently unsystematic variations during the experiment.

Superimposed on the density contours is the equivalent-altitude trajectory of the rocket. The significance of the superposition is that it helps in recognizing and accounting for extraneous echoes from the skin of the rocket or the exhaust trail, especially when received on sidelobes of the radar antenna. In this case, Figure 36 reveals only one density enhancement coinciding with the equivalent-altitude trajectory (0346 UT); thus we may conclude that, except for this single possibility, there is no significant contamination in the density measurements due to rocket echoes.

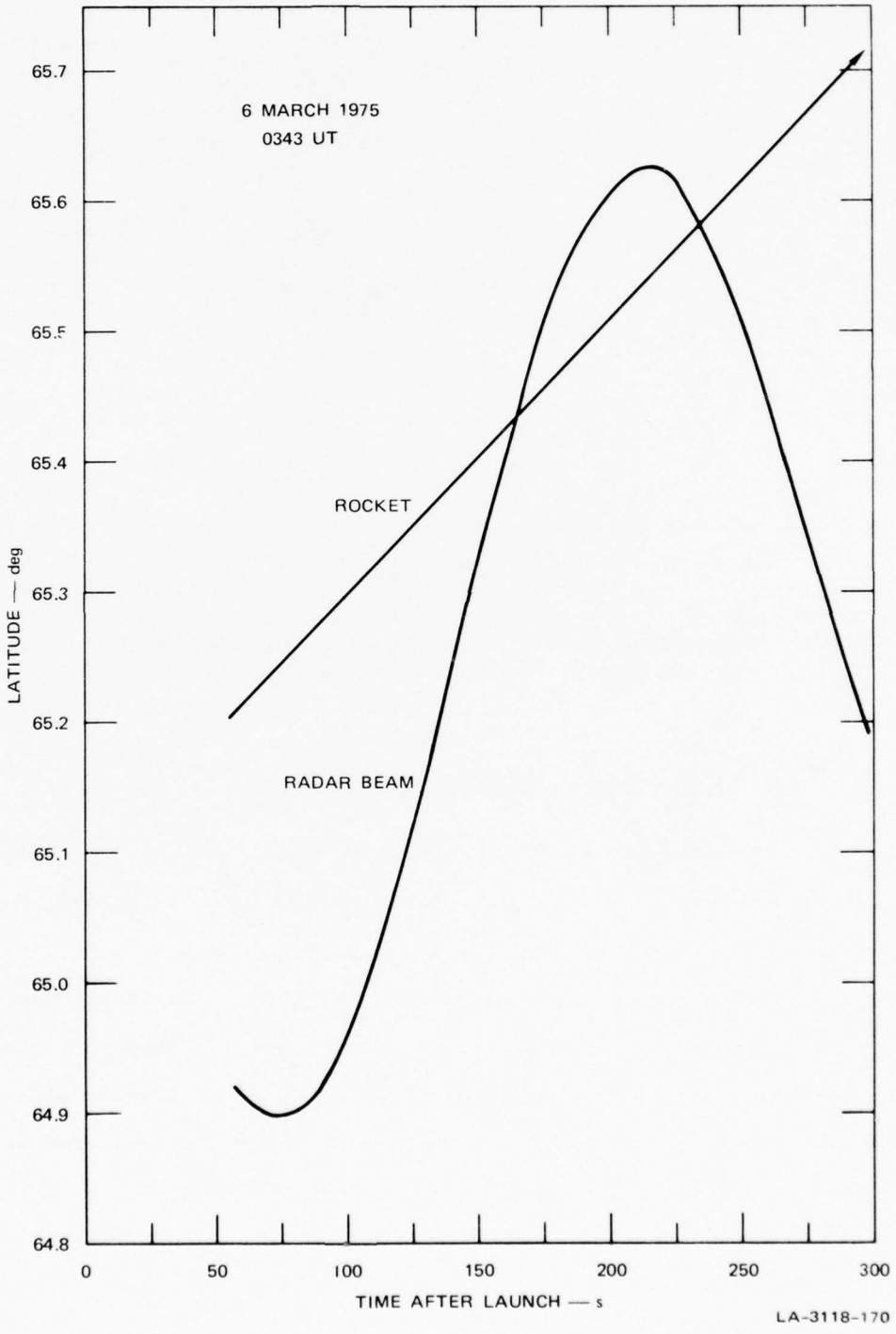

FIGURE 34 LATITUDINAL SEPARATION BETWEEN THE RADAR BEAM AND THE ROCKET FOR THE FLIGHT OF 0343 UT, 6 MARCH 1975

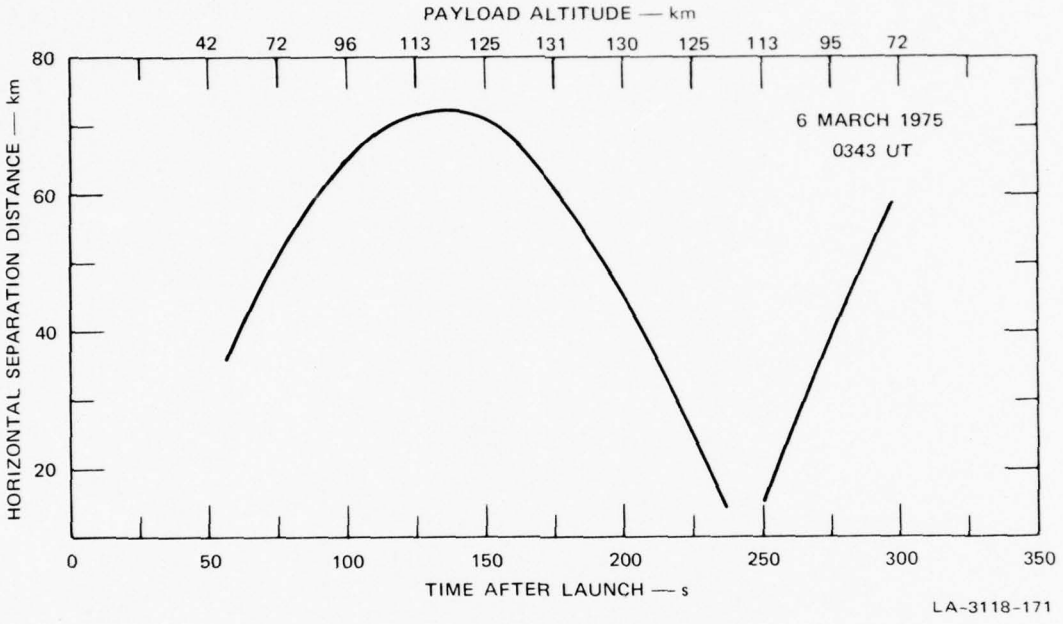

FIGURE 35 HORIZONTAL SEPARATION DISTANCE BETWEEN THE RADAR BEAM AND THE ROCKET FOR THE FLIGHT OF 0343 UT, 6 MARCH 1975

4. Correlated Measurements--0616:30 UT

a. Separation Between Rocket and Radar Beam

During the second rocket flight on 6 March (0616:30 to 0623 UT) the radar operated continuously in an azimuth scan mode. Figures 37 and 38 illustrate the longitudinal and latitudinal positions, respectively, of the rocket and the intersection of the radar beam with the rocket altitude, and Figure 39 illustrates the total horizontal separation distance. Several representative altitudes of the rocket are also indicated at various points along the piot. It can be seen that, in contrast to the first flight discussed above, horizontal separation distance between the rocket and the radar beam is large (i.e., >30 km) everywhere in the D- and E-regions.

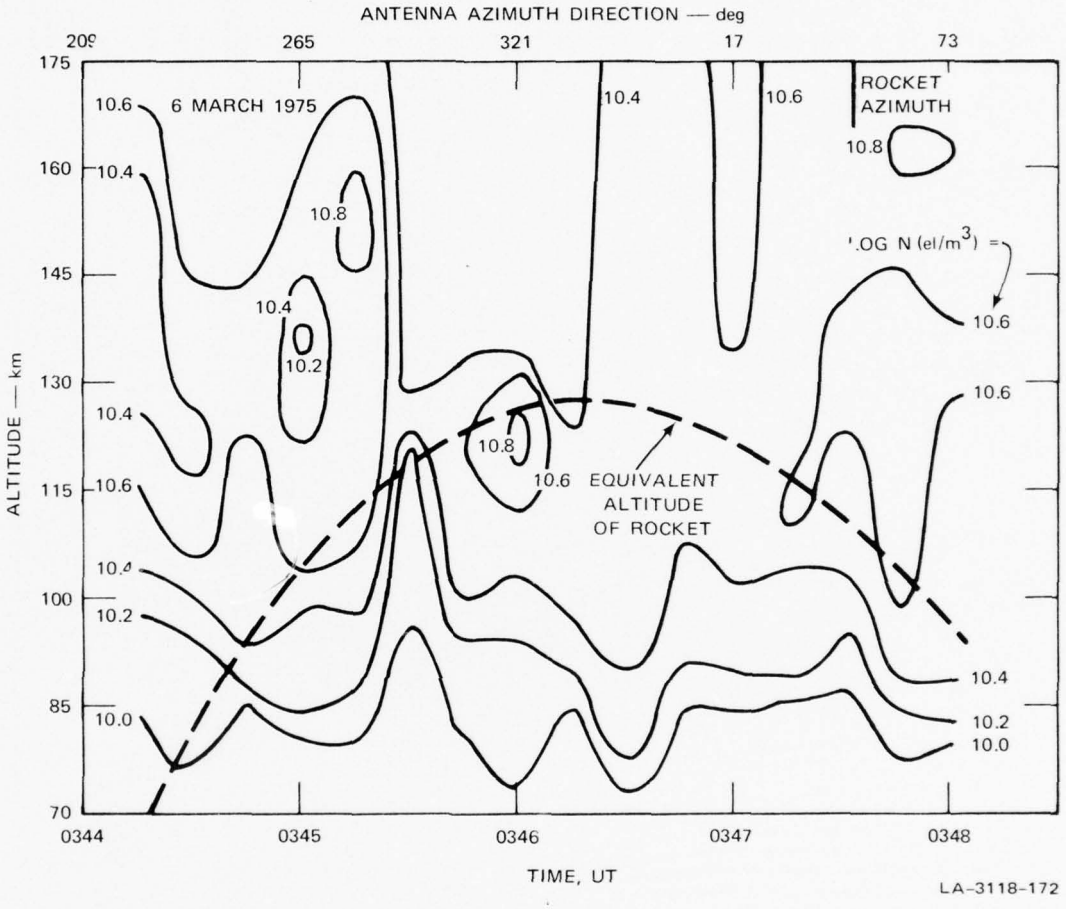

FIGURE 36 CONTOURS OF ELECTRON DENSITY AND THE EQUIVALENT ALTITUDE OF THE ROCKET DURING THE FLIGHT OF 0343 UT, 6 MARCH 1975

b. Electron Density

Figure 40 illustrates contour plots of electron density obtained by the radar during the flight of the rocket. The contours were prepared by drawing smooth curves through data points spaced at 15-s intervals, corresponding to the integration intervals of the radar. As in the case of the earlier launch on this date, densities are generally low ($<1.6 \times 10^5/cm^3$) throughout the altitude range of interest and during the entire flight of the rocket. The contours illustrate density fluctuations with no discernible systematic pattern.

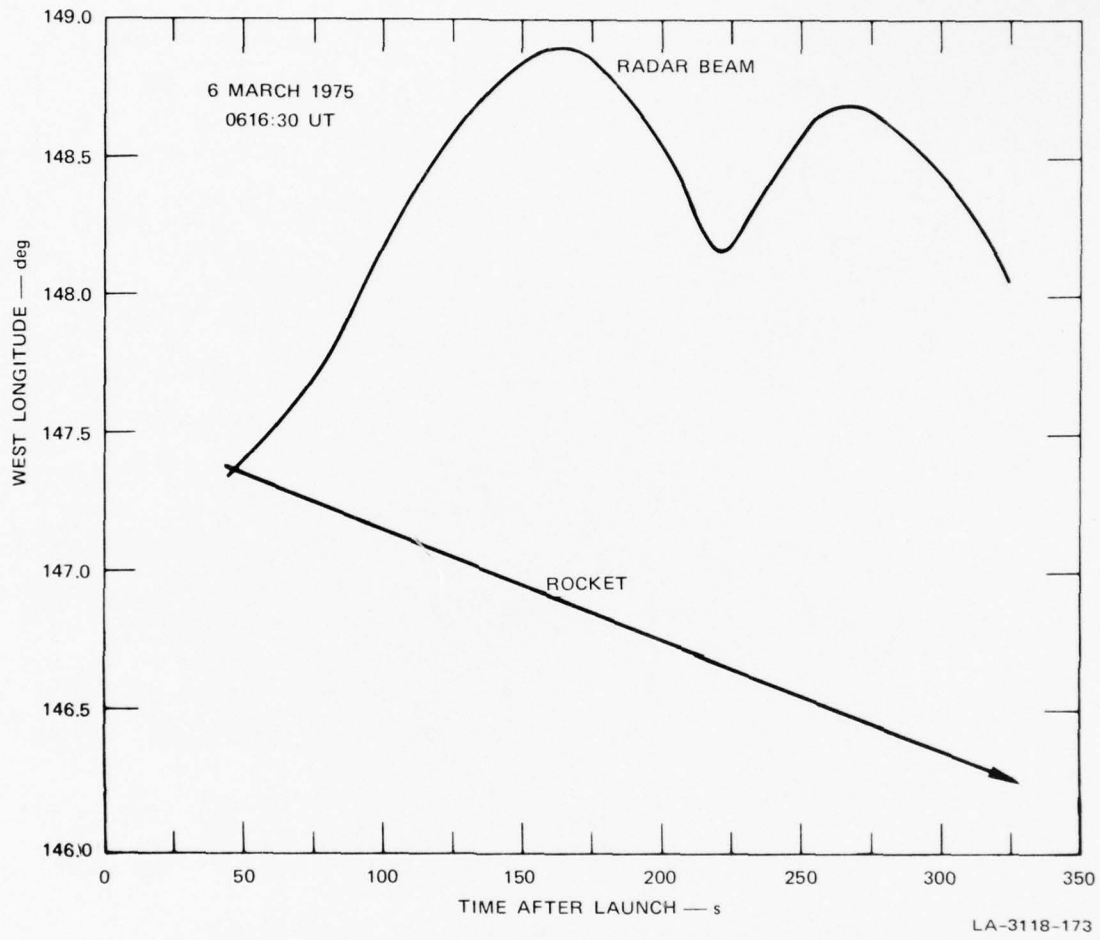

FIGURE 37 LONGITUDINAL SEPARATION BETWEEN THE RADAR BEAM AND THE ROCKET FOR THE FLIGHT OF 0616:30 UT, 6 MARCH 1975

The equivalent altitude of the rocket is superimposed on the density contours. The superposition of the equivalent-altitude-trajectory plot and the electron-density contours indicates no evidence of density enhancements along the trajectory. We thus conclude that no significant contamination, due to skin echoes from the rocket, is present in the electron-density measurements.

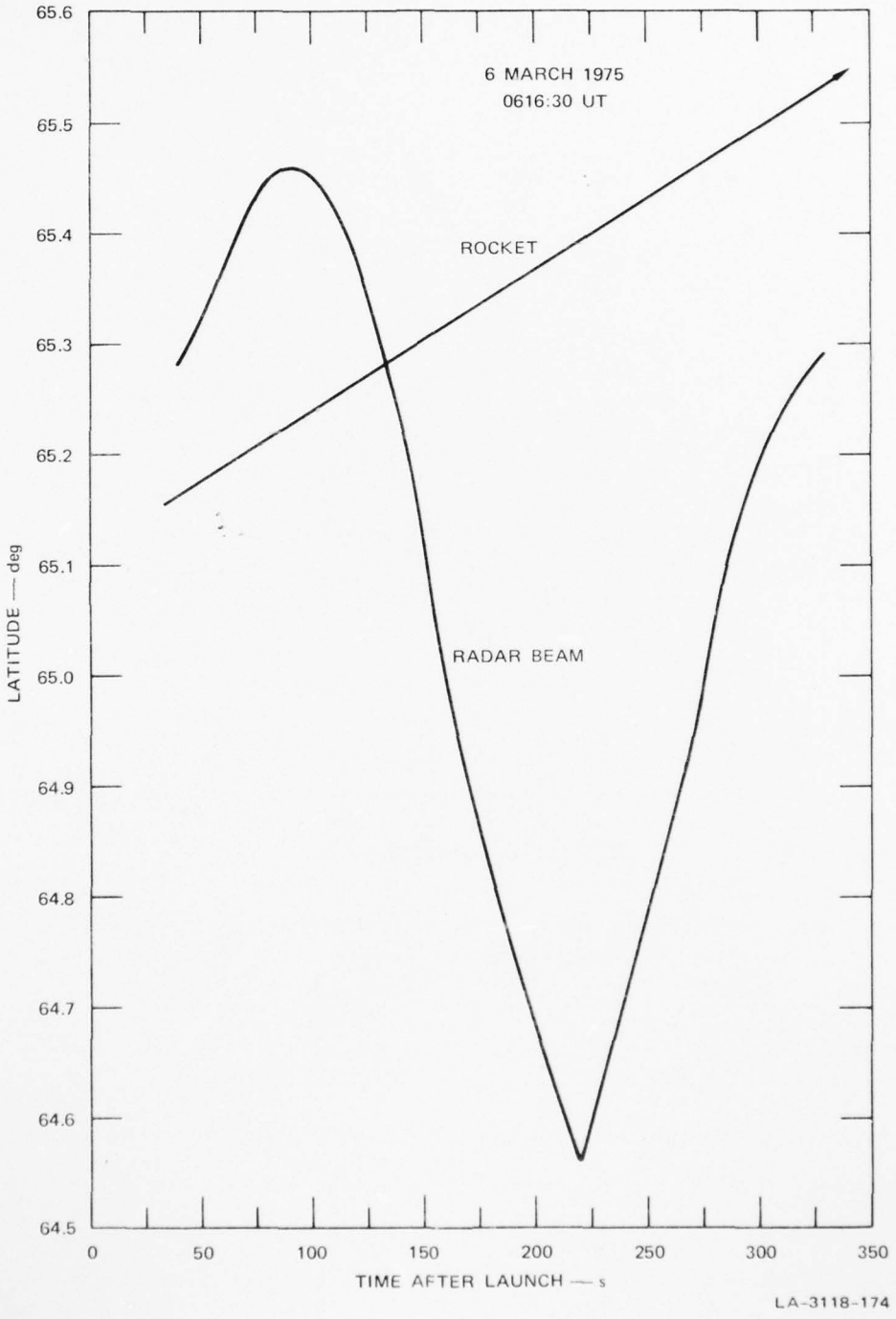

FIGURE 38 LATITUDINAL SEPARATION BETWEEN THE RADAR BEAM AND THE ROCKET FOR THE FLIGHT OF 0616:30 UT, 6 MARCH 1975

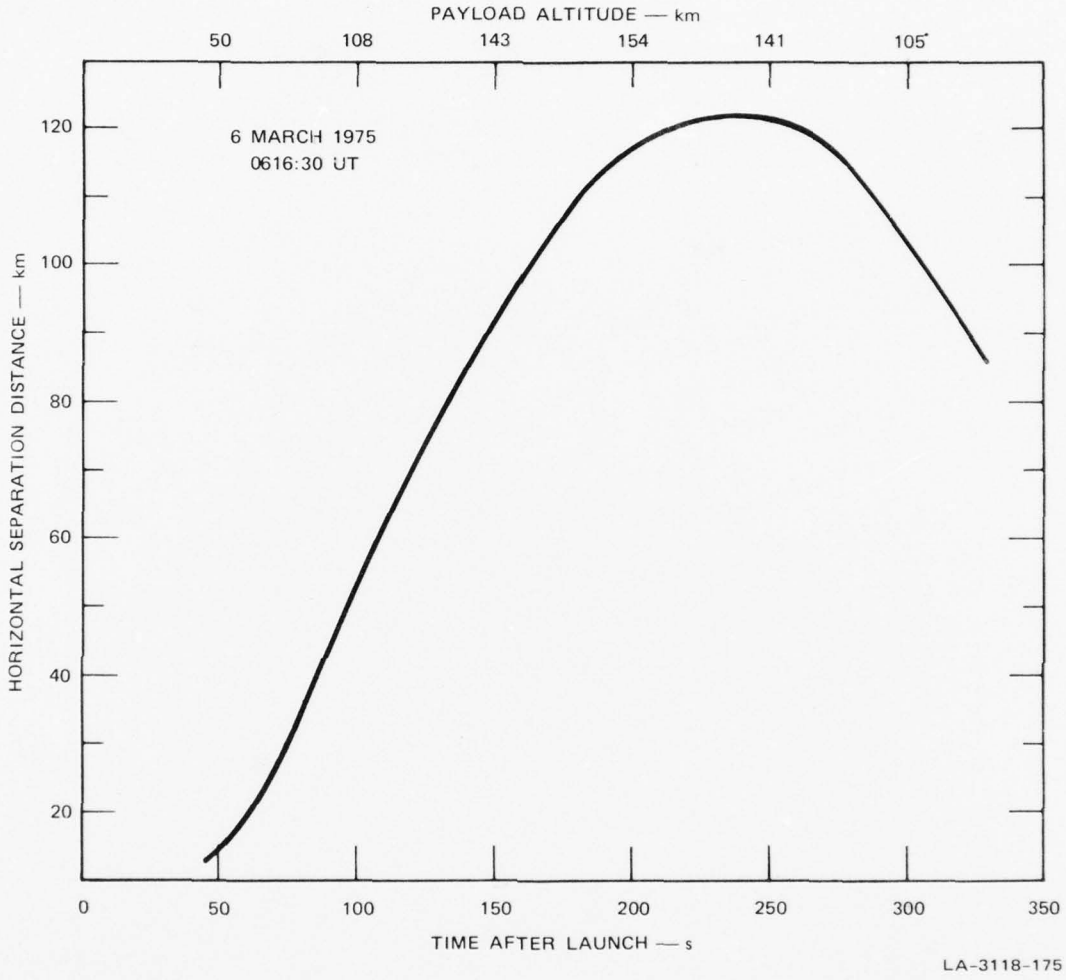

FIGURE 39 HORIZONTAL SEPARATION DISTANCE BETWEEN THE RADAR BEAM AND THE ROCKET FOR THE FLIGHT OF 0616:30 UT, 6 MARCH 1975

c. Energy Spectrum of Auroral Electrons

An analysis of the energy distribution of the auroral electrons responsible for the E-layer ionization near the rocket trajectory is shown in Figure 41. The ionization profile shown represents an average over a 70° sector of the azimuth scan centered near the azimuth of the rocket trajectory. The diamonds indicate the density profile that would be produced by the derived electron energy distribution. It can be seen

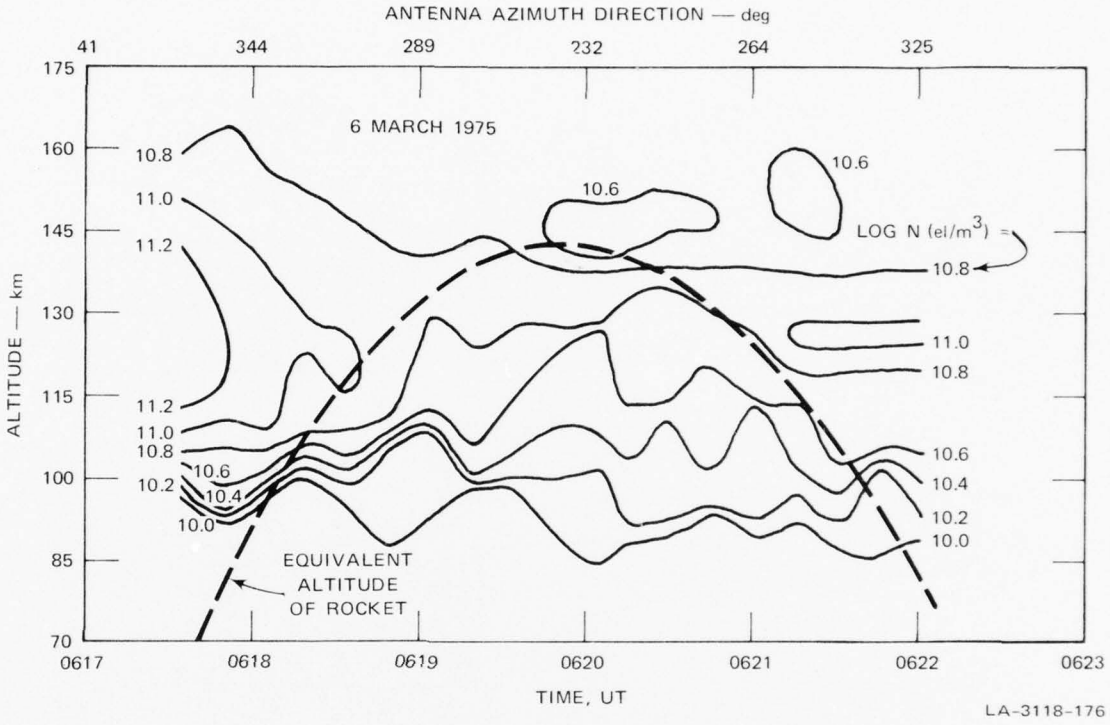

FIGURE 40 CONTOURS OF ELECTRON DENSITY AND THE EQUIVALENT ALTITUDE OF THE ROCKET DURING THE FLIGHT OF 0616:30 UT, 6 MARCH 1975

that the incoming auroral electrons had a fairly soft energy distribution with a mean energy of about 3 keV and a differential flux of 10-keV electrons less than 10^7 cm^{-2}-s^{-1}-keV^{-1}. A similar analysis was made of the ionization profiles on portions of the scan south of the rocket trajectory. The shape of the energy distribution there was similar to that shown in Figure 41, although the flux intensity was lower, as would be expected from the smaller electron densities to the south.

5. Summary

A Nike-Hydac rocket (IC 507.11-1A), the first of two missions, was launched at 0343 UT on 6 March to measure LWIR emission profiles of CO_2, NO, and O_3 during twilight. There was little geomagnetic disturbance during this launch interval. Low E-region peak electron densities (less

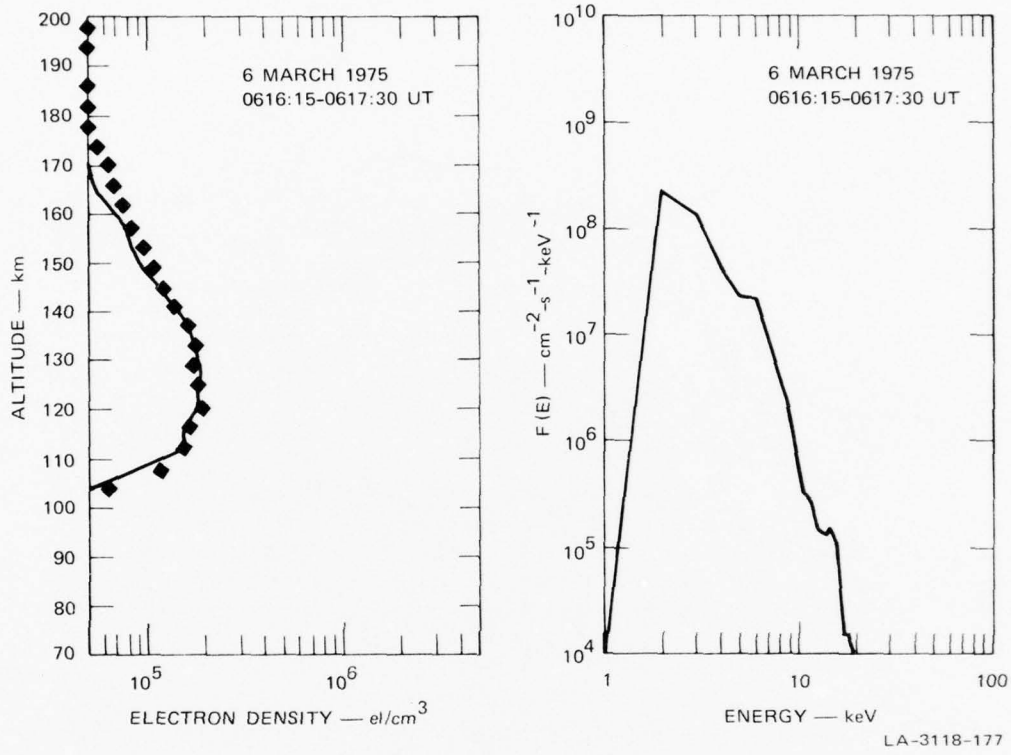

FIGURE 41 ENERGY SPECTRUM OF AURORAL ELECTRONS AND ASSOCIATED ELECTRON-DENSITY PROFILE FOR THE PERIOD 0616:15-TO-0617:30 UT, 6 MARCH 1975. Details are given in the text.

than $10^5/cm^3$) and a weak (5 mV/m) northward electric field resulted in a very small total energy deposition rate of less than 0.1 ergs/cm^2-s.

The second launch of a Nike-Hydac rocket (IC 507.11-3) took place during the evening at 0616:30 UT to measure LWIR emission profiles of CO_2, NO, and O_3 under quiet night conditions. During this launch the eastward electrojet increased to a moderate level of 0.12 A/m. E-layer electron densities increased slightly to just greater than $10^5/cm^3$ at 130 km altitude. D-region densities ranged from 1 to 4 x $10^4/cm^3$. The northward-directed electric field increased in intensity to about 40 mV/m during this second launch interval. This increased electric field and electron precipitation resulted in a moderate total energy deposition

rate of 2.2 ergs/cm^2-s with the joule dissipation rate being about 50% greater than the energy deposited by precipitating electrons.

E. 10 March 1975--Nike Hydac

1. General

A Nike-Hydac rocket (IC 507.11-2A) was launched from Poker Flat at 0912:20 UT on 10 March. The rocket carried a liquid-N_2-cooled radiometer, and the purpose of the experiment was to measure IR emission profiles under bright auroral-breakup conditions. The rocket reached an apogee of 152 km at 206 s after launch, and was above 70 km altitude during the time interval 68 to 332 s after launch.

The Chatanika radar was operated in support of the rocket experiment from 0548 UT to 1150 UT. During this period the radar antenna was operated almost entirely in a two-position mode. The elevation angle was held fixed at 60°. Two azimuth angles, symmetrically placed about magnetic north (29.0°) were used. Between 0548 UT and 0828 UT, azimuth angles ±22.5° away from geomagnetic north were used. Between 0828 UT and 0913 UT, and between 0922 UT and 1150 UT, azimuth angles ±45° away from geomagnetic north were used. During the two-position operation, the antenna dwelled for about five minutes in each position. Electric fields, currents, joule heating, and neutral winds were derived from the measurements under the assumption that the plasma velocity parallel to the earth's magnetic field was zero.

Between 0914 UT and 0921 UT, the radar antenna was pointed at the predicted E-region penetration point of the rocket (36° azimuth, 76° elevation).

2. Background Measurements

a. Geomagnetic Conditions

Geomagnetic conditions during the launch period can be characterized as active. An enhancement of the ionospheric overhead eastward current system resulted in the positive enhancement seen in the College magnetogram (Figure 42) from about 0715 UT until about 0855 UT. At this time the transition region between the eastward and westward current regions passed overhead. At launch time the College magnetogram indicated a large negative bay of more than 500 γ, which resulted from an intensification of the westward electrojet. The H component began to recover while the Z component (not shown) decreased to -350 γ, indicating that the locus of the electrojet had moved poleward. At Fort Yukon (Figure 43) at the time of rocket apogee, the H-component was depressed to -250 γ although the sudden large negative excursion of the H-component did not occur until about 0920 UT. The large positive bay recorded at Honolulu at about 0900 UT is another indication of substorm activity.

b. Auroral Conditions

Brilliant and dynamic auroral displays characterized the evening of 10 March. So intense was the aurora during the launch interval that even the two-second exposures of the Chatanika all-sky data were overexposed. All-sky photos from Fort Yukon have been included to augment the Chatanika data (Figure 44). Chatanika radar boresight television photographs have also been included.*

---

*See Section V-E-3-b, Figure 56.

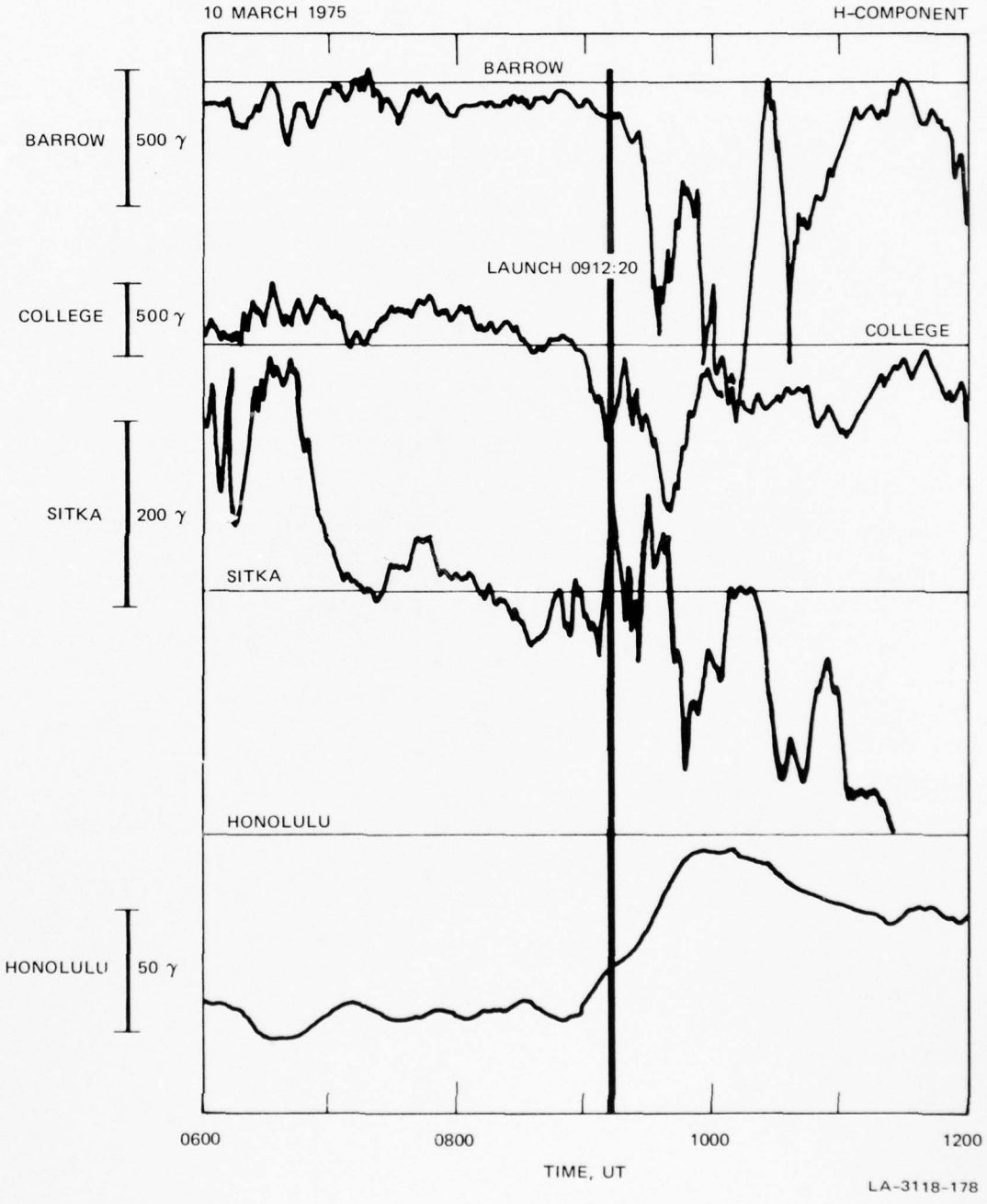

FIGURE 42 H-COMPONENT MAGNETOGRAMS ON 10 MARCH 1975 FROM FOUR STATIONS DISTRIBUTED IN LATITUDE BUT IN THE SAME LOCAL TIME SECTOR AS THE ROCKET TRAJECTORY

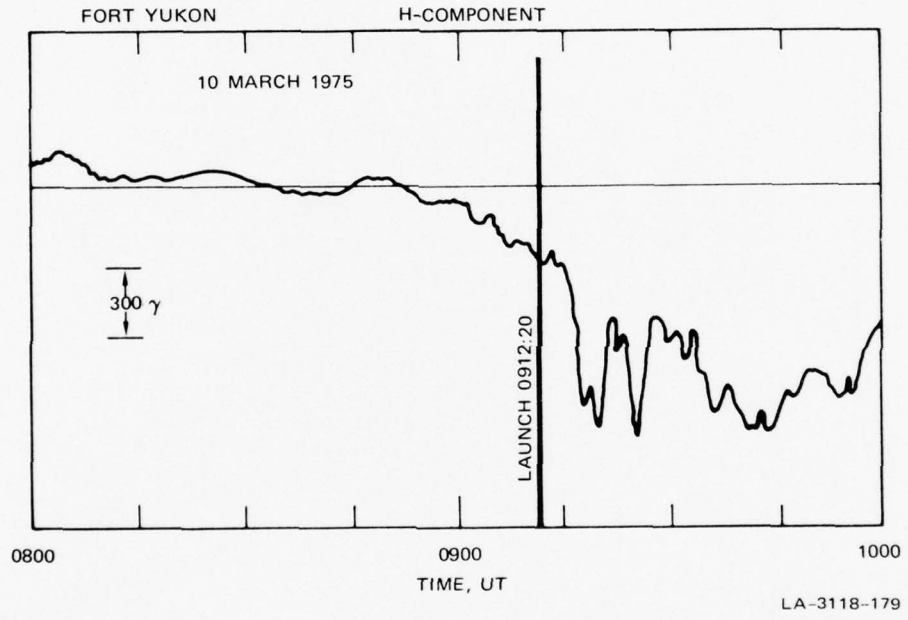

FIGURE 43 H-COMPONENT MAGNETOGRAM ON 10 MARCH 1975 FROM FORT YUKON

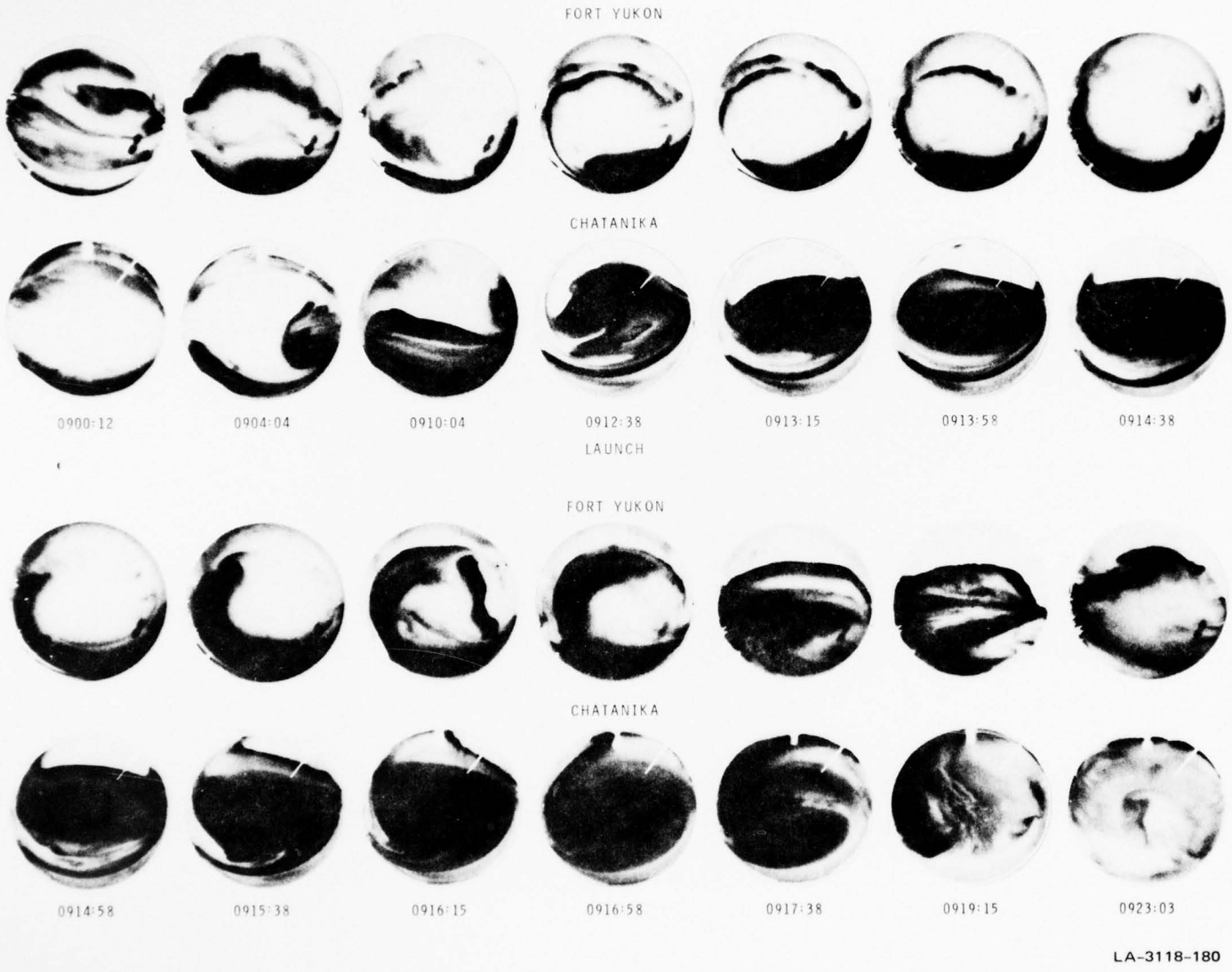

FIGURE 44 ALL-SKY PHOTOGRAPHS FROM CHATANIKA AND FORT YUKON FOR THE PERIOD 0900-TO-0923 UT, 10 MARCH 1975

c. Absorption

Figure 45 illustrates absorption measured by the College riometer for the period 0700 to 1000 UT on 10 March. Also illustrated is the same time period for 9 March, used as a quiet-day reference. It can be seen that a period of strong absorption begins at about 0900 UT and reaches a peak at about 0920 UT.

d. Electron Density

Figure 46 illustrates density contours for the period 0827 UT to 0935 UT. Each data point was obtained by averaging over a pair of antenna azimuth angles symmetrically located about geomagnetic north. The contours are parametric in the logarithm, to the base 10, of density in el/m^3; that is, the contour labeled 11 indicates a density of 10^{11} el/m^3.

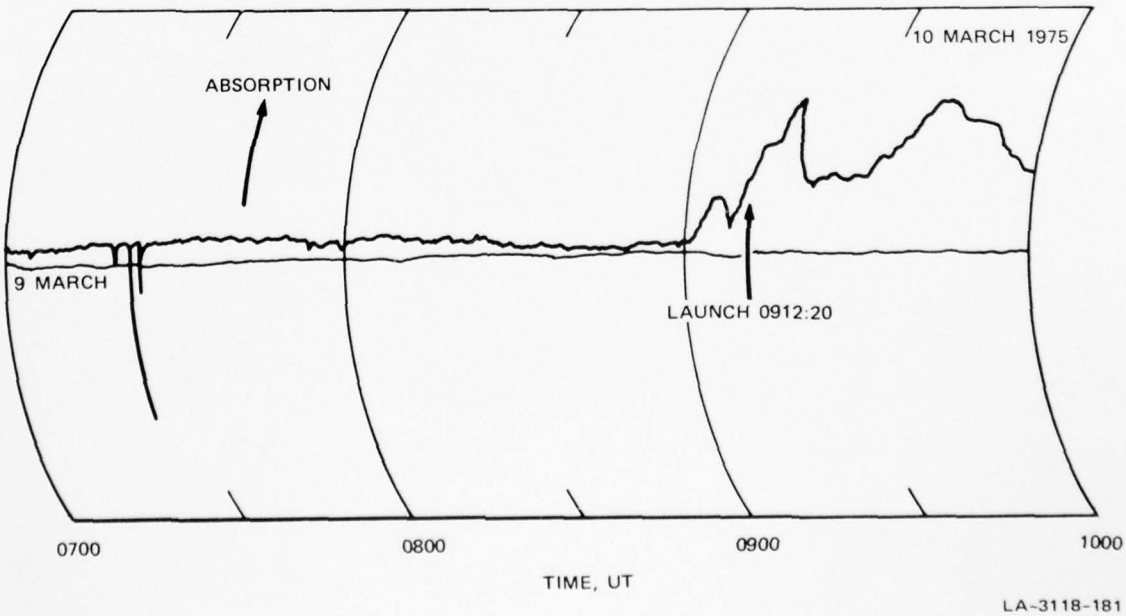

FIGURE 45 COLLEGE RIOMETER RECORD FOR 10 MARCH 1975. The record for 9 March 1975 is representative of a quiet day.

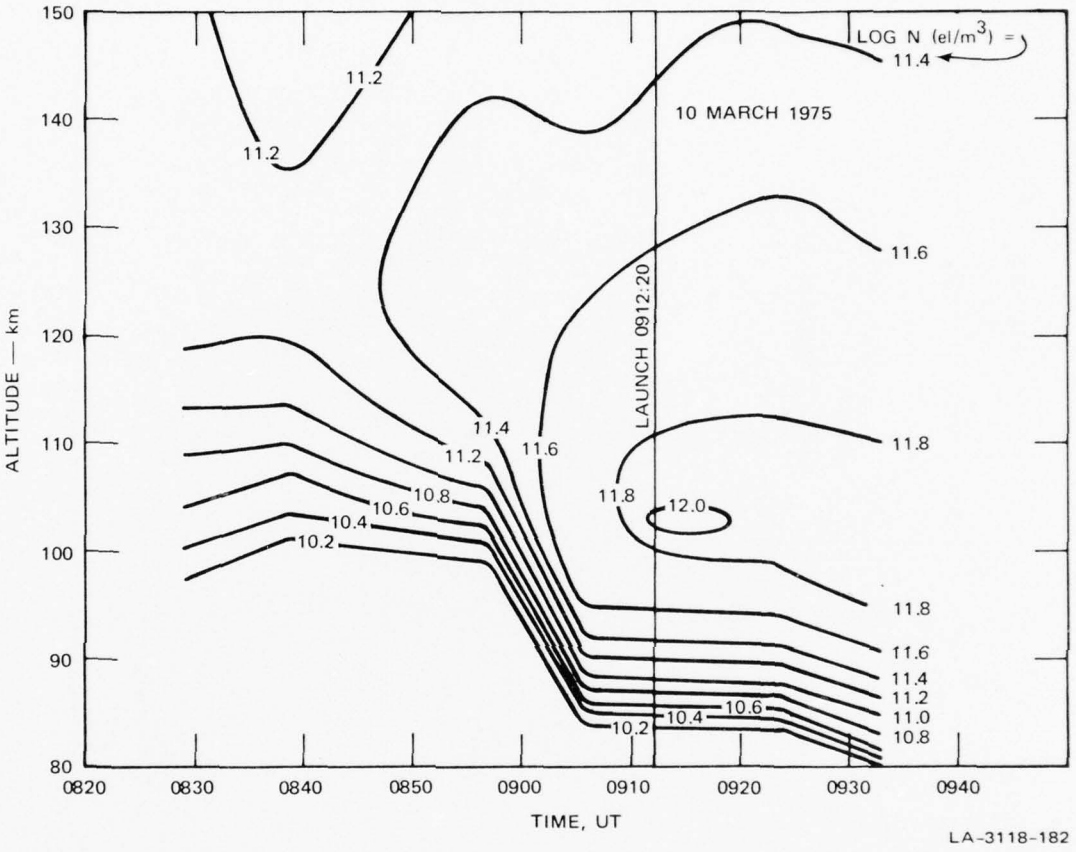

FIGURE 46 BACKGROUND CONTOURS (10-Minute Averages) OF ELECTRON DENSITY FOR THE EXPERIMENT ON 10 MARCH 1975

It can be seen that an auroral-E layer began to form at about 0840 UT, and that below 100 km a rapid buildup in density began at about 0900 UT, consistent with the onset of increasing absorption shown in Figure 45.

Figure 47(a) illustrates a plot of the maximum observed electron density in the E-region for the period 0605 to 1145 UT, and Figure 47(b) illustrates the height at which the maximum density occurs, for the same time period. The values are based on 5-minute integrations. These plots contain less information than contour plots, but are useful to indicate variations in the amplitude of flux and the hardness of the

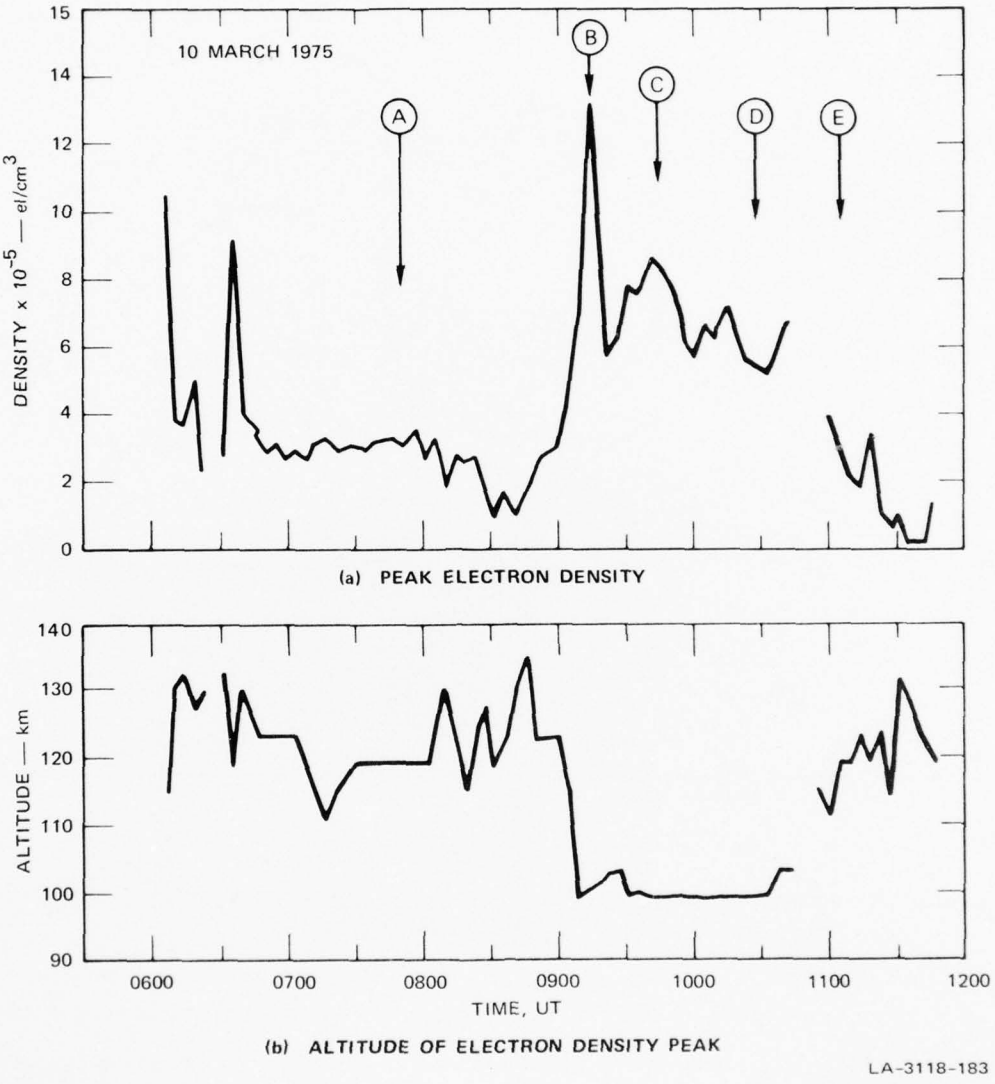

FIGURE 47 DENSITY AND ALTITUDE OF THE E-LAYER PEAK FOR 10 MARCH 1975. The five selected times are explained in the text.

spectrum of precipitating particles. An increase in the maximum density indicates an increase in flux, and a decrease in the height of the maximum density indicates a hardening of the spectrum.

In Figure 47, five points in time have been indicated by the letters A through E. These points were selected for analysis of energy spectra, to be discussed later. We note for now that Point B corresponds to the time of the rocket flight.

e. Height-Integrated Conductivities

In accordance with the high level of electron precipitation the height-integrated Hall and Pedersen conductivities (Figure 48) were quite large during this experiment. The Pederson conductivity varied from about 3 to 12 mhos during the hour preceeding launch, but at launch time it had a value of about 13 mhos. The Hall conductivity ranged from 3.7 to almost 28 mhos in the hour before launch. During the launch period the Hall conductivity increased further from about 47 to 85 mhos.

f. Electric Field

The ionospheric electric field, as determined from data taken in the 208-km altitude range gate, is shown in Figure 49. The

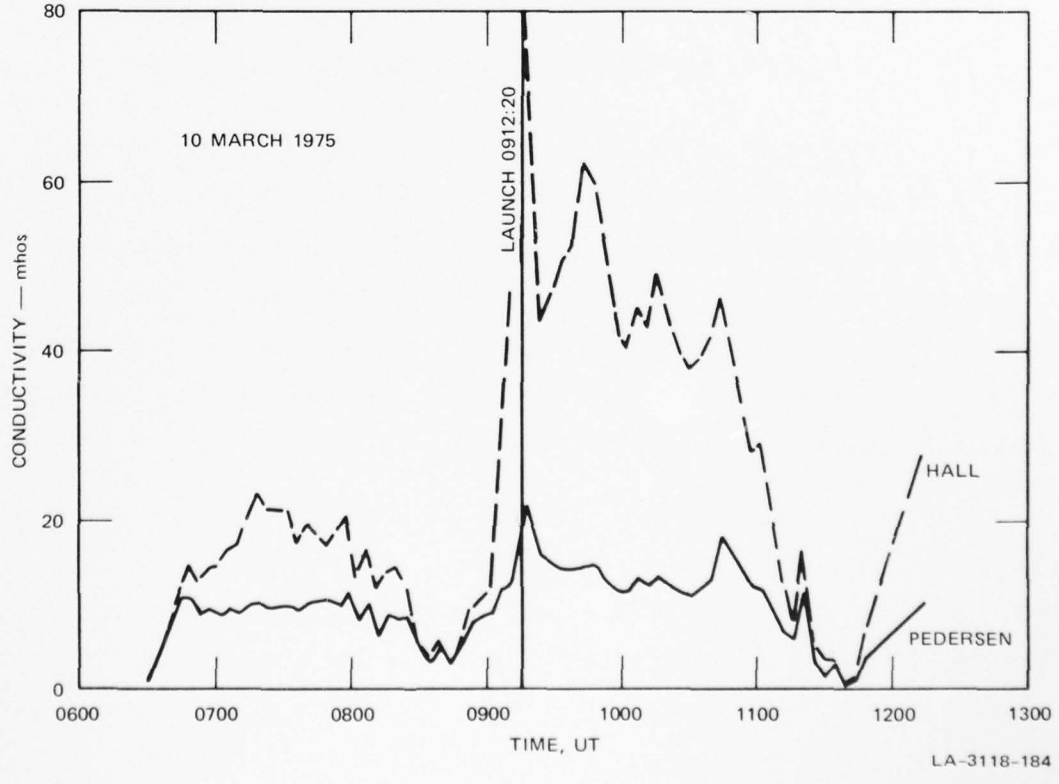

FIGURE 48 HEIGHT-INTEGRATED CONDUCTIVITIES FOR THE EXPERIMENT ON 10 MARCH 1975

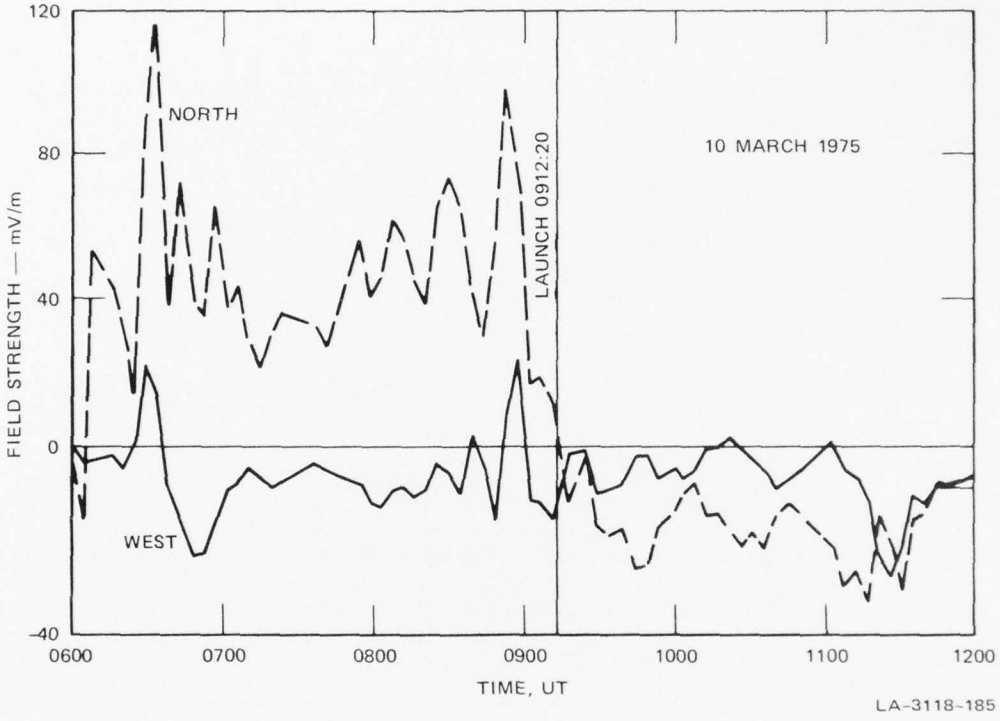

FIGURE 49 ELECTRIC FIELD FOR THE EXPERIMENT ON 10 MARCH 1975

geomagnetic north-south component is shown by the dashed line, and the east-west component by the solid line. From 0600 to 0900 UT a substantial northward electric field (generally in excess of 40 mV/m) was present. At about 0900 UT, the electric field reversed and remained southward (20 to 30 mV/m) for the rest of the evening. During most of the evening, the east-west component of electric field was small compared to the north-south component, and primarily westward-directed.

The electric field reversal at about 0900 UT indicates a transition from eastward electrojet conditions to westward electrojet conditions. In other words, the Harang discontinuity passed through the region above Chatanika at about 0900. This conclusion is verified by the local magnetometer H-component records, which show a positive bay prior to 0900 and a large negative bay after 0900.

AD-A038 259 STANFORD RESEARCH INST MENLO PARK CALIF F/G 4/1
ICECAP '75--CHATANIKA RADAR RESULTS.(U)
MAY 76 P D PERREAULT, R R VONDRAK, T M WATT DNA001-74-C-0167
UNCLASSIFIED DNA-4086T NL

2 OF 2
AD
AD38259

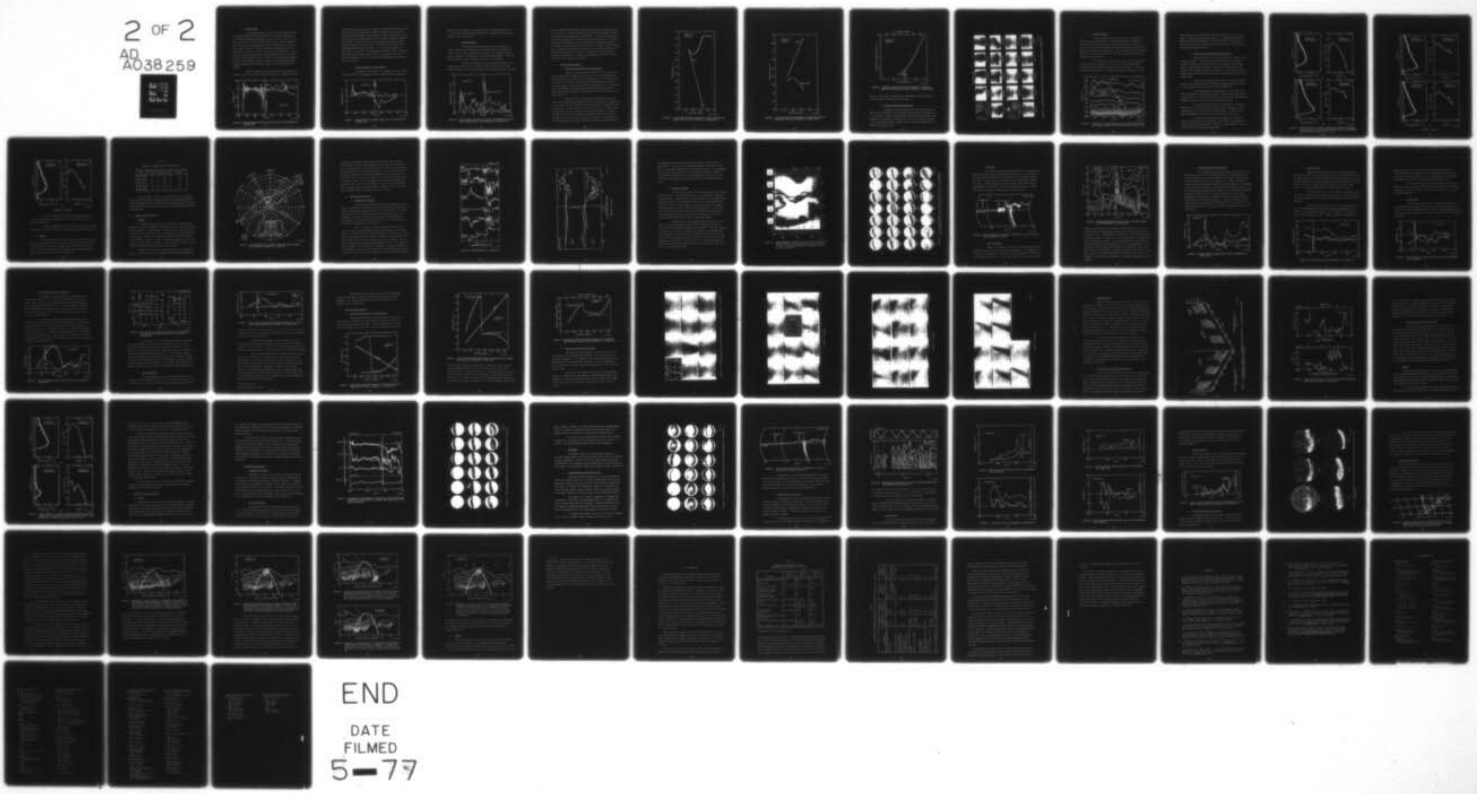

END

DATE
FILMED
5-77

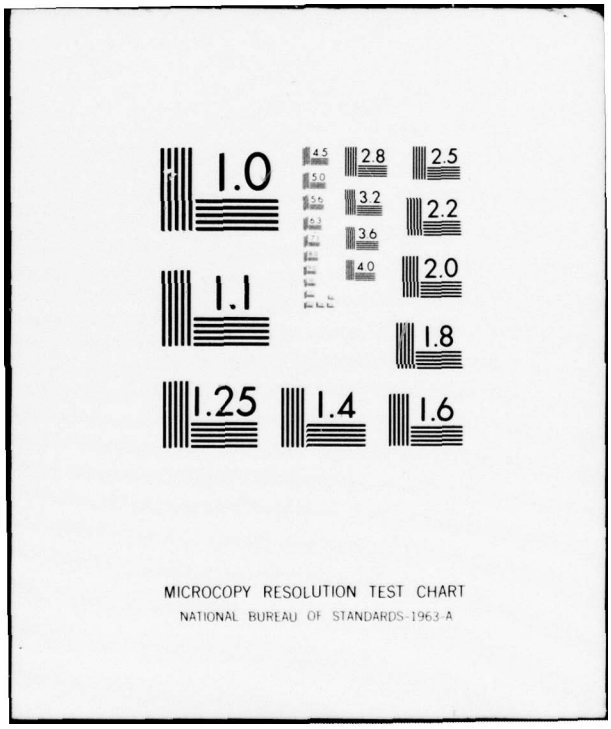
1.0
1.1
1.25
1.4
1.6
1.8
2.0
2.2
2.5
2.8
3.2
3.6
4.0
4.5
5.0
5.6
MICROCOPY RESOLUTION TEST CHART
NATIONAL BUREAU OF STANDARDS-1963-A

g. Neutral Wind

The E-region horizontal neutral wind was computed using the method described by Baron and Chang.[7] The neutral wind computed by this method represents a weighted average over 40 to 50 km of altitude. Since it is known from vapor-trail releases that the E-region neutral-wind vector substantially changes in magnitude and direction as a function of altitude, the height-averaged radar estimates of this quantity may not give an accurate picture of the wind behavior. For example, the radar measurements are heavily weighted toward the altitude of peak electron density. As the altitude of the peak density changes by 10 to 20 km, apparent temporal changes in neutral wind may simply represent changes in the altitude at which the neutral wind is being sampled.

Figure 50 shows the E-region neutral-wind estimates as a function of time. The rapid variations shown prior to 0900 UT should be

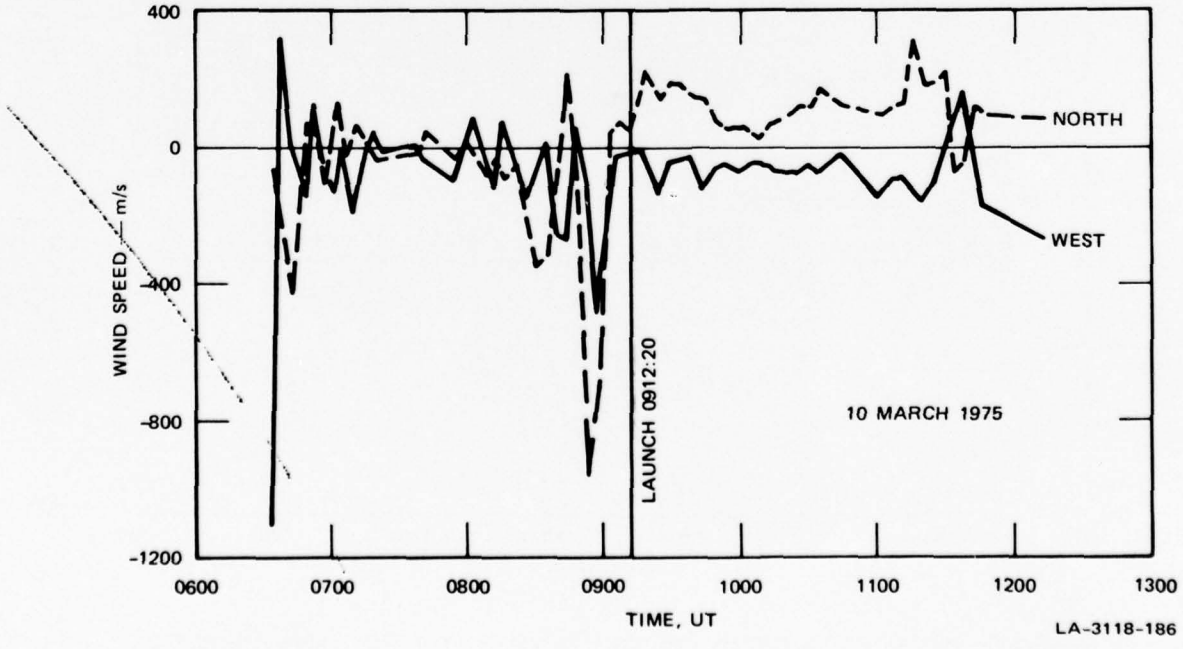

FIGURE 50 HEIGHT-AVERAGED E-REGION NEUTRAL WIND FOR THE EXPERIMENT ON 10 MARCH 1975

viewed with caution because the altitude of maximum ionization was changing (see Figure 47) and because the SNR was weakest during this time. The neutral-wind estimates between 0900 and 1100 UT are probably the most reliable because the SNR was high and the altitude of maximum ionization was constant. During this time period there was a relatively steady westward component of about 50 m/s. The north-south component varied smoothly from about 150 m/s at 0915 UT to about 20 m/s at 1000 UT, to about 100 m/s at 1030 UT. During this period (0900 to 1100) the neutral-wind direction was between about 60° west of geographic north and 30° east of geographic north. The neutral-wind magnitude was between about 50 m/s and 150 m/s.

h. Height-Integrated Current Density

From 0630 UT until launch the ionospheric current (Figure 51) was generally northeastward, having a moderate Pedersen component.

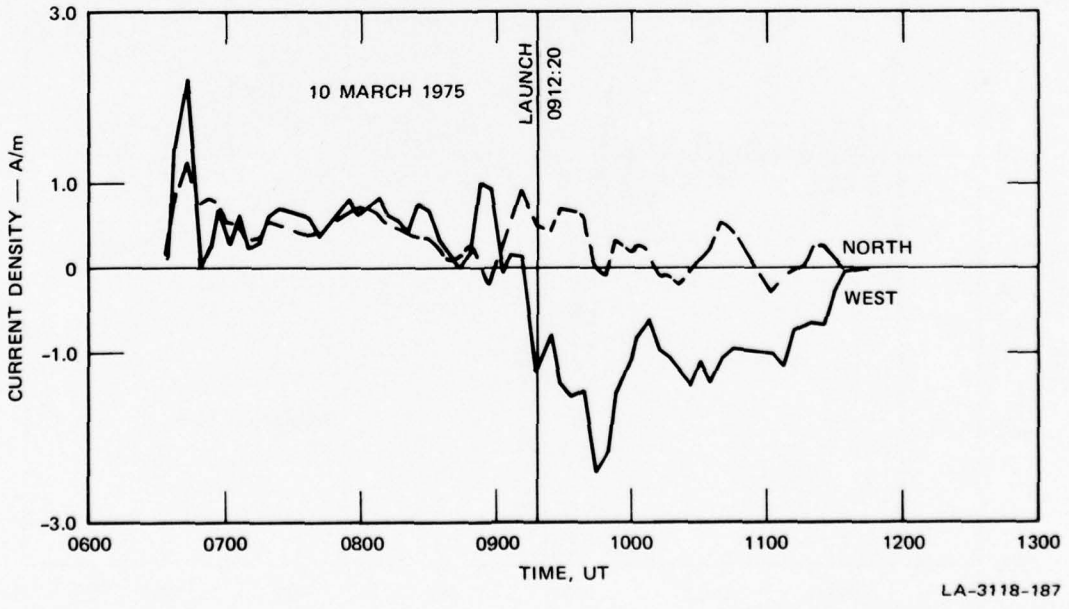

FIGURE 51 HEIGHT-INTEGRATED CURRENT DENSITY FOR THE EXPERIMENT ON 10 MARCH 1975

During the launch period, in conjunction with the reversal of the electric field the current direction rotated to a westward direction and increased to more than 1.8 A/m.

i. Energy Deposition

The calculated energy deposited from joule heating is shown in Figure 52. Although the joule heating rate as a function of time is quite variable throughout the evening, it is generally larger prior to 0900 (in the eastward electrojet) than after 0900 UT. The joule heating is quite large, averaging in excess of 10 ergs/cm^2-s.

Figure 52 also shows the rate of energy deposition by the precipitating electrons as a function of time. Early in the evening, 0600 to 0700 UT, there was an enhancement as arcs passed through the radar

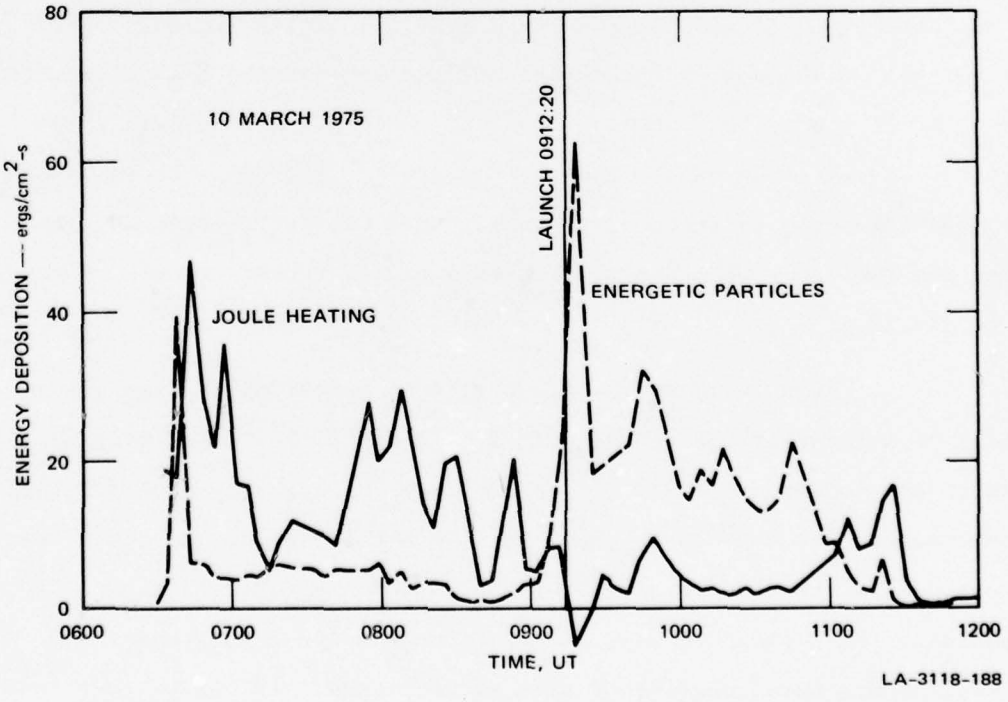

FIGURE 52 JOULE HEATING AND ENERGETIC PARTICLE CONTRIBUTIONS TO TOTAL ENERGY DEPOSITION FOR THE EXPERIMENT ON 10 MARCH 1975

beam. Between 0700 and 0900 UT the energy deposition was relatively low (<5 ergs/cm^2-s). This was followed by a two-hour period (0900 to 1100 UT) of enhanced energy deposition (>15 ergs/cm^2-s). The period of increased deposition corresponds to the westward-electrojet period when the electric field was southward-directed and the electron precipitation was harder, as indicated by the relatively low altitude of the E-layer maximum (Figure 46). The peak following launch occurred when the radar was pointed at an azimuth and elevation of 36° and 76°. This period of enhanced energy deposition corresponds to the period of enhanced 391-Å and 1.27-μm emissions measured by Utah State University.

3. Correlated Measurements

a. Separation Between Rocket and Radar Beam

During the period 0914:22 to 0920:59 UT the radar antenna was held fixed at 36° azimuth and 76° elevation. It was intended that this antenna position would place the antenna beam at the E-layer penetration point of the rocket. By the time the antenna was placed in this position, however, the rocket had reached 130 km altitude. It is instructive, nevertheless, to consider the horizontal separation between the rocket and the radar beam for that portion of the rocket flight occurring after 0914:22 UT.

Figures 53 and 54 illustrate as functions of time after launch, plan views of the geomagnetic longitude and latitude, respectively, for both the rocket and the point on the radar beam at the same altitude as the rocket. In both cases the reversal in the plot of the radar beam corresponds to the time of apogee of the rocket trajectory. Figure 55 illustrates the horizontal separation distance between the rocket and the radar beam, as a function of time after launch. It can be seen that the initial separation distance (at 130 km altitude) is less than 10 km,

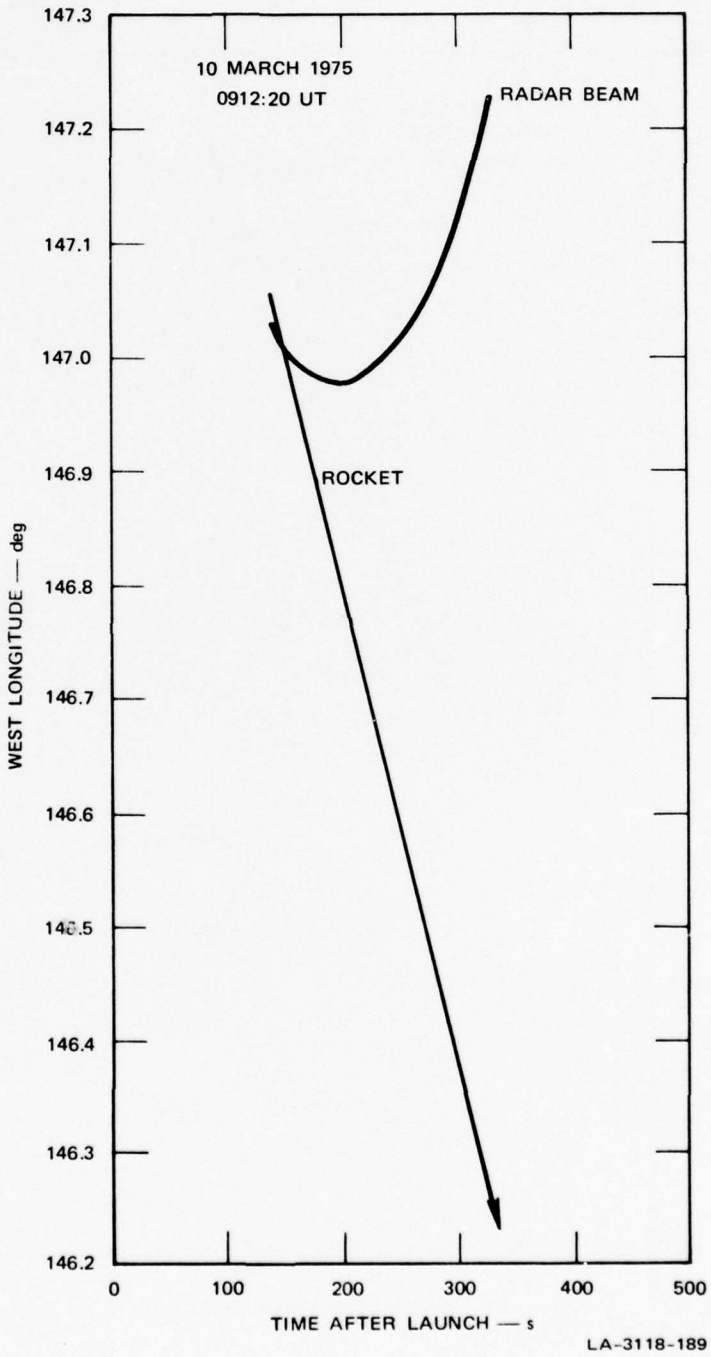

FIGURE 53 LONGITUDINAL SEPARATION BETWEEN THE RADAR BEAM AND THE ROCKET FOR THE FLIGHT OF 0912:20 UT, 10 MARCH 1975

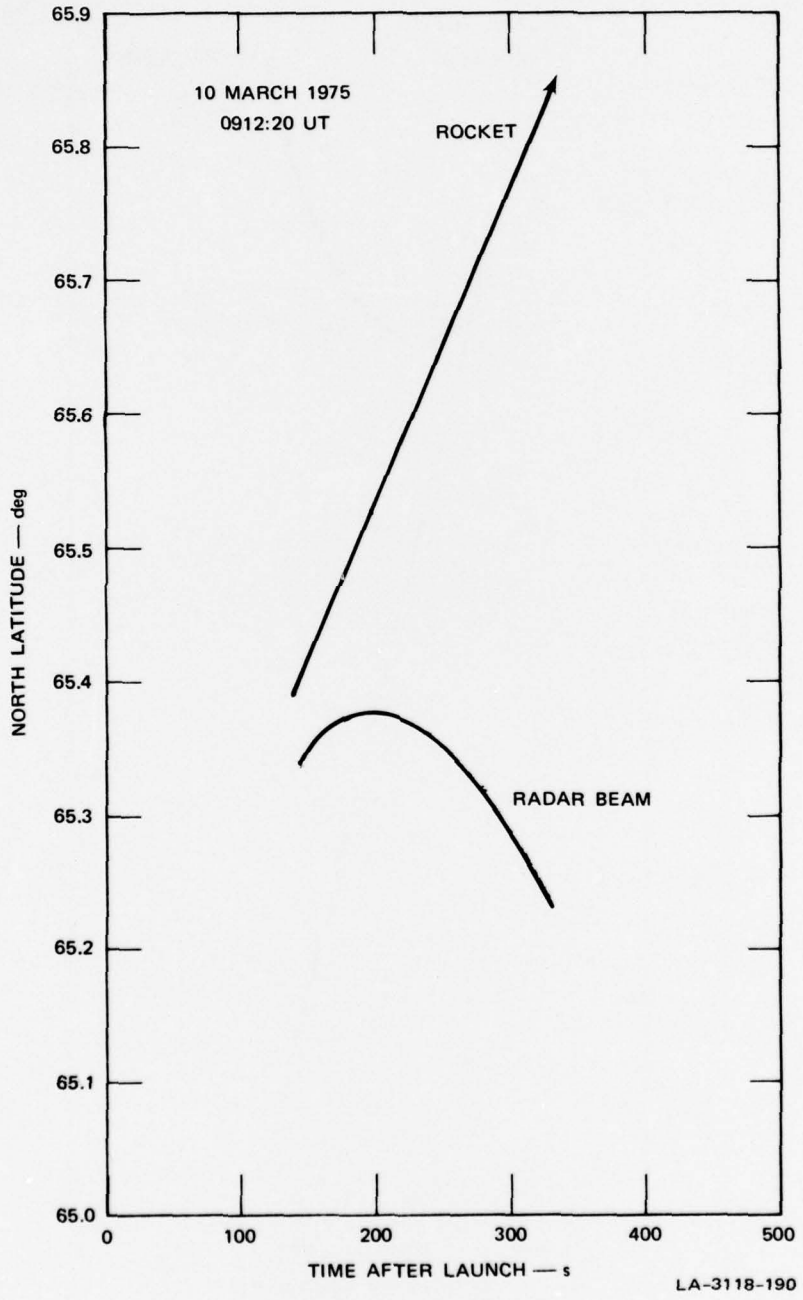

FIGURE 54 LATITUDINAL SEPARATION BETWEEN THE RADAR BEAM AND THE ROCKET FOR THE FLIGHT OF 0912:20 UT, 10 MARCH 1975

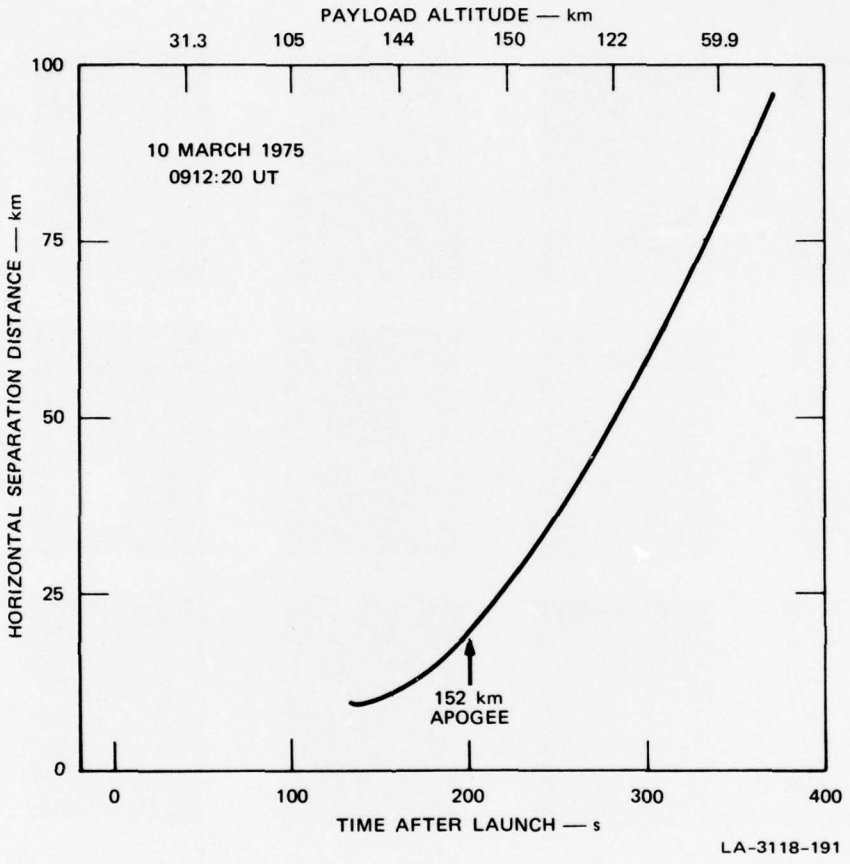

FIGURE 55 HORIZONTAL SEPARATION DISTANCE BETWEEN THE RADAR BEAM AND THE ROCKET FOR THE FLIGHT OF 0912:20 UT, 10 MARCH 1975

which is close enough to suggest that reasonable correlations between rocket and radar measurements could be made.

b. Boresite Television Observations

To augment the pulsed radar data, observations were also made using a low-light-level television camera mounted and boresited on the radar dish. Images collected during the launch interval (Figure 56) display in a narrow-field format (35.5° x 46.7°) the activity recorded by the all-sky photographs. Notice that the rocket was launched into a region of brilliant aurora.

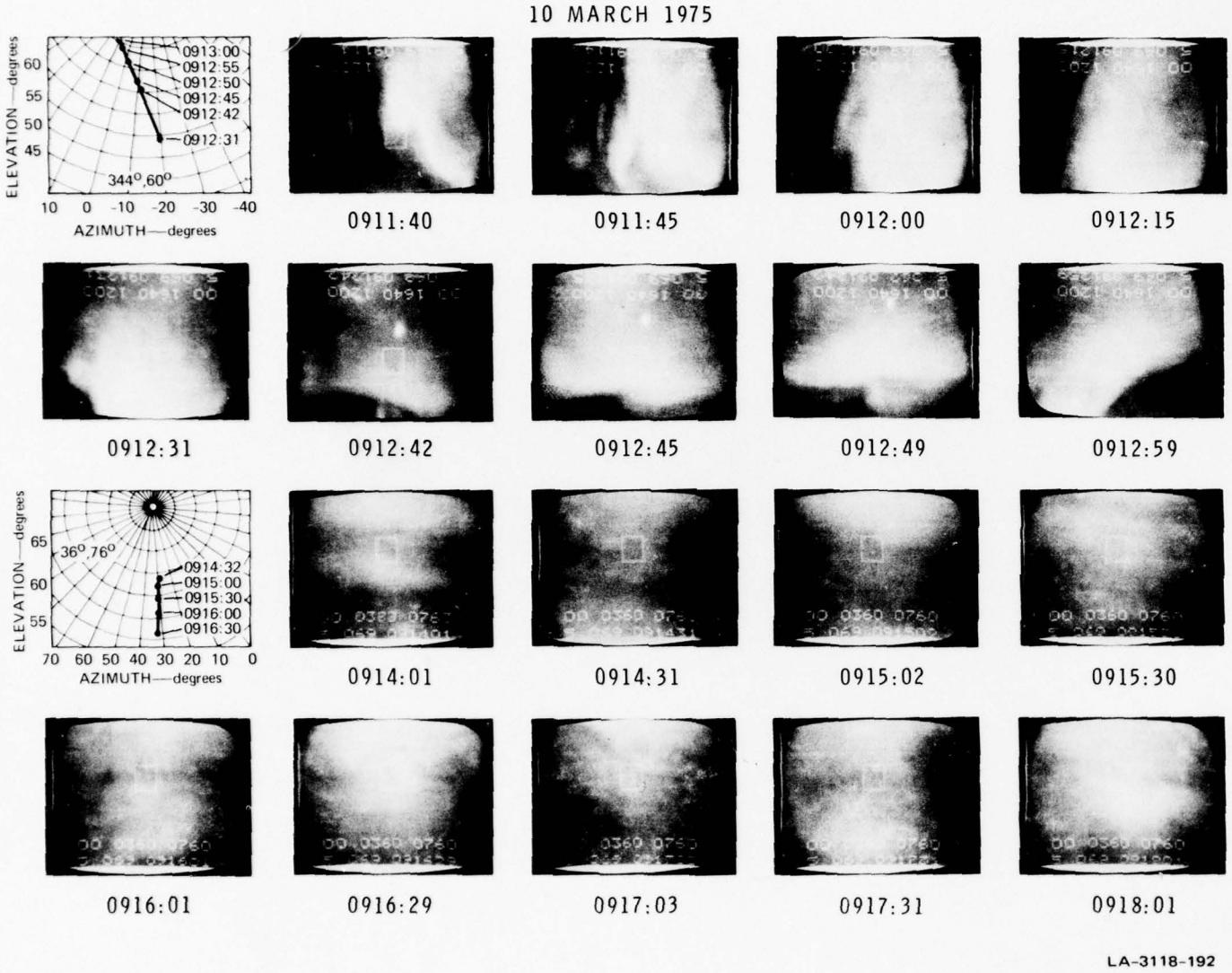

FIGURE 56 CHATANIKA BORESIGHT TELEVISION PHOTOGRAPHS FOR THE EXPERIMENT ON 10 MARCH 1975

c. Electron Density

Figure 57 illustrates contour plots of the logarithm of radar-derived electron density for the period 0914:22 to 0920:08 UT, when the radar antenna was fixed at 36° azimuth and 76° elevation. The contours were prepared by drawing smooth curves through the data points, which were obtained at 10-s intervals. Also illustrated is the equivalent altitude of the rocket, plotted as a function of time and calculated as described in Section III-E.

By comparison of these contour values with the background density contours in Figure 46, it can be seen that D- and E-region densities were greatly enhanced during the rocket flight, over the pre-existing background levels. E-layer peak densities, occurring at about

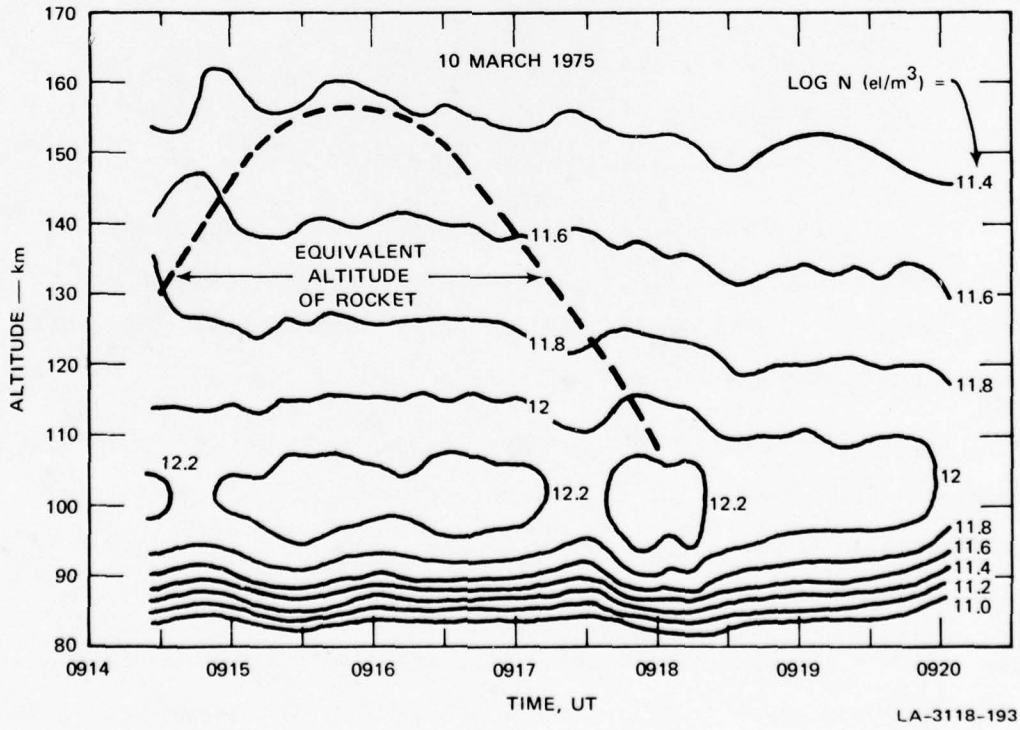

FIGURE 57 CONTOURS OF ELECTRON DENSITY AND THE EQUIVALENT ALTITUDE OF THE ROCKET DURING THE FLIGHT OF 0912:20 UT, 10 MARCH 1975

100 km altitude, exceeded $10^6/cm^3$ during practically all of the rocket flight. These enhanced densities suggest a corresponding enhancement in energetic-particle precipitation. We can also observe from Figure 47 that just prior to the rocket flight, rapid increases in flux amplitude and spectrum hardness occurred.

d. Energy Spectra of Precipitating Electrons

Energy spectra have been computed for five different times during the evening. The times chosen are indicated by the letters A through E on Figure 47, and correspond to the computed energy spectra shown in Figures 58(a) through (e), respectively. Also shown are the measured electron density profile (solid line) and the electron density profile (diamonds) that would be produced by the derived electron energy distribution.

All the spectra show a small "bump" at about 15 to 16 keV energy. This bump is an artifact induced by the transition from 1 keV to 2 keV energy resolution at 16 keV in the UNTANGLE code.

The energy spectrum corresponding to a time before the 0900 UT enhancement [Figure 58(a)] shows a relatively soft spectrum with a peak flux at 2 to 3 keV and a mean energy of about 4 keV. The spectrum exhibits a relatively steep power-law decay with altitude.

The spectrum [Figure 58(b)] corresponding to the initial enhancement peak shows a substantial hard (~10 keV) component of flux superimposed on the soft spectrum of Figure 58(a). The number flux is almost independent of energy and the mean energy is about 10 keV.

The spectra [Figures 58(c) and 58(d)] for times later during the enhancement event also show a hard component superimposed on the soft spectrum of Figure 58(a). However the hard component is not as intense as at the initial peak enhancement.

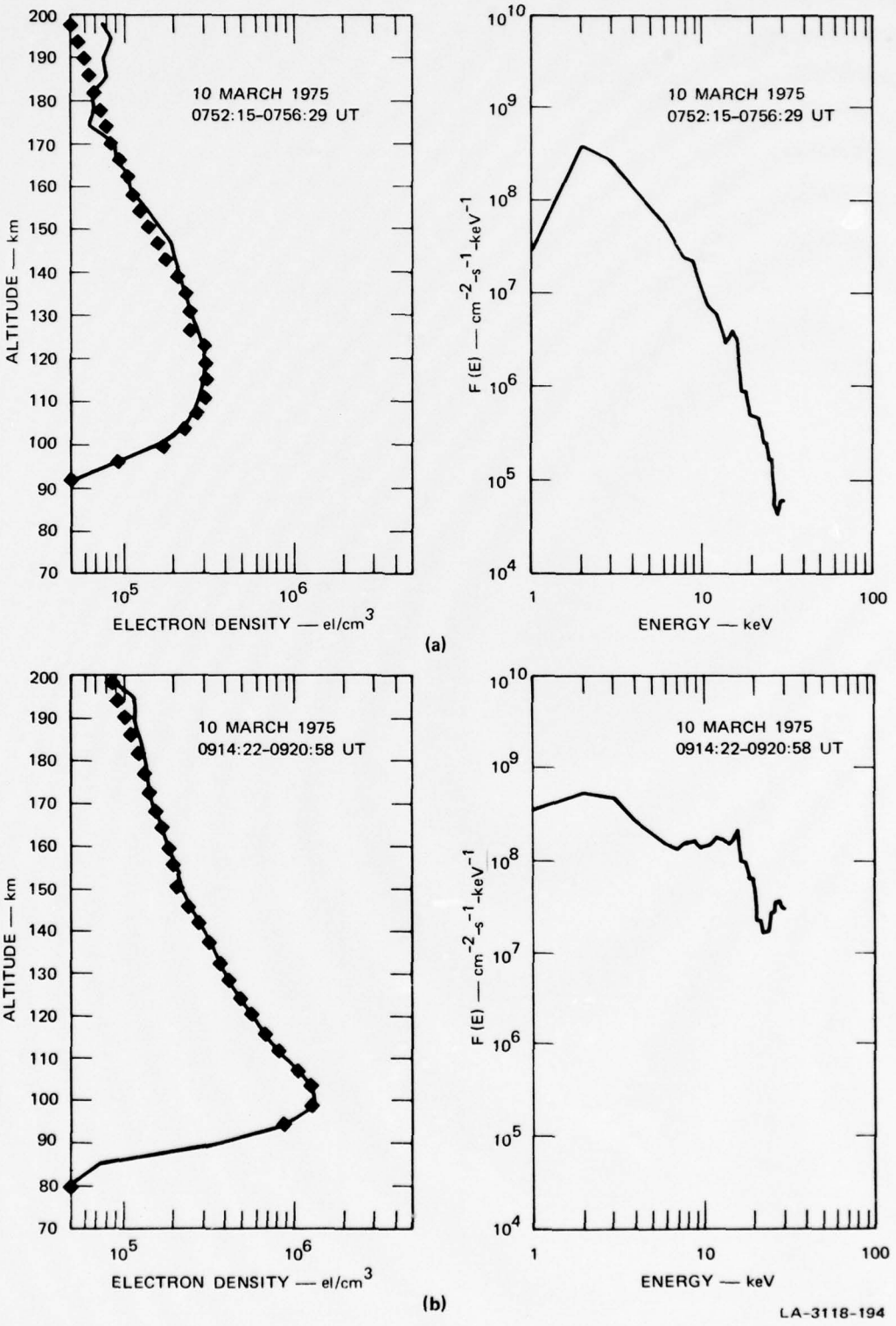

FIGURE 58 ENERGY SPECTRA OF AURORAL ELECTRONS AND ASSOCIATED ELECTRON-DENSITY PROFILES FOR FIVE SELECTED PERIODS DURING THE EXPERIMENT ON 10 MARCH 1975. Details are given in the text.

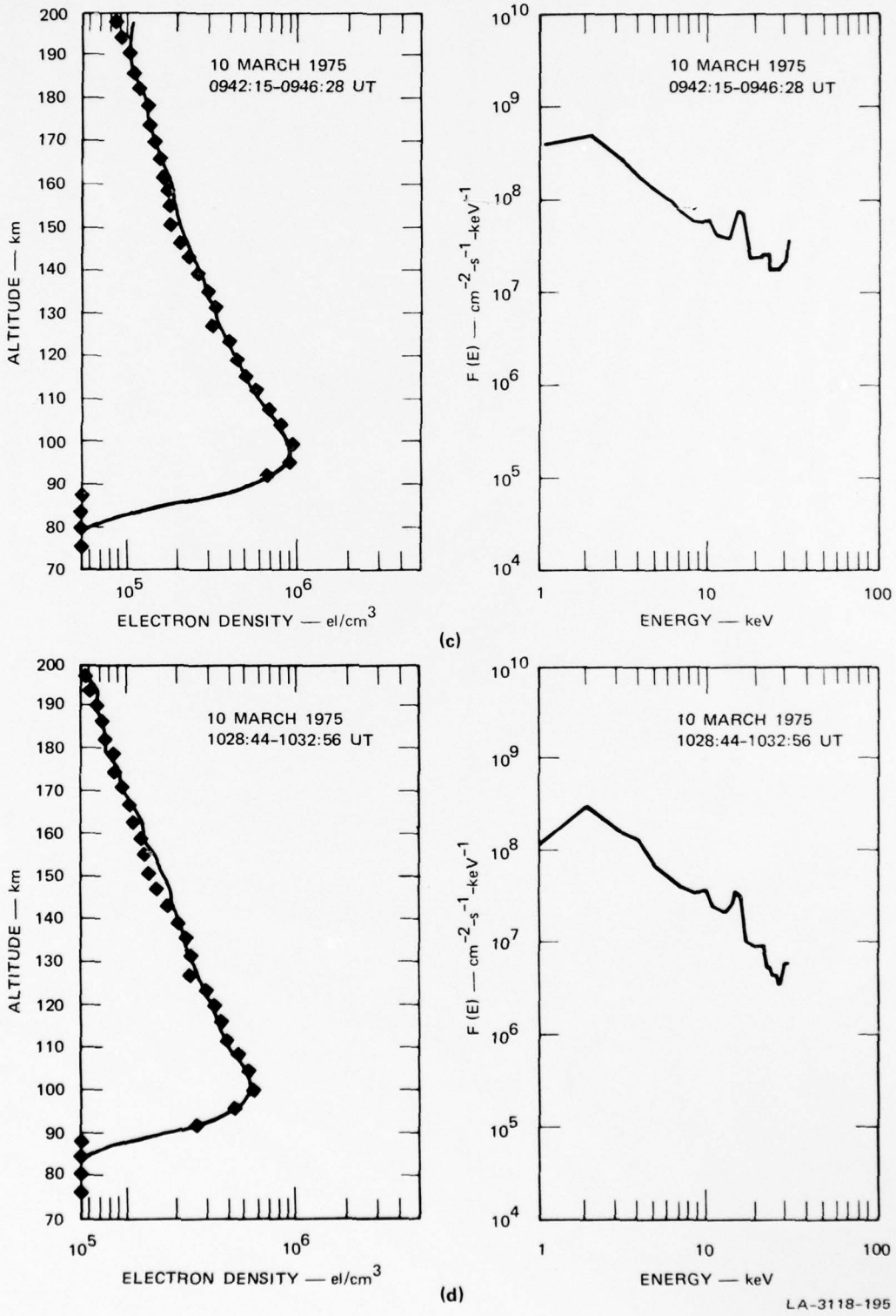

FIGURE 58 (Continued)

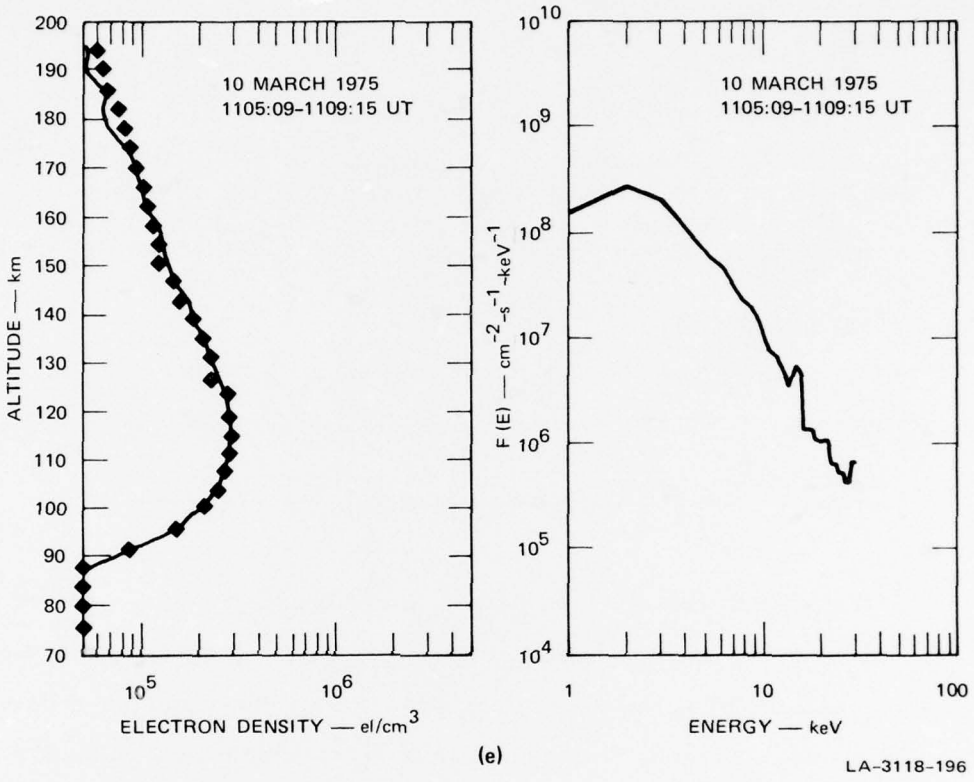

FIGURE 58 (Concluded)

The energy spectrum [Figure 58(e)] corresponding to the recovery phase after the enhancement is almost identical to the pre-enhancement spectrum.

Table 5 summarizes the behavior of the electron flux during the period of interest. All quantities represent 5-minute averaged data.

4. Summary

The period 0700 to 0900 UT was characterized by high northward-directed electric fields (40 mV/m), moderate electron density produced by soft precipitation, eastward electrojet flow, large amounts of joule heating (15 to 20 ergs/cm^2-s on the average), and modest energy deposition by precipitating electrons (~5 ergs/cm^2-s).

Table 5

SUMMARY OF UNTANGLE RESULTS FROM FIGURE 58

Time (UT)	Mean Energy (keV)	Energy Flux (ergs/cm^2-s)	Parallel Current (μA/m^2)
0752-0756	4.1	7.5	1.8
0914-0921	11.3	65.0	5.7
0942-0946	6.8	32.0	4.8
1028-1033	7.8	14.0	1.8
1105-1109	4.6	6.8	1.5

The period 0900 to 1200 UT was characterized by a southward electric field (~20 mV/m), somewhat higher electron densities produced by harder precipitation, westward electrojet flow, moderate joule heating ($\lesssim$10 ergs/cm^2-s), and large energy deposition by precipitating electrons (>20 ergs/cm^2-s).

F. 11 March 1975--Nike Javelin

1. General

An Honest-John-Javelin (1C 511.21) vehicle, carrying instrumentation to measure ionospheric electric fields, was launched from Poker Flat at 0633:09 UT on 11 March 1975. A second rocket, launched two minutes later, was to deposit a trail of aluminum vapor to make visible the neutral winds. However, the second stage failed to ignite, rendering this experiment a failure. Figure 59 contains a composite picture of the rocket trajectory and an auroral arc, seen in the fields of view of the boresighted television camera and the all-sky camera.

During this evening, the radar was operated in two different modes. From 0049 to 0626 UT an independent six-position experiment was

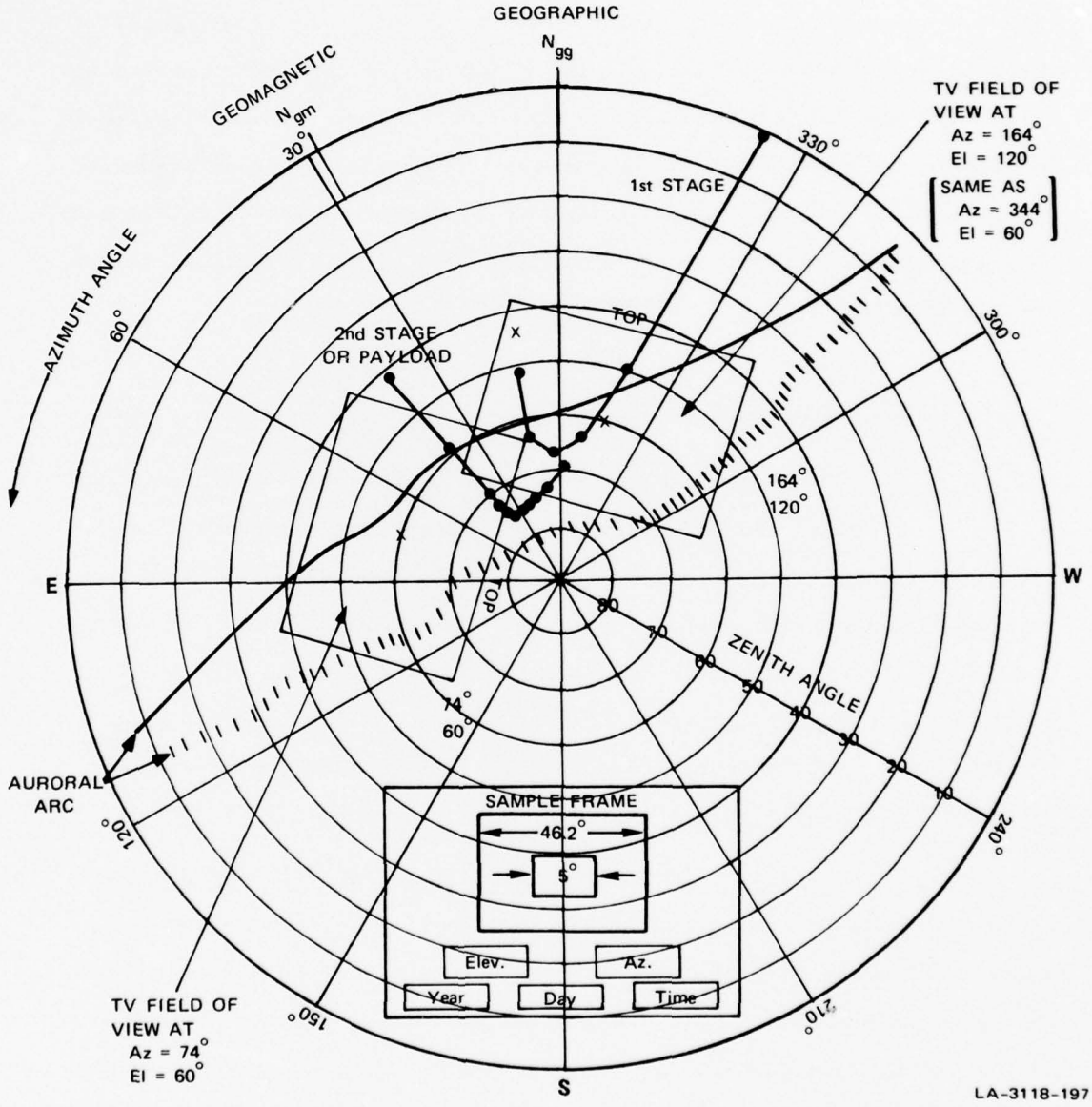

FIGURE 59 SKY PROJECTIONS OF THE ROCKET TRAJECTORY FROM CHATANIKA FOR THE FLIGHT OF 0633:09 UT, 11 MARCH 1975

conducted to investigate latitudinal gradients of the electric field. Then, in support of this ICECAP launch and to obtain better time resolution of electric fields in the vicinity of the rocket, the radar observing mode was changed to a two-position experiment. Here the beam elevation was held at 60° while the azimuth was alternated every three minutes between 344° and 74°. This put the radar line of sight 45° on either side of geomagnetic north. At these azimuths the radar was not aligned with the path of the rocket, and interference by rocket echoes was minimized. This two-position mode was used from 0627 to 0707 UT. After the flight, the six-position mode was resumed, from 0717 to 1950 UT.

2. Background Measurements

a. Geomagnetic Conditions

This launch occurred during disturbed geomagnetic conditions. A geomagnetic storm had begun at about 0200 UT on 10 March and had reached a maximum provisional Dst of -79 γ at about 2300 UT. By launch time the storm was recovering and the provisional Dst was -42 γ. The geomagnetic records for Barrow, College, and Sitka are presented in Figure 60(a). The records of Poker Flat and Fort Yukon in an expanded time scale are displayed in Figure 60(b).

Prior to launch, the College magnetometer recorded the field of a well developed eastward current system located to the south. However, at about 0635 UT the College H-component turned strongly negative while the Z-component remained negative, indicating that an intense westward current, located north of College, had begun to dominate. Changes in the Z-component then became rapid and poorly recorded. As a result of these conditions it was difficult to determine the subsequent location of the electrojet. At Fort Yukon, although the H-component had turned negative at about 0635 UT, the sudden enhancement (-750 γ in the H-component)

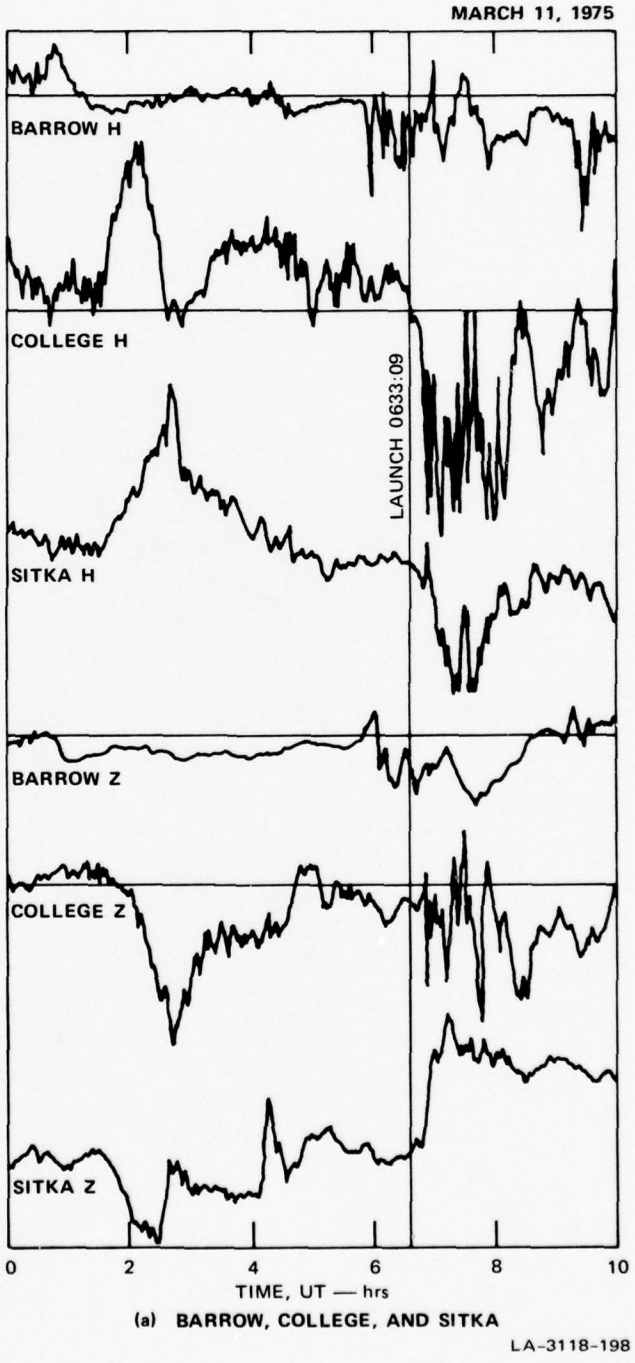

FIGURE 60 MAGNETOGRAMS ON 11 MARCH 1975

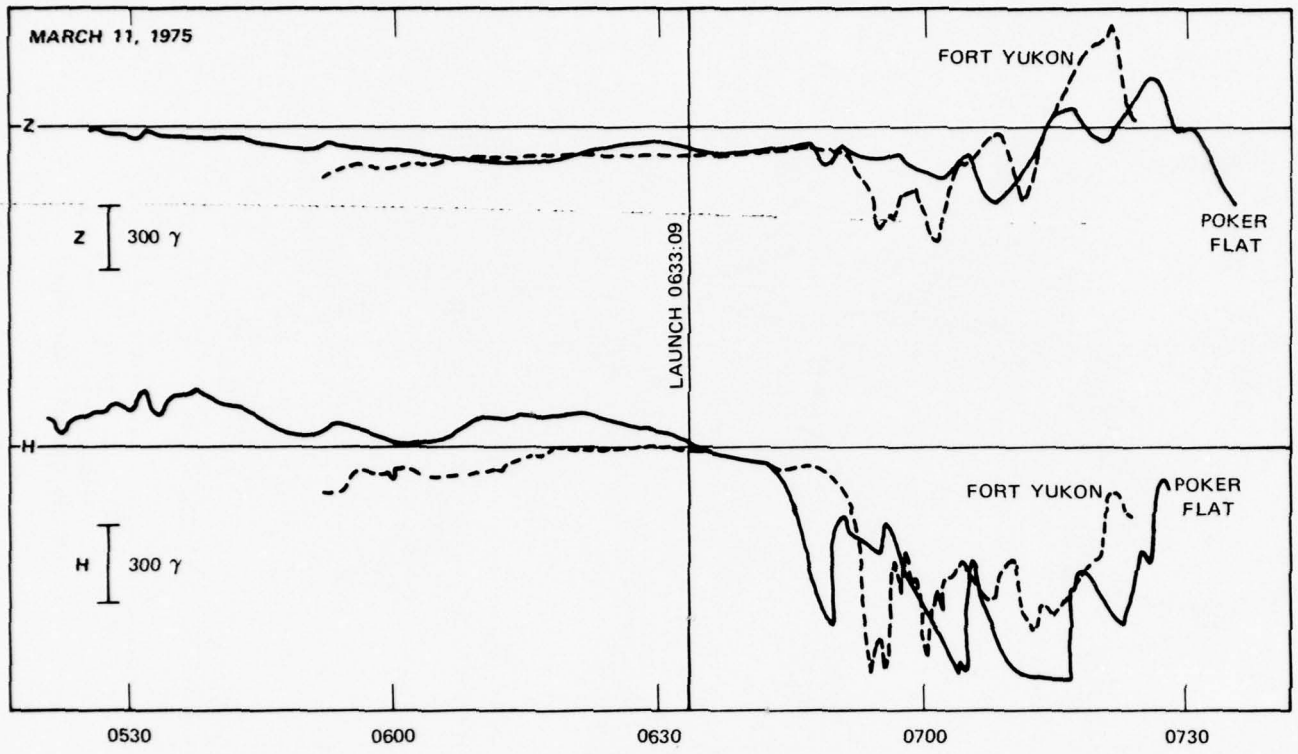

(b) POKER FLAT AND FORT YUKON

LA-3118-199

FIGURE 60 (Concluded)

of westward current was not observed until almost 15 minutes later, at about 0650 UT. At Barrow, the sudden enhancement was observed at about 0655 UT. The Barrow Z-component indicated that the center of the westward-current system was located even more poleward than Barrow. However, for a few minutes after 0655 UT, as the surge passed by, the center of the current system expanded equatorward and was located between College and Barrow.

b. Auroral Conditions

The evening of 11 March 1975 was characterized by increasing auroral activity, from a bright quiet arc to the passage of a westward-traveling surge. A Defense Meteorological Satellite Program (DMSP) photograph labeled 0647 UT (equatorial crossing time of the southward-bound satellite), taken over the midnight sector of the auroral oval, shows a complicated pattern of active auroral forms (Figure 61). If that surge-like structure, located near 100° longitude and 65° latitude, was the same westward-traveling surge that passed over Chatanika at 0651 UT, it propagated westward at about 1.2 km/s (a reasonable speed).

Chatanika all-sky photographs (Figure 62) indicate that a bright auroral arc was located just poleward of Chatanika and that it slowly drifted equatorward of Chatanika until 0638 UT. A typical westward-traveling surge is clearly visible in the sequence of photographs that begin at 0646 UT. The surge passed overhead at about 0651 UT, about the same time that a deep negative bay was recorded on the College and Poker H-component magnetograms. Note that since the all-sky photographs are displayed in the sky projection, the westward-traveling surge moves from left to right across the figure.

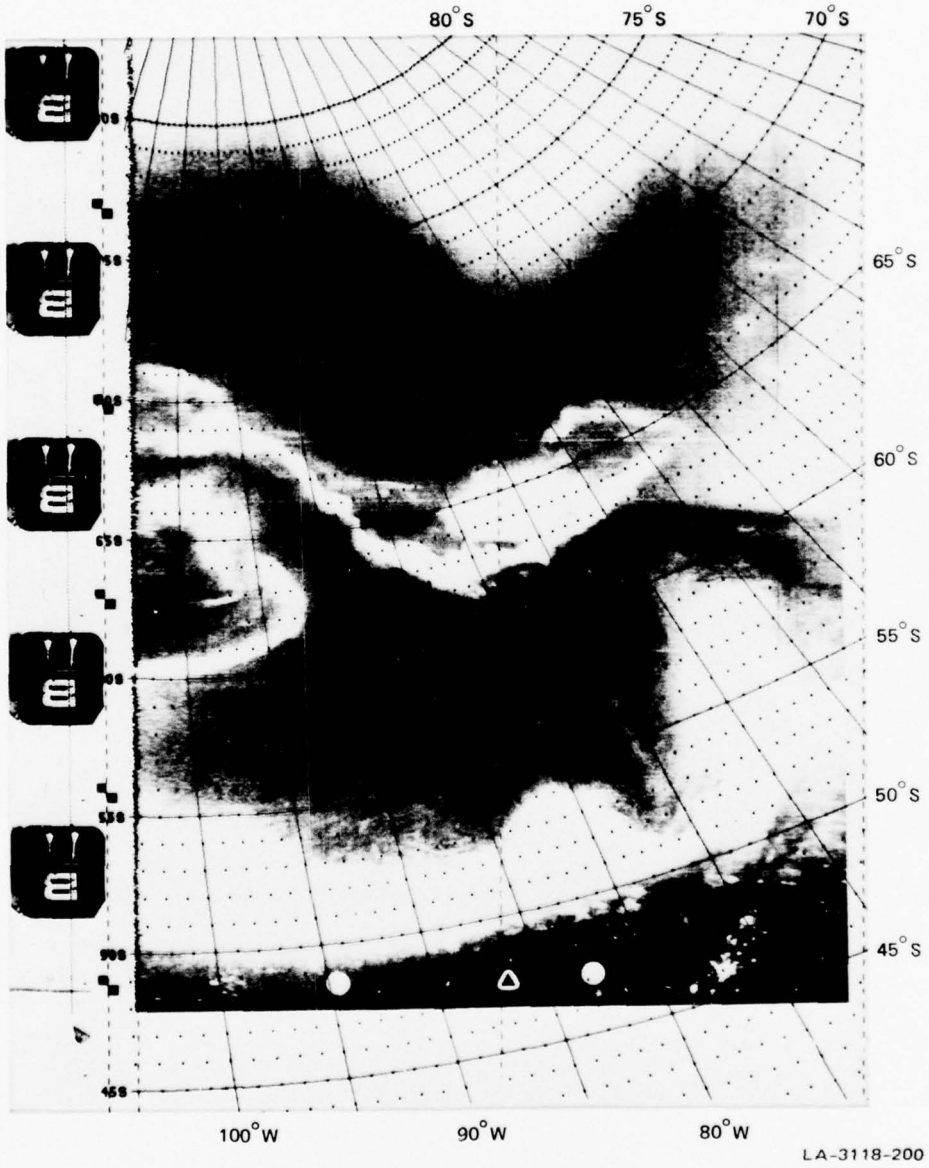

FIGURE 61 DMSP PHOTOGRAPH TAKEN ON 11 MARCH 1975 ILLUSTRATING THE MIDNIGHT SECTOR OF THE AURORAL OVAL. The triangle indicates the position of the southward-bound satellite at 0633:09 UT, the launch time of the ICECAP rocket.

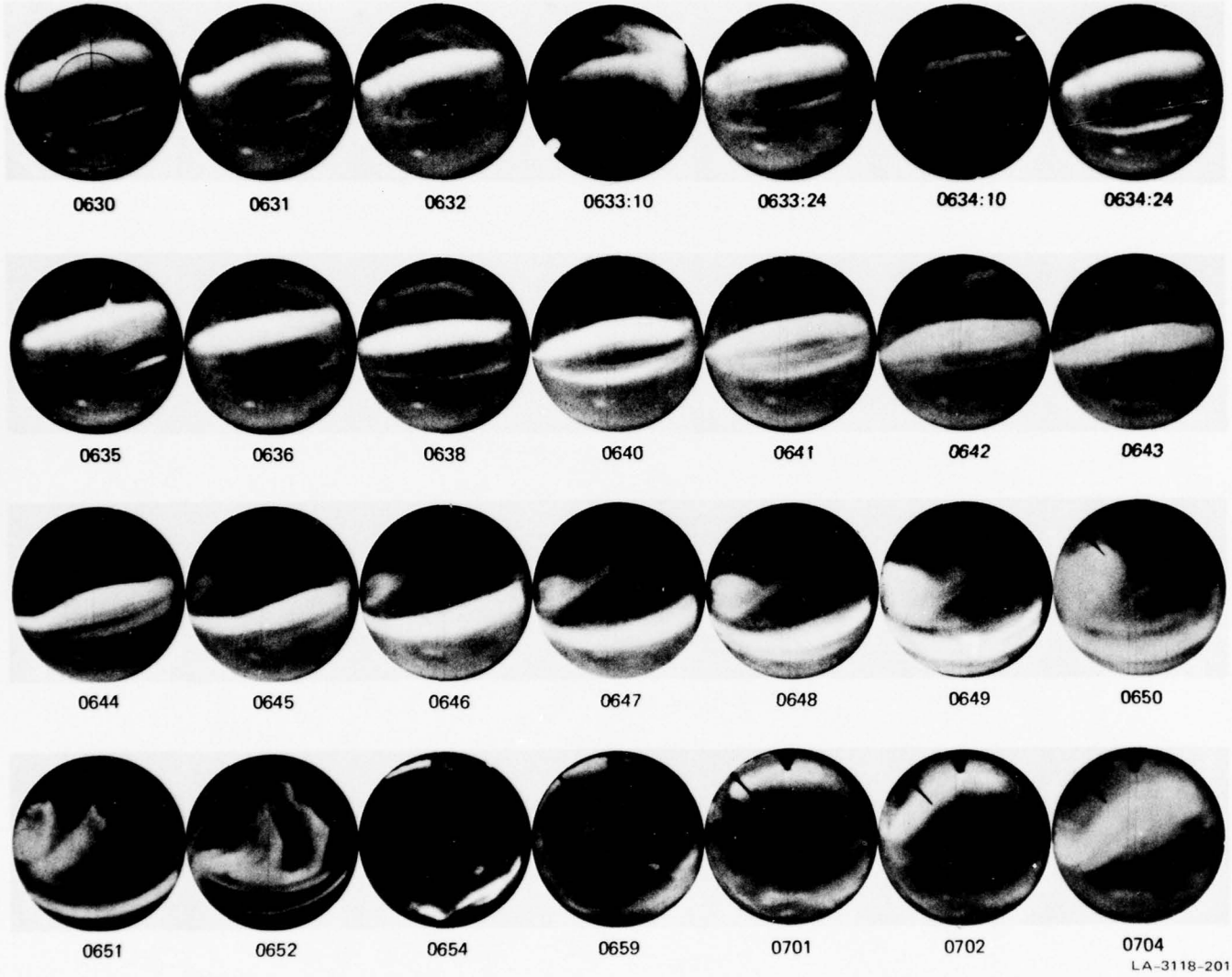

FIGURE 62 ALL-SKY PHOTOGRAPHS TAKEN FROM CHATANIKA DURING THE EXPERIMENT ON 11 MARCH 1975. East is to the left and north is at the top of each image.

c. Absorption

The cosmic-radio-noise absorption levels for the quiet day (9 March) and for 11 March are presented in Figure 63. A small amount of D-layer ionization before launch is indicated by the absorption during this time. At about launch time, however, radio interference degraded the record. A large absorption event did begin at about 0649 UT, and corresponds to the arrival at College of an auroral westward traveling surge and its associated enhanced electron precipitation.

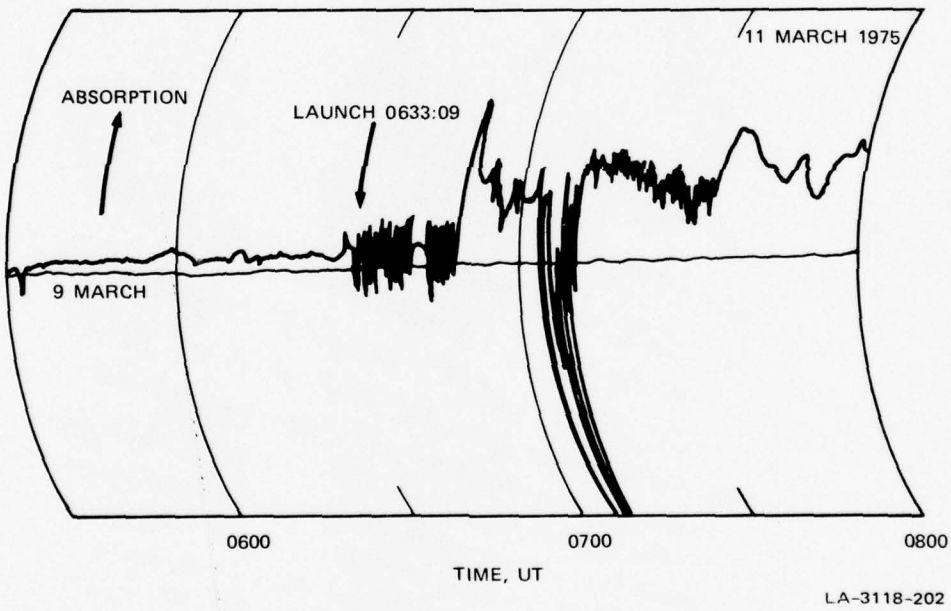

FIGURE 63 COLLEGE RIOMETER RECORD FOR 11 MARCH 1975. The record for 9 March 1975 is representative of a quiet day.

d. Electron Density

Figure 64 illustrates contours of the logarithm of electron density obtained by the radar during this experiment. In viewing these contours, it is important to bear in mind that two distinct antenna modes are represented by the data. Before 0627 UT and after 0717 UT, the radar

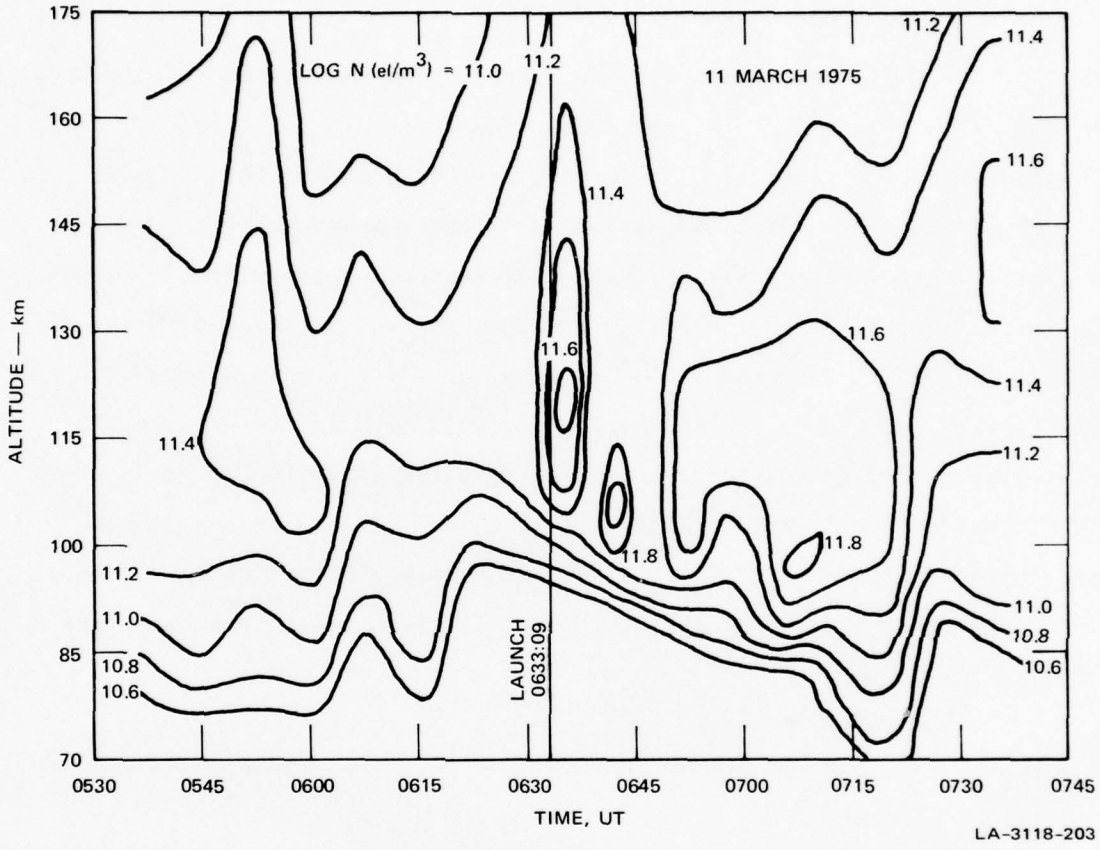

FIGURE 64 BACKGROUND CONTOURS (6-Minute Averages) OF ELECTRON DENSITY FOR THE EXPERIMENT ON 11 MARCH 1975

antenna was operating in a six-position azimuth-scan mode, and the contours are based on measurements averaged over the entire scan and over 6 minutes in time. Between 0627 UT and 0707 UT the antenna direction was alternately placed 45° either side of geomagnetic north at a frequency of about 3 minutes per position. The contours within this time period are based on measurements taken separately at each antenna position. The enhancements occurring during the times 0633 to 0636, 0640 to 0643, and 0646 to 0649 UT correspond to an antenna azimuth position of 344°, during which times the antenna boresight passed through an auroral arc. It is apparent, then, that these enhancements are primarily spatial rather than temporal.

e. Height-Integrated Conductivities

The height-integrated Pedersen and Hall conductivities are presented in Figure 65. The Pedersen conductivity ranged between 3 and 9 mhos during the interval 0400 to 0600 UT (not shown). Before launch, the Hall conductivity fell to less than 2 mhos. However, as auroral activity increased, especially during the overhead passage of the westward-traveling surge, both the Hall and Pedersen conductivities increased. The Hall conductivity variations closely parallel the enhancements in density observed by the radar, and in auroral activity seen in the all-sky photographs (Figure 62). The westward-traveling surge, which marks the leading edge of the westward electrojet, a region of intense electron precipitation, was intercepted by the radar beam at about 0651 UT. From this time until the end of the run, the Hall conductivity averaged more than 20 mhos.

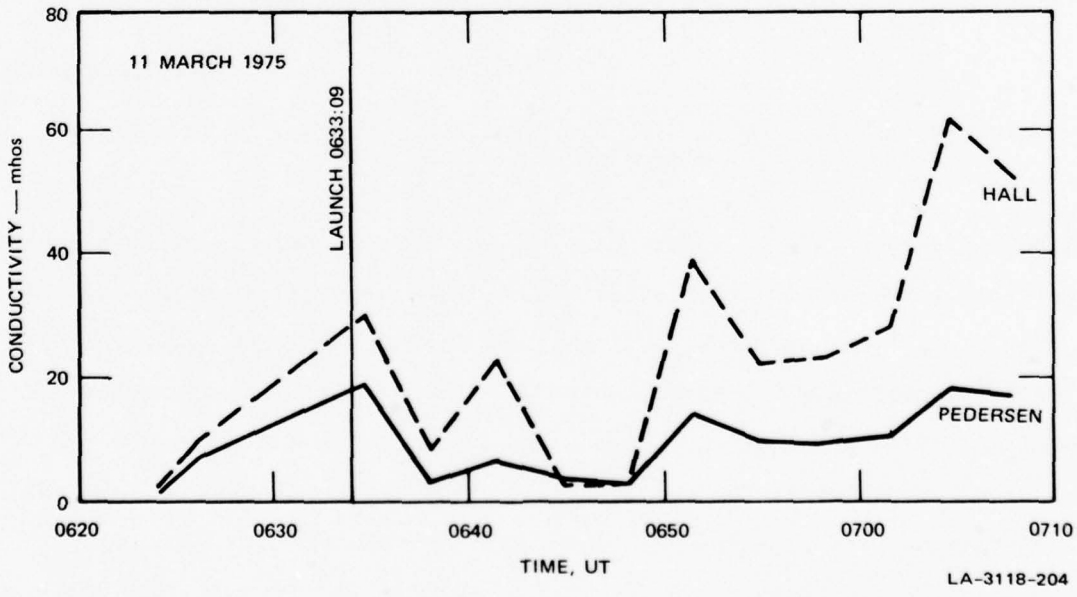

FIGURE 65 HEIGHT-INTEGRATED CONDUCTIVITIES FOR THE EXPERIMENT ON 11 MARCH 1975

f. Electric Field

Electric field components are illustrated in Figure 66. As mentioned earlier, the radar was operated in a two-position mode during the launch period. Assuming stationarity, homogeneity, and that the ion velocity parallel to the earth's magnetic field is negligible, an electric field vector can be resolved for each 3-minute change of the radar azimuth. The angular spread between the radar positions was 90°.

In the calculation of current density, joule heating, etc., the electric field used is the average of that from the second and third range gates which, at this elevation, gives an average centered at 178 km altitude.

During the interval 0633 to 0707 UT, the calculated electric field was predominantly northward-directed, with magnitudes up to 69 mV/m in the north-south component. Up to 0646 UT the field was intense and slightly east of north. However, subsequent measurements

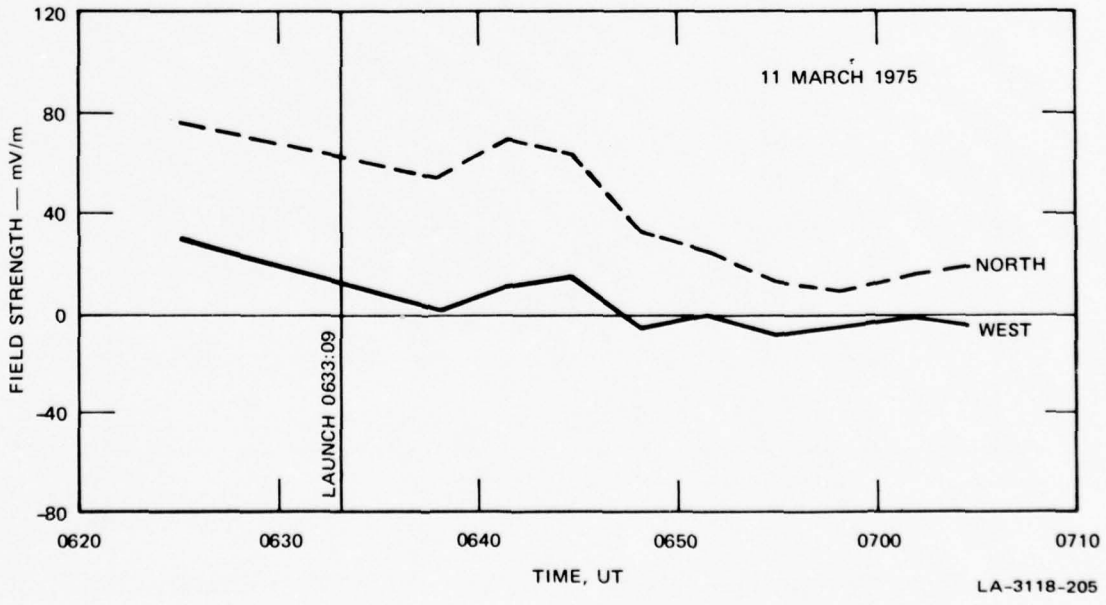

FIGURE 66 ELECTRIC FIELD FOR THE EXPERIMENT ON 11 MARCH 1975

indicated that the field had decreased in magnitude and rotated to a slight west-of-north orientation. This reduction and rotation of the field direction was coincident with the overhead passage of a westward-traveling surge as seen in the all-sky photographs (Figure 62).

Note that although the College H-component changed from a positive to a negative bay, a feature that some ascribe to the Harang discontinuity, the electric field in the region probed did not reverse its northward orientation.

g. Neutral Wind

The height-averaged E-region neutral wind, estimated for the altitude region between 73 and 126 km, was generally southwestward (Figure 67) during the launch interval. However, as the westward-traveling auroral surge passed overhead, the neutral winds rotated to a northwesterly direction.

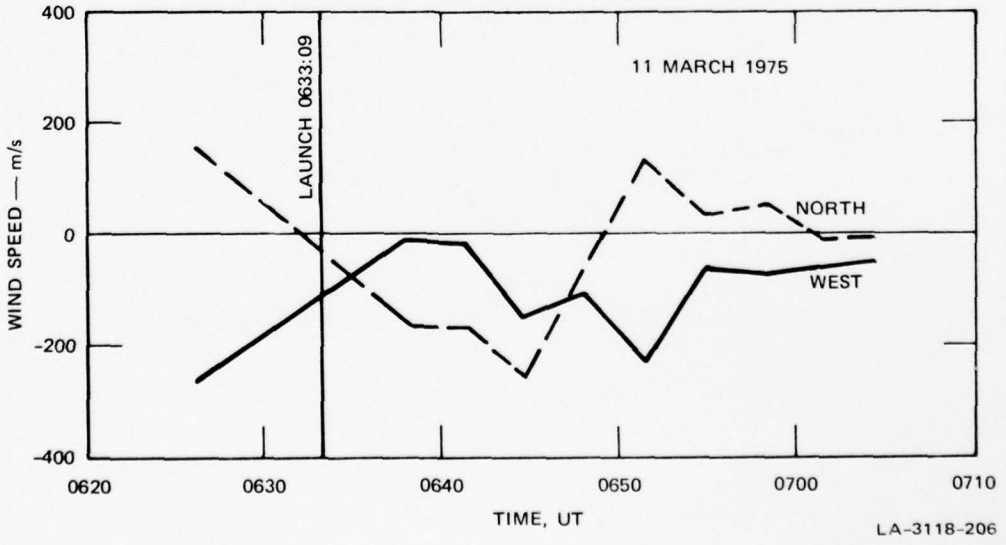

FIGURE 67 HEIGHT-AVERAGED E-REGION NEUTRAL WIND FOR THE EXPERIMENT ON 11 MARCH 1975

h. Height-Integrated Current Density

The ionospheric height-integrated current density is illustrated in Figure 68. The current direction during the interval 0633 to 0707 UT, in the 73-to-126-km region, was generally eastward. Current density ranged from about 0.1 to 1.2 A/m. During the passage of the westward-traveling surge, however (after 0651 UT), the current direction rotated about 45° to a more northerly direction, then back to the east after 0700 UT.

The eastward ionospheric current direction derived from radar measurements is puzzling, because the magnetometer data indicated that the equivalent current system changed from a strong eastward to a stronger westward current. However, it must be recognized that complex auroral activity--i.e., a westward-traveling surge--occurred during this time. The radar was probing a region about 65 km northeast of Chatanika, between the Poker Flat and Fort Yukon magnetometer, both of which indicated a westward ionospheric current.

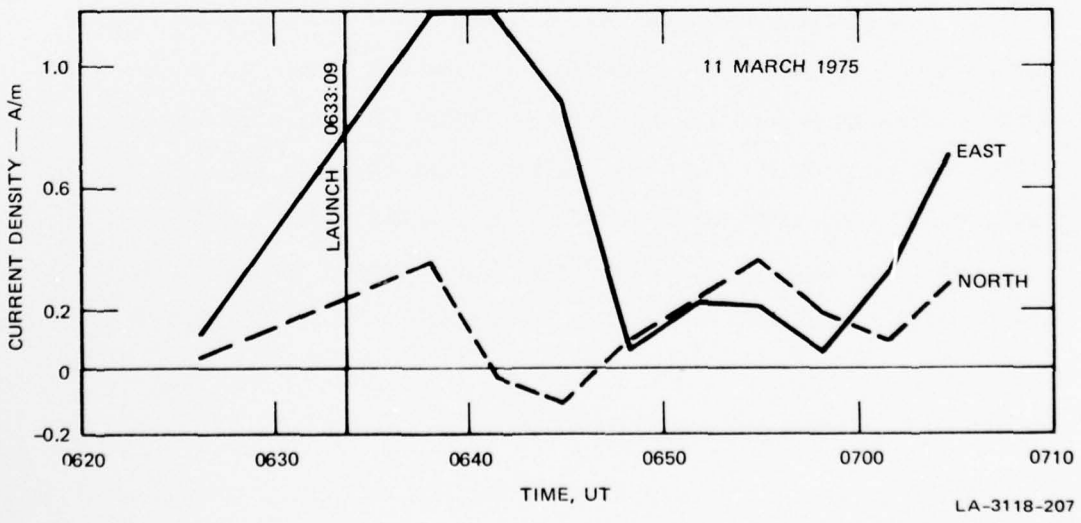

FIGURE 68 HEIGHT-INTEGRATED CURRENT DENSITY FOR THE EXPERIMENT ON 11 MARCH 1975

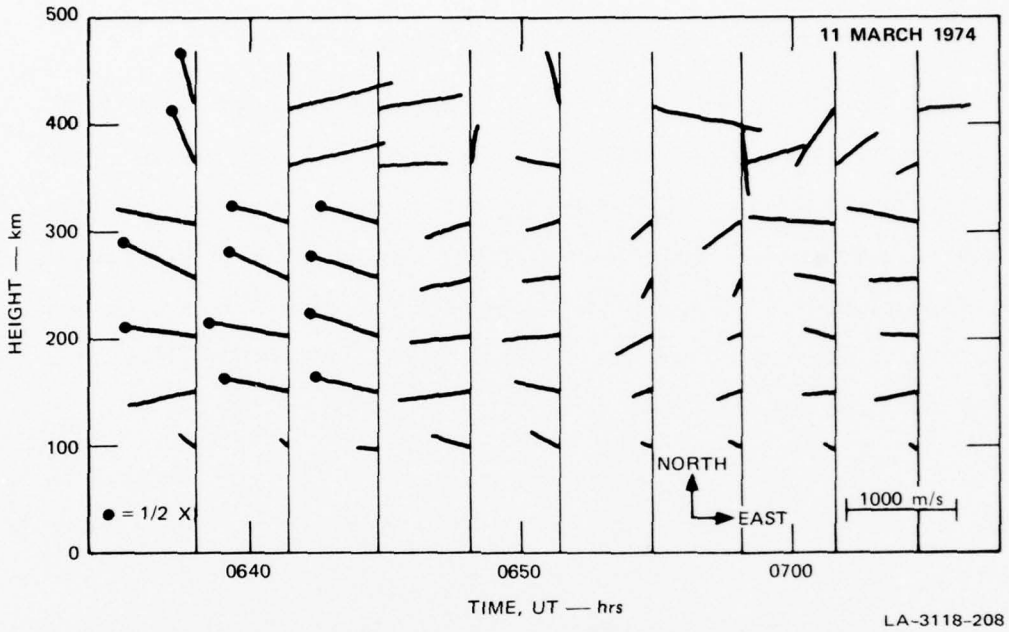

FIGURE 69 PLAN VIEW OF ION VELOCITIES OBTAINED AT EACH RADAR RANGE GATE FOR SEVERAL TIMES JUST FOLLOWING THE LAUNCH ON 11 MARCH 1975

In Figure 69 the ion velocities determined at each range gate are presented. The ion drift does correspond to a convection electric field directed northward in Range Gates 1 through 5. But in Gates 6 and 7 the drift is reversed. Although the SNR is low here, the trend is consistent and is most likely real. The horizontal distance to the subionospheric radar penetration point is about 300 km, thus putting the flow-reversal region north of the geomagnetic latitude of Fort Yukon and thus near the arc boundary. The electric field, which is consistent with this flow, would also be associated with a westward current.

i. Energy Deposition

The energy-deposition rate due to precipitating auroral electrons for the interval 0626 to 0707 UT is presented in Figure 70. In the early part of the evening it appears that particle precipitation was

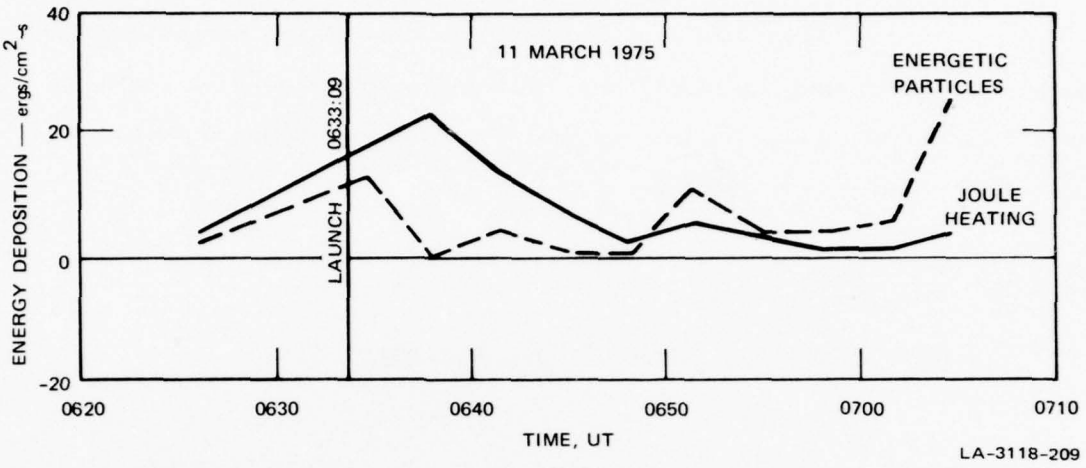

FIGURE 70 JOULE HEATING AND ENERGETIC PARTICLE CONTRIBUTIONS TO TOTAL ENERGY DEPOSITION FOR THE EXPERIMENT ON 11 MARCH 1975

moderate and fairly uniform across the sky. Then, as auroral arcs drifted equatorward, density enhancements were observed when the beam intersected regions of auroral precipitation.

Joule heating estimates are also presented in Figure 70. In the time between 0626 and 0636 UT the joule dissipation rose from 4.4 ergs/cm^2-s to a high of 23.7 ergs/cm^2-s. By 0650 UT the heating rate had dropped to about 6 ergs/cm^2-s, and continued to fall slightly until 0707 UT.

When the radar resumed two-position-mode operation, auroral arcs were present near the radar beam, as seen in the television photographs.* At times when the radar was probing an auroral arc, the energy-deposition rate exceeded the joule heating; at 0649 UT the rates were 14 and 5.9 ergs/cm^2-s, respectively. When the total energy-deposition rate and the joule dissipation rate are summed and averaged over the 35-minute period immediately following the launch, 0633 to 0707 UT, the average energy input to the ionosphere is about 16.5 ergs/cm^2-s, more than 10 times the quiet-time level.

*See Section V-F-3-b, Figure 74.

Although the Hall and Pedersen conductivities had dropped to about 8 and 3 mhos, respectively, during the period of high joule dissipation, the electric field was quite intense, reaching a total magnitude of more than 54 mV/m.

3. Correlated Measurements

a. Separation Between Rocket and Radar Beam

The radar was operated in a two-position mode during the rocket launch. At 0636 UT the radar azimuth was changed from 344° to 74°; the elevation being held at 60°. In Figures 71 and 72 the longitude and latitude of the rocket and the spot illuminated by the radar

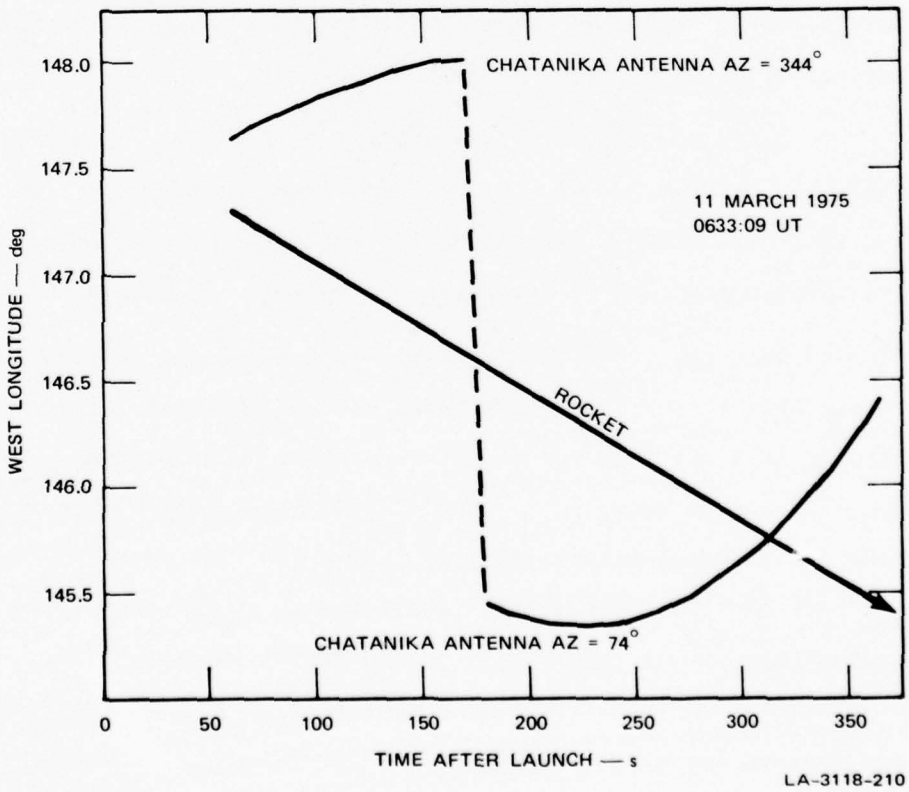

FIGURE 71 LONGITUDINAL SEPARATION BETWEEN THE RADAR BEAM AND THE ROCKET FOR THE FLIGHT OF 0633:09 UT, 11 MARCH 1975

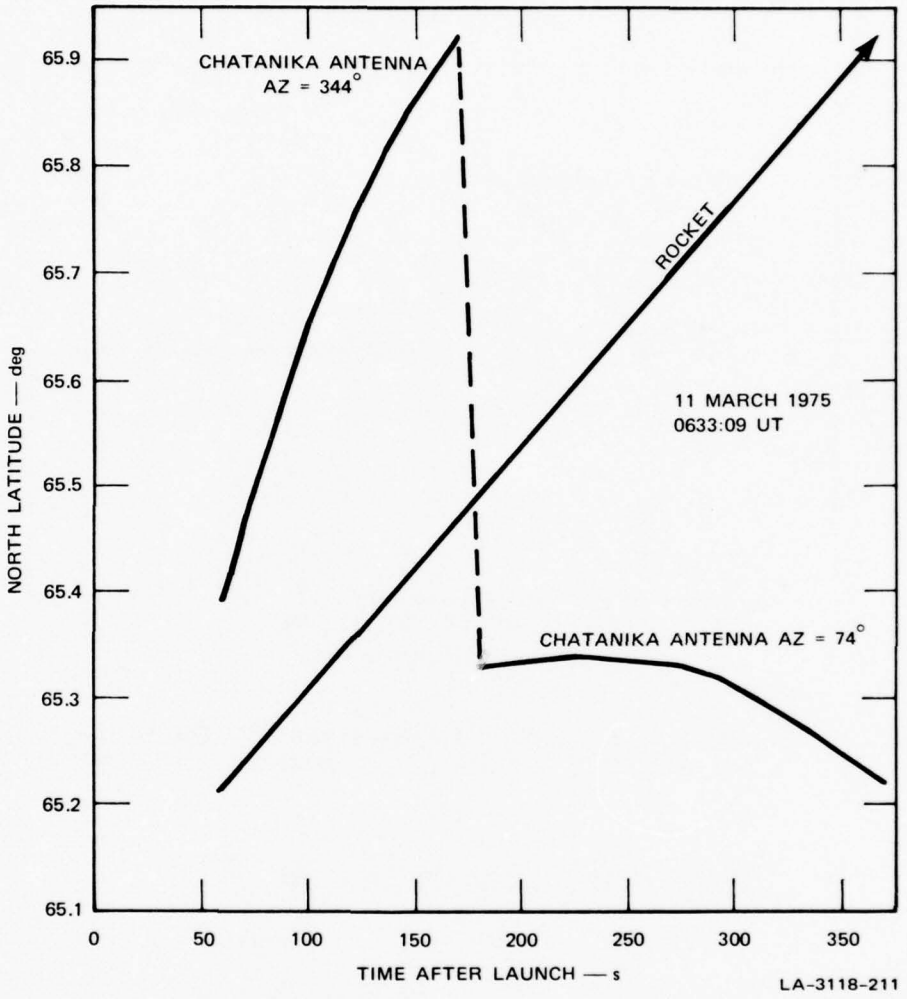

FIGURE 72 LATITUDINAL SEPARATION BETWEEN THE RADAR BEAM AND THE ROCKET FOR THE FLIGHT OF 0633:09 UT, 11 MARCH 1975

beam at rocket altitude are presented as a function of time. The horizontal separation distance between the radar beam and rocket at the rocket altitude is displayed in Figure 73. From these figures it is seen that in the upleg above 110 km the radar beam probed a volume that was northwest of the rocket by between 60 to 80 km, whereas near apogee and on the downleg, the beam was southeast of the rocket by between 50 and 70 km.

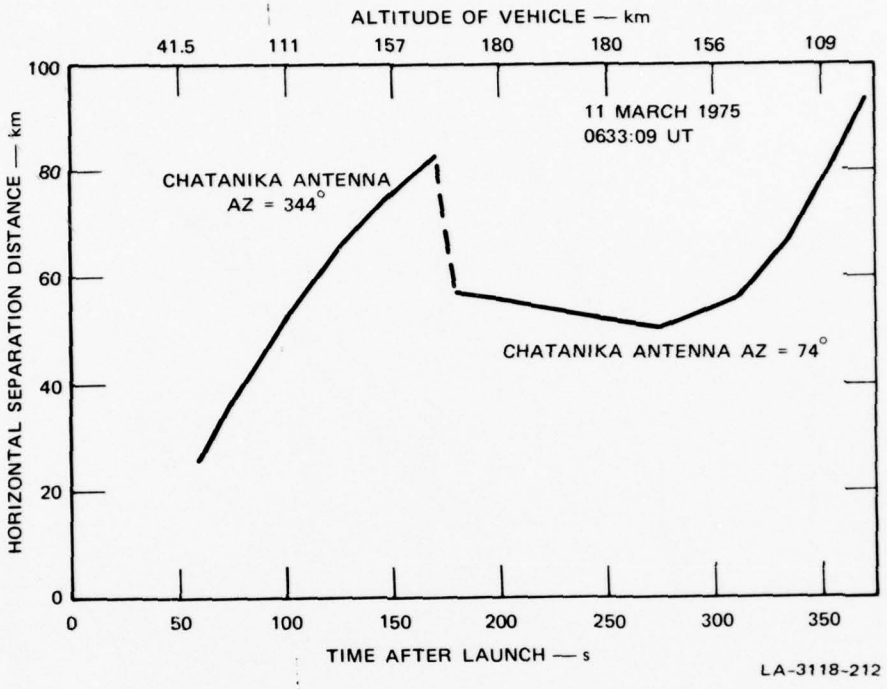

FIGURE 73 HORIZONTAL SEPARATION DISTANCE BETWEEN THE RADAR BEAM AND THE ROCKET FOR THE FLIGHT OF 0633:09 UT, 11 MARCH 1975

b. Boresight Television Observations

The Chatanika radar boresight television pictures, which were selected from recordings made throughout the launch period, are displayed in Figure 74. Up to 0635 UT, the television camera zoom lens was adjusted for a narrow field of view (13.5° by 17.6°), permitting the arc structure to be seen. Then it was opened up to a 35.5° by 46.2° field of view.

The flare of the rocket's first stage and its subsequent burnout are clearly seen in the sequence of images between 0633:32 and 0634:10 UT. The spent first stage is seen near the center of the image at 0633:34 UT, while the ascending second stage is visible near the bottom.

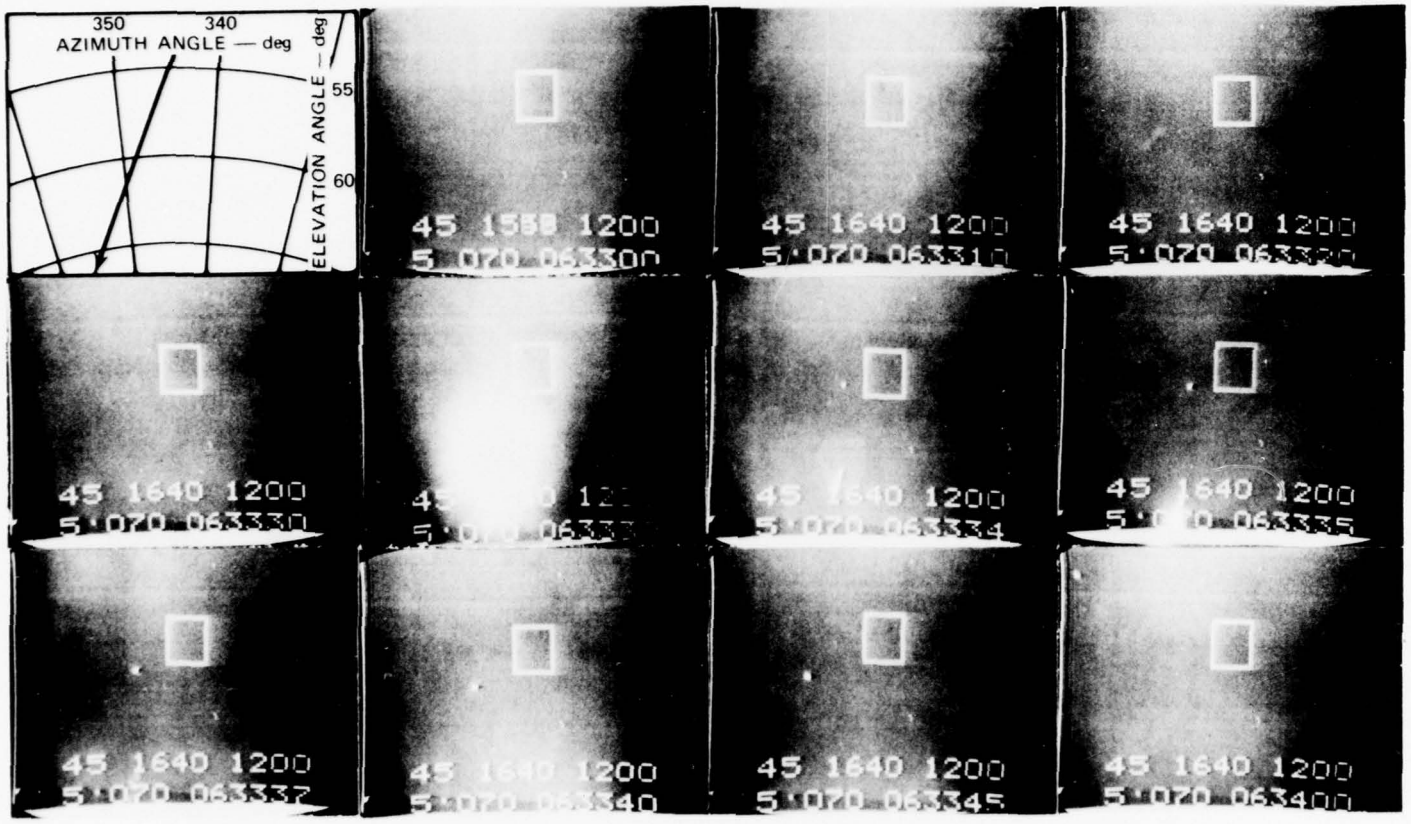

FIGURE 74 CHATANIKA BORESIGHT TELEVISION PHOTOGRAPHS FOR THE EXPERIMENT ON 11 MARCH 1975

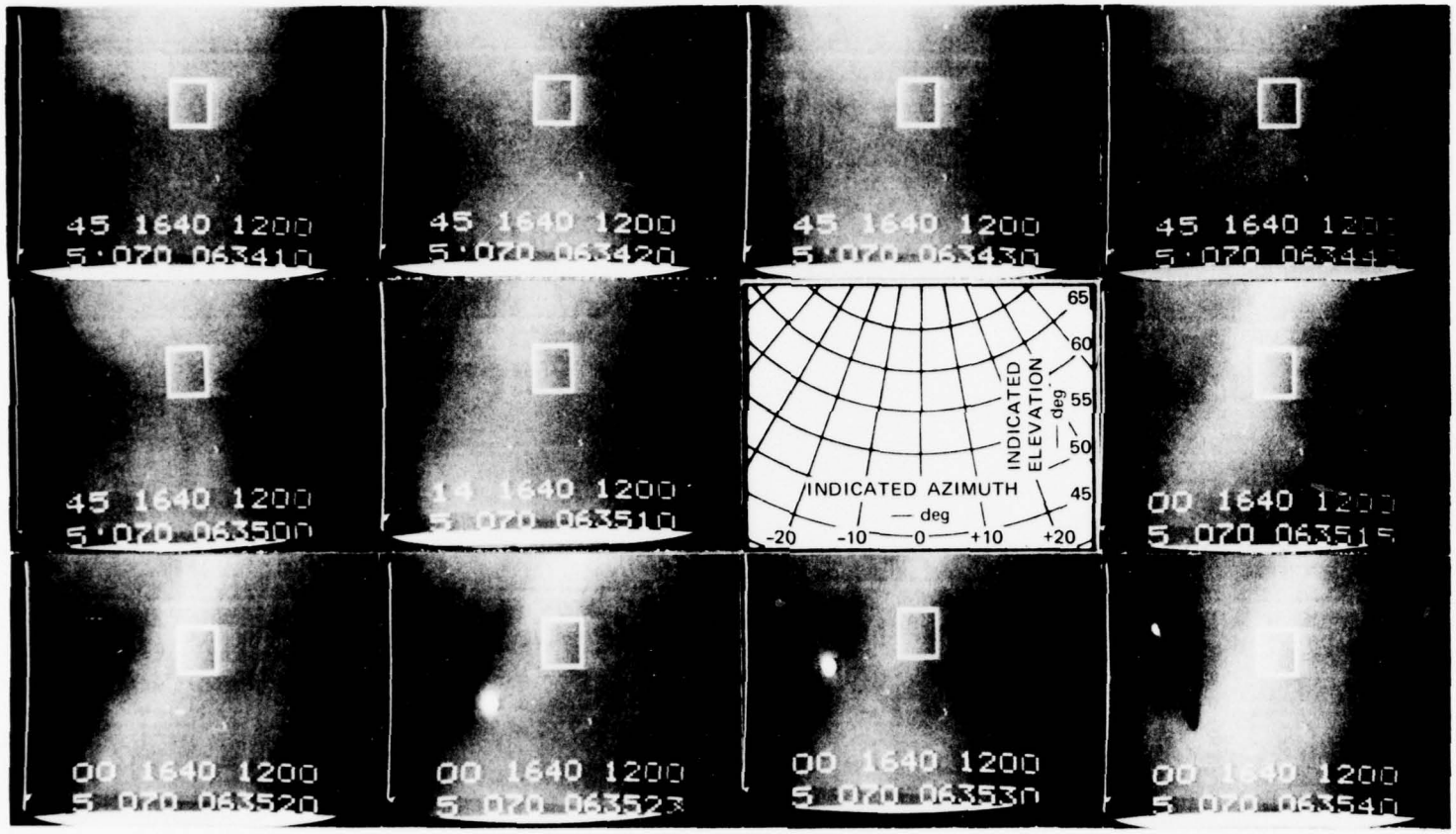

FIGURE 74 (Continued)

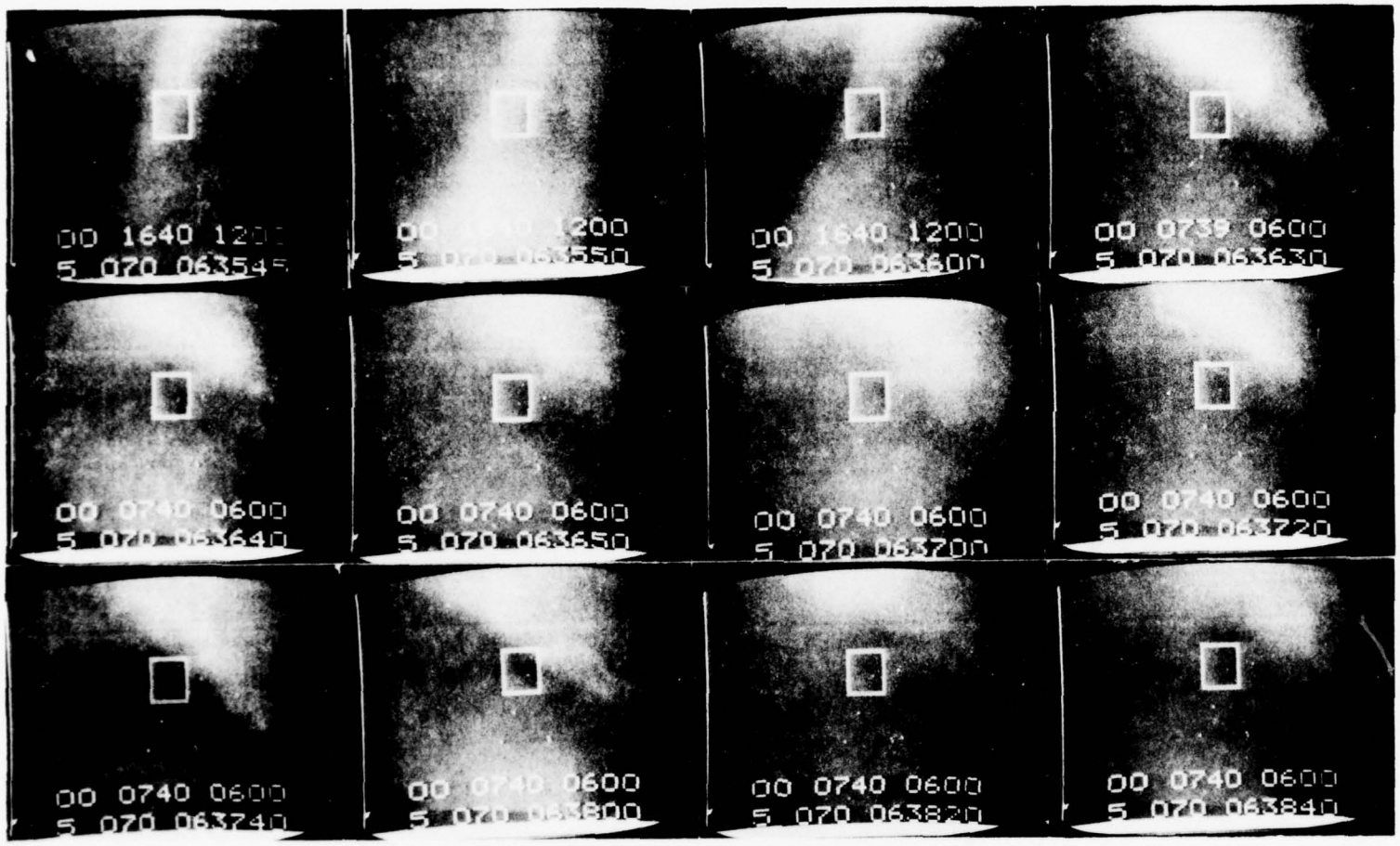

LA-3118-215

FIGURE 74 (Continued)

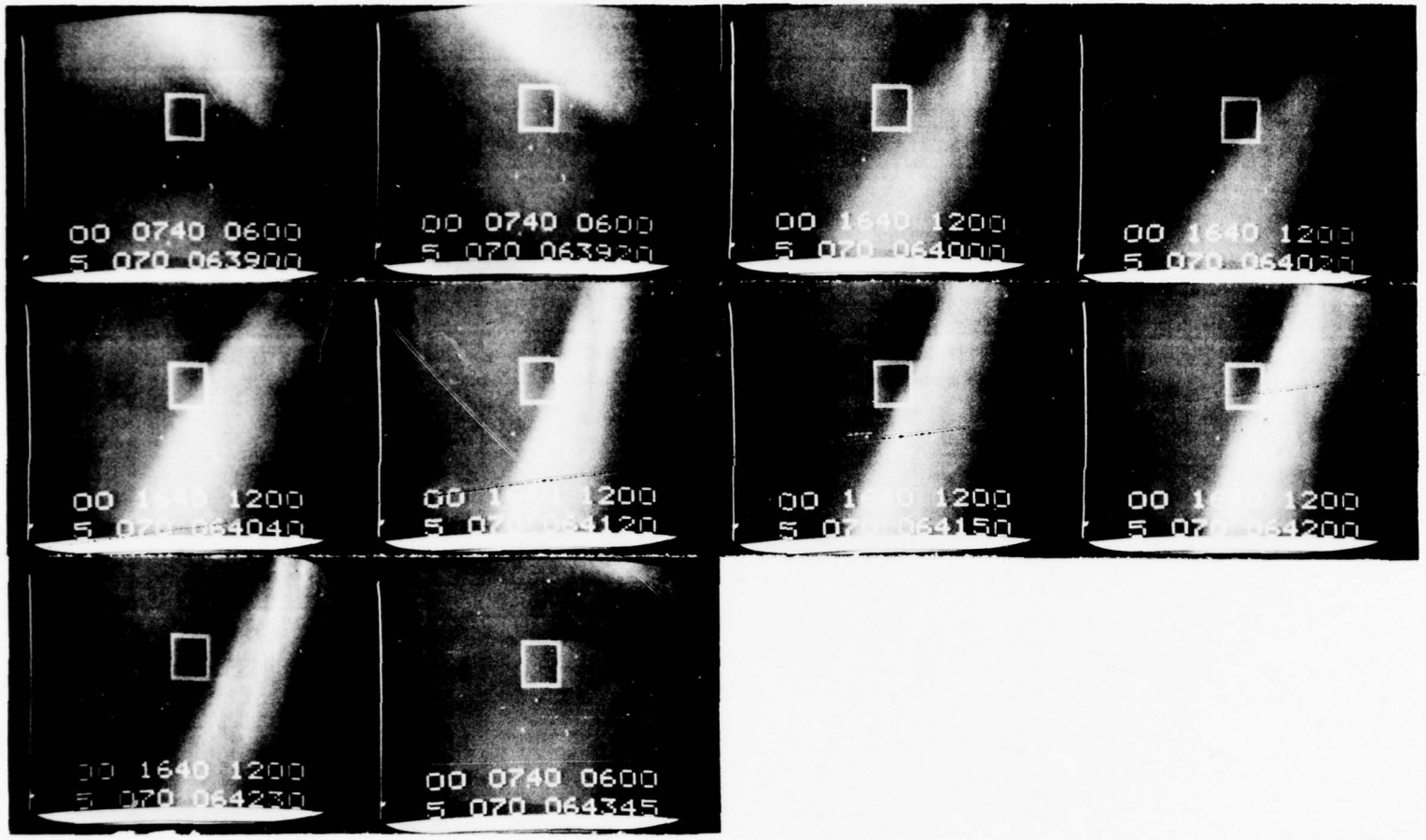

LA-3118-216

FIGURE 74 (Concluded)

c. Electron Density

Typical peak electron density of about $2 \times 10^5/cm^3$ was observed prior to 0625 UT at an altitude of 120 km in the geomagnetic southwest direction. Between this time and 0633 UT the radar operating mode was being changed and no data were taken. However, when measurements were resumed, densities up to $8 \times 10^5/cm^3$ at 120 km were observed in the western sky. Figure 75 displays the density profiles observed at the two antenna azimuth positions used during the launch period (344° and 74°). The profiles on the left were taken at an azimuth of 344° and the ones on the right at an azimuth of 74°. When these results are compared with the boresight TV photographs, it is obvious that the enhancements in density closely correspond to the enhancements in auroral luminosity.

In Figure 76 the 30-s averaged peak density and peak density altitudes are given. Some of the apparent large variations in peak density are due to spatial inhomogeneities between the two regions probed by the radar. However, the large variations in the data taken at one azimuth may be due to temporal variations or drifting of structures into the beam. It is evident from the variation in peak altitudes that the spectrum of the precipitating particles softened considerably at about 0634 UT and hardened again at 0650 UT during the passage of the westward-traveling surge.

d. Correlated Electric Field Measurements

Electric field measurements were made by the radar throughout the experiment, as discussed in Section V-F-2-f above. During the launch period, measurements of electric field were available from each pair of individual vector measurements. The radar began operating in the two-position azimuth mode at 0627:48 UT in support of the rocket experiment, launch of the rocket occurred at 0633:09 UT, and the first pair of vector measurements after launch was complete at 0636:09 UT.

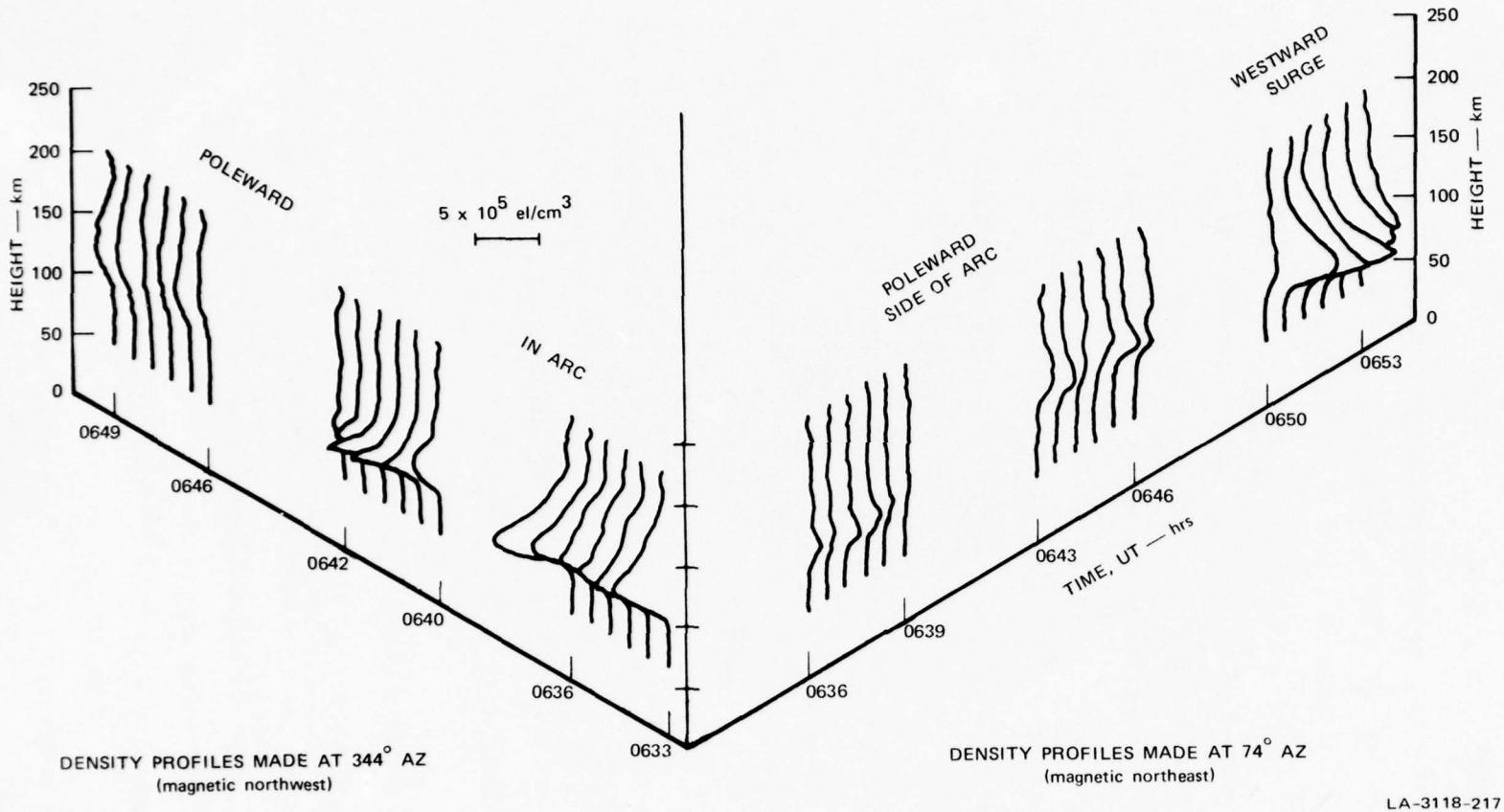

FIGURE 75 ELECTRON-DENSITY PROFILES AT ANTENNA AZIMUTH POSITIONS OF 74° AND 344° DURING THE PERIOD OF THE ROCKET FLIGHT ON 11 MARCH 1975

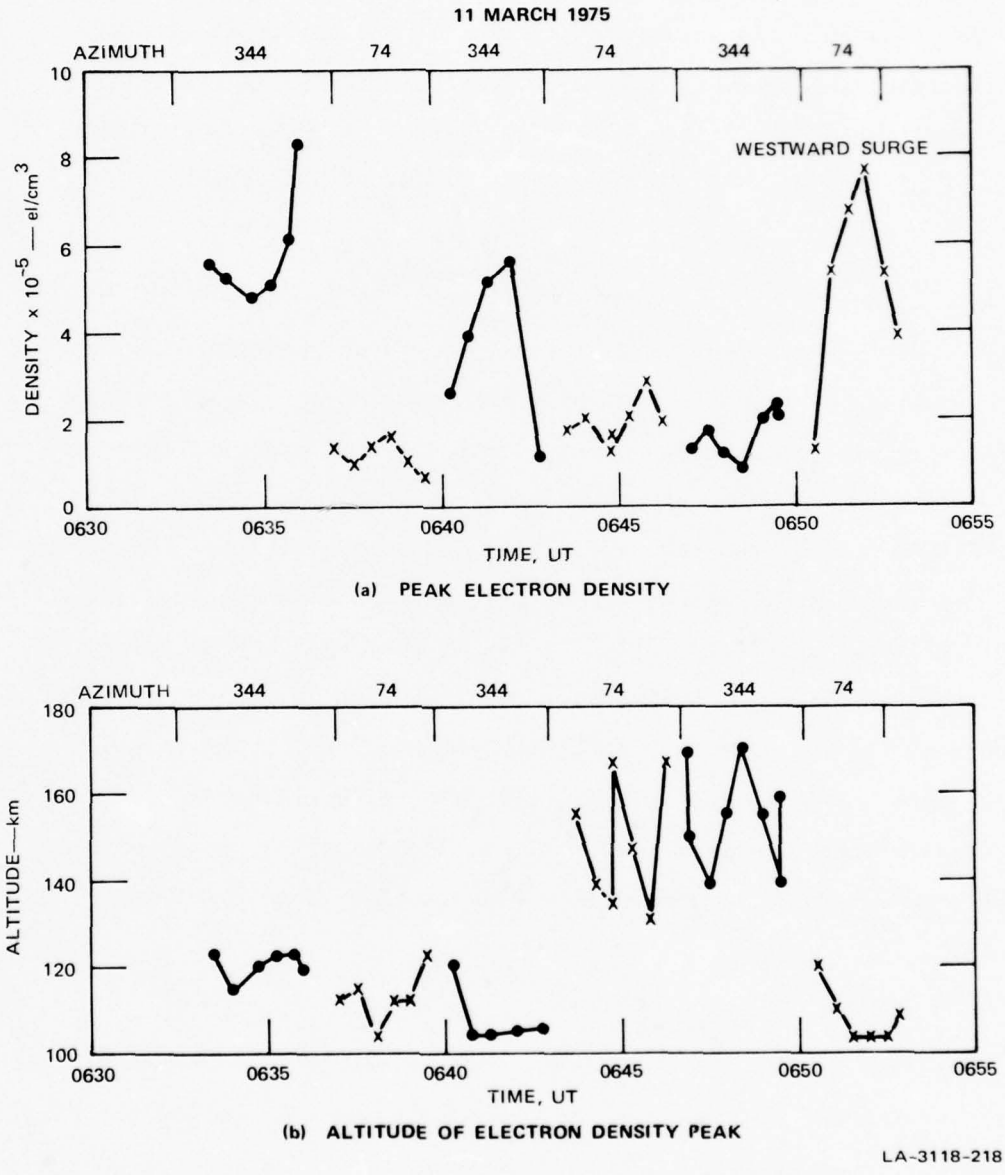

FIGURE 76 DENSITY AND ALTITUDE OF THE E-LAYER PEAK DURING THE PERIOD OF THE ROCKET FLIGHT ON 11 MARCH 1975

The data available at this time represent time averages over the period 0627 to 0636 UT and a spatial average over about 150 km at a geomagnetic latitude of 65.78°. They also represent the closest correlation of electric field measurements available from the radar. Electric field measurements obtained at this time were characterized by an eastward component of 3.7 mV/m and a northward component of 54.3 mV/m.

e. Energy Spectrum of Auroral Electrons

The ionization profiles measured at two different time periods during the rocket flight have been used to obtain an estimate of the incoming auroral electron energy distribution. Figures 77(a) and 77(b) correspond to times when the radar was measuring ionization profiles within the arc and poleward of the arc, respectively. The differential energy distribution within the arc is characterized by very high fluxes, although the distribution is fairly soft with a mean energy of only 3.5 keV. Although the incoming electron flux is greatly reduced poleward of the arc [Figure 77(b)], the energy distribution is actually harder, with a mean energy near 4.4 keV. The relative hardness of the two distributions can be seen directly by comparing the relative shapes of the associated ionization profiles, particularly above 115 km.

4. Summary

This Honest-John Nike-Javelin rocket vehicle was launched into active auroral and geomagnetic conditions. During this period the ring current was recovering from a moderate geomagnetic storm. A large substorm, which began a few minutes after launch, was marked by the passage of a westward-traveling auroral surge.

Just before launch, geomagnetic activity observed by the College magnetometer was under the influence of an eastward equivalent current

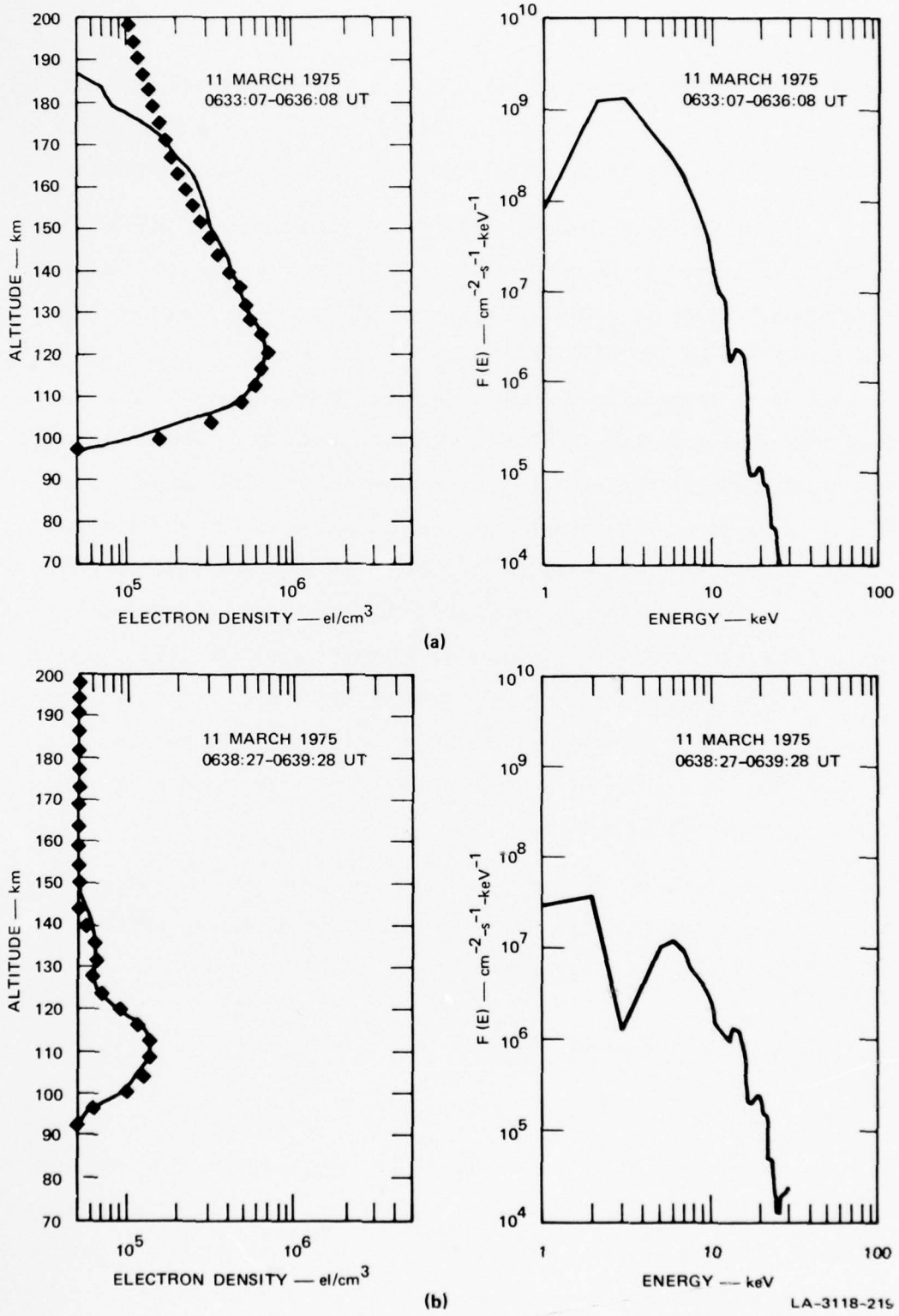

FIGURE 77 ENERGY SPECTRA OF AURORAL ELECTRONS AND ASSOCIATED ELECTRON DENSITY PROFILES FOR TWO TIME PERIODS DURING THE ROCKET FLIGHT OF 0633:09 UT, 11 MARCH 1975. Details are given in the text.

system. But by the time of rocket apogee a strong westward auroral electrojet had developed. However, the radar-derived current densities at 110 km north of Chatanika were highest in the eastward direction.

Electric-field measurements obtained during the launch period by the radar showed a generally northward field that averaged above 50 mVm. The eastward component was smaller and ranged between -6 and 17 mVm. From inspection of the resolved velocities at each range gate, a latitudinal profile of convection electric field could be inferred. The electric field was northward-directed from near Chatanika out to 200 km poleward of the radar, where the electric field reversed direction. Although this field reversal was observed in the higher range gates, which tend to have lower SNRs; the trend is consistent in time and indicates that there may be local regions of eastward current even in situations when magnetometer readings are dominated by westward current. It is interesting that auroral arcs are observed within the region of a northward electric field. It was believed by some that discrete auroral arcs are observed only in regions of southward electric field which lie poleward of the northward field region.

Note that the reversal of the east-west electric field component occurs at about the same time the Poker Flat magnetometer indicated a development of the westward electrojet.

G. 12 March 1975--Sergeant Hydac

1. General

A Sergeant Hydac rocket (IC 519-07-1B) was launched on 12 March at 07:48:10 UT over a bright auroral form. The rocket reached an apogee of 184 km at 225 s after launch, and was above 70 km altitude during the time interval 68 to 381 s after launch (0749:18 to 0754:31 UT). The rocket carried a MULTI payload designed to measure a variety of auroral

and ionospheric phenomena. Instrumentation included infrared radiometers and spectrometers, photometers, an auroral electron analyzer (1 to 30 keV), probes to measure electron density and temperature, and an ion-neutral mass spectrometer.

For several hours before the MULTI launch the Chatanika radar was operated in a continuous azimuthal scan mode (65° elevation) in order to measure ionospheric transport, electron density, and neutral winds. Approximately two minutes before launch the radar mode of operation was changed to a continuous scan in elevation, with the radar azimuth fixed in the geomagnetic meridian. The objective of operating in this manner was to measure the latitudinal variation of auroral ionization and related parameters.

2. Background Measurements

a. Geomagnetic Conditions

Geomagnetic records for the evening of 12 March are shown in Figure 78. At College, starting at 0500 UT a positive enhancement of less than 80 γ developed, indicating an eastward electrojet. At approximately 0730 UT the geomagnetic H-component turned negative, culminating as a nearly 200-γ negative bay at 0745 UT. The onset of this bay occurred simultaneously with the equatorward motion of the bright auroral arc as seen in the Chatanika all-sky photographs. This negative bay is presumably due to a westward electrojet associated with the visible arc.

b. Auroral Conditions

The evening of 12 March was characterized by very active aurora. Auroral conditions as monitored by the Chatanika all-sky camera are shown in Figure 79. During the hour before launch the only aurora visible was near the northern horizon. At about 0740 UT the aurora

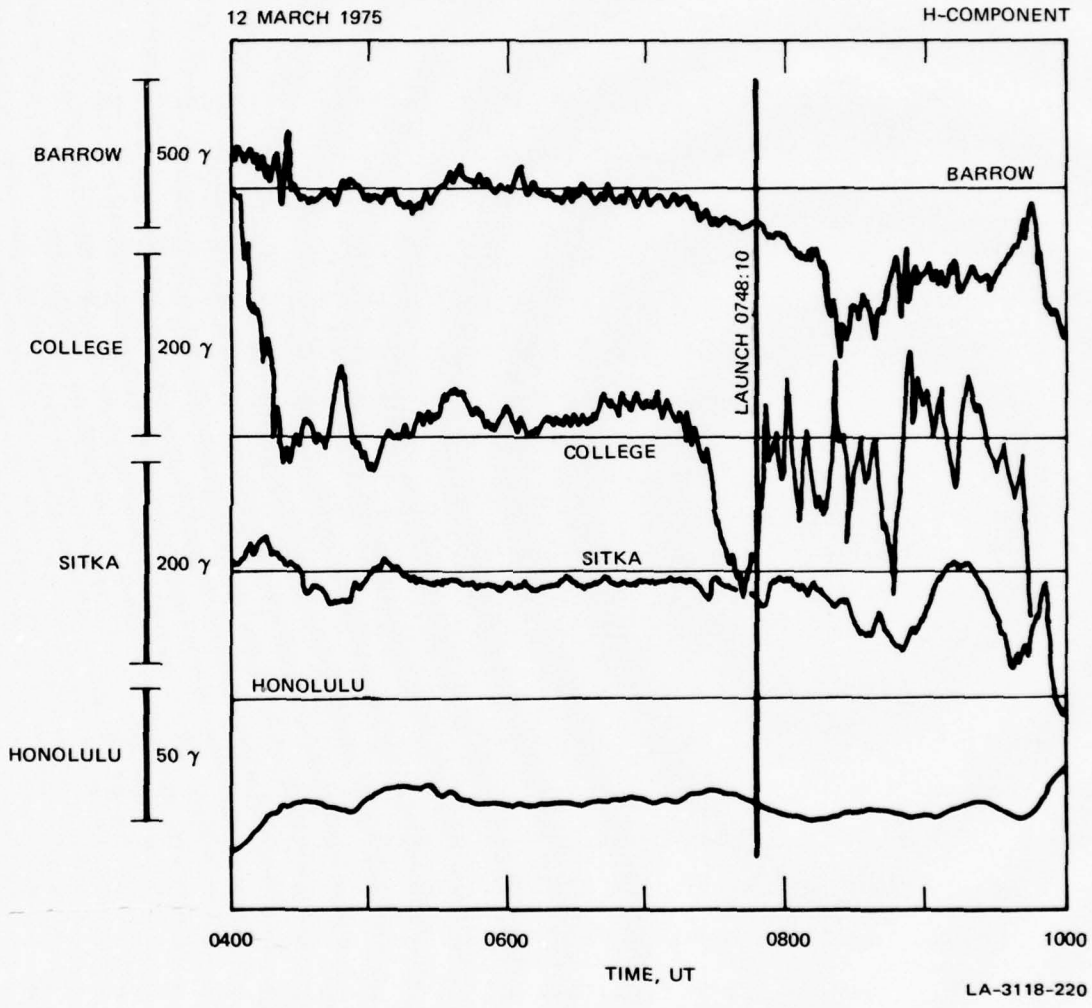

FIGURE 78 H-COMPONENT MAGNETOGRAMS ON 12 MARCH 1975 FROM FOUR STATIONS DISTRIBUTED IN LATITUDE BUT IN THE SAME LOCAL TIME SECTOR AS THE ROCKET TRAJECTORY

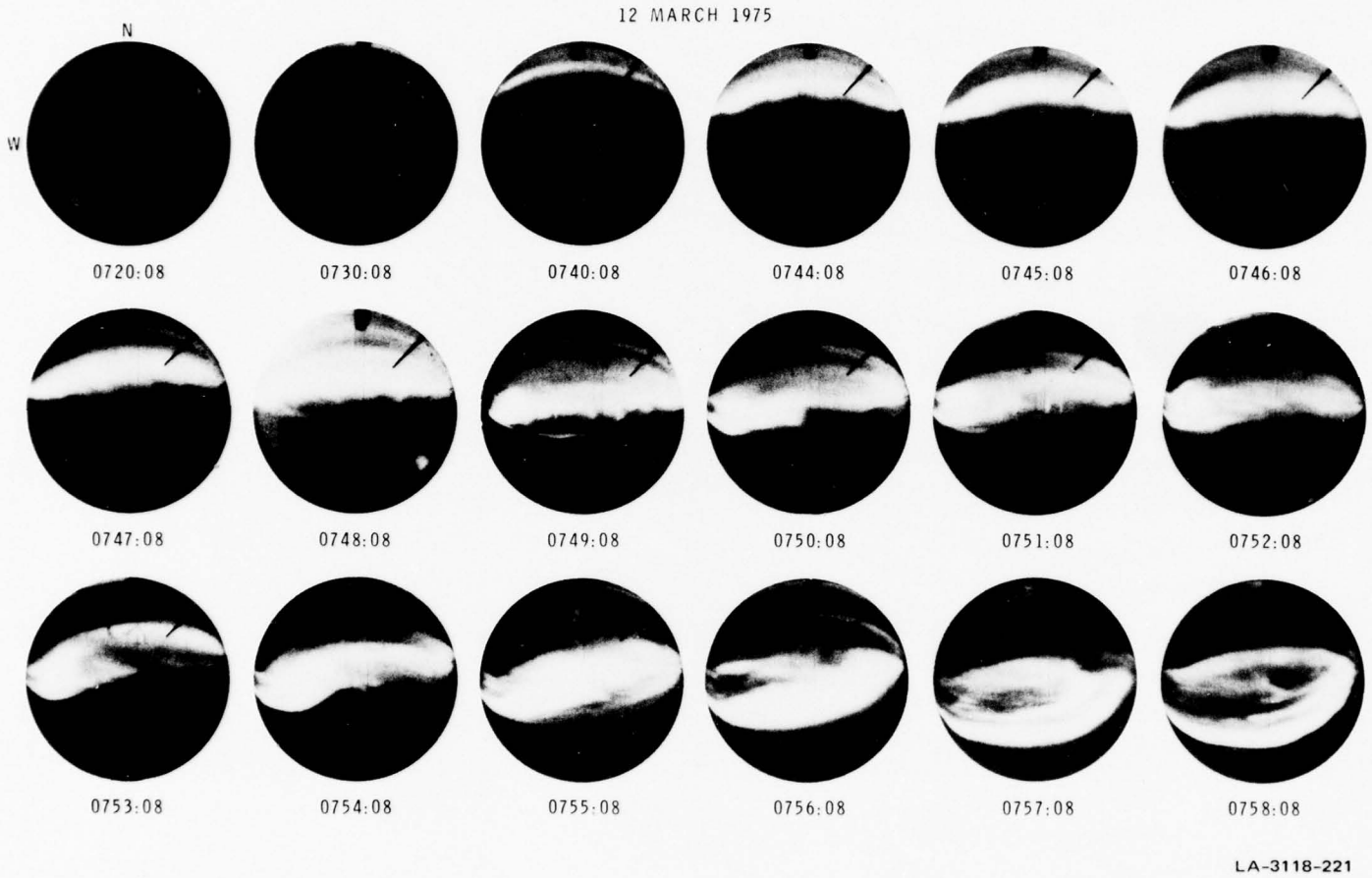

FIGURE 79 ALL-SKY PHOTOGRAPHS FROM CHATANIKA FOR THE PERIOD 0720-0758 UT, 12 MARCH 1975

moved southward, followed by a substantial brightening at approximately 0745 UT. At 0750 UT a westward-traveling surge could be seen at the eastern horizon; it passed over Chatanika sometime after 0755 UT.

The aurora was also photographed from Fort Yukon as shown in Figure 80. A bright arc near zenith was visible there as early as 0700 UT. The rapid southward motion at 0740 is quite apparent.

c. Absorption

The College riometer record is shown in Figure 81. In the early evening (0600 to 0730 UT) there was a modest level of relatively constant absorption. At 0740 UT there was a sharp rise in absorption, coinciding with the southward motion and brightening of the visual aurora. The riometer trace from 0800 to 0810 UT was degraded by radio interference.

d. Electron Density and Conductivities

Contours of electron density for the time period 0630 to 0736 UT are shown in Figure 82. Data were obtained while the radar was scanning in azimuth at an elevation of 65°, with 6 minutes required for each scan. As a result, the variations in density on time scales less than 6 minutes probably represent spatial rather than temporal changes. No data were obtained in the time interval between 0640 UT and 0646 UT.

The azimuth of the radar is indicated in the upper part of Figure 82. Also noted (vertical shaded bars) is the azimuth along which the MULTI rocket was later launched. A general increase in electron density is evident during this one-hour period prior to launch. This is consistent with the increasing magnetic and auroral activity.

The spatial and temporal variation of the electron density at the time of the MULTI flight is discussed in Section V-G-3.

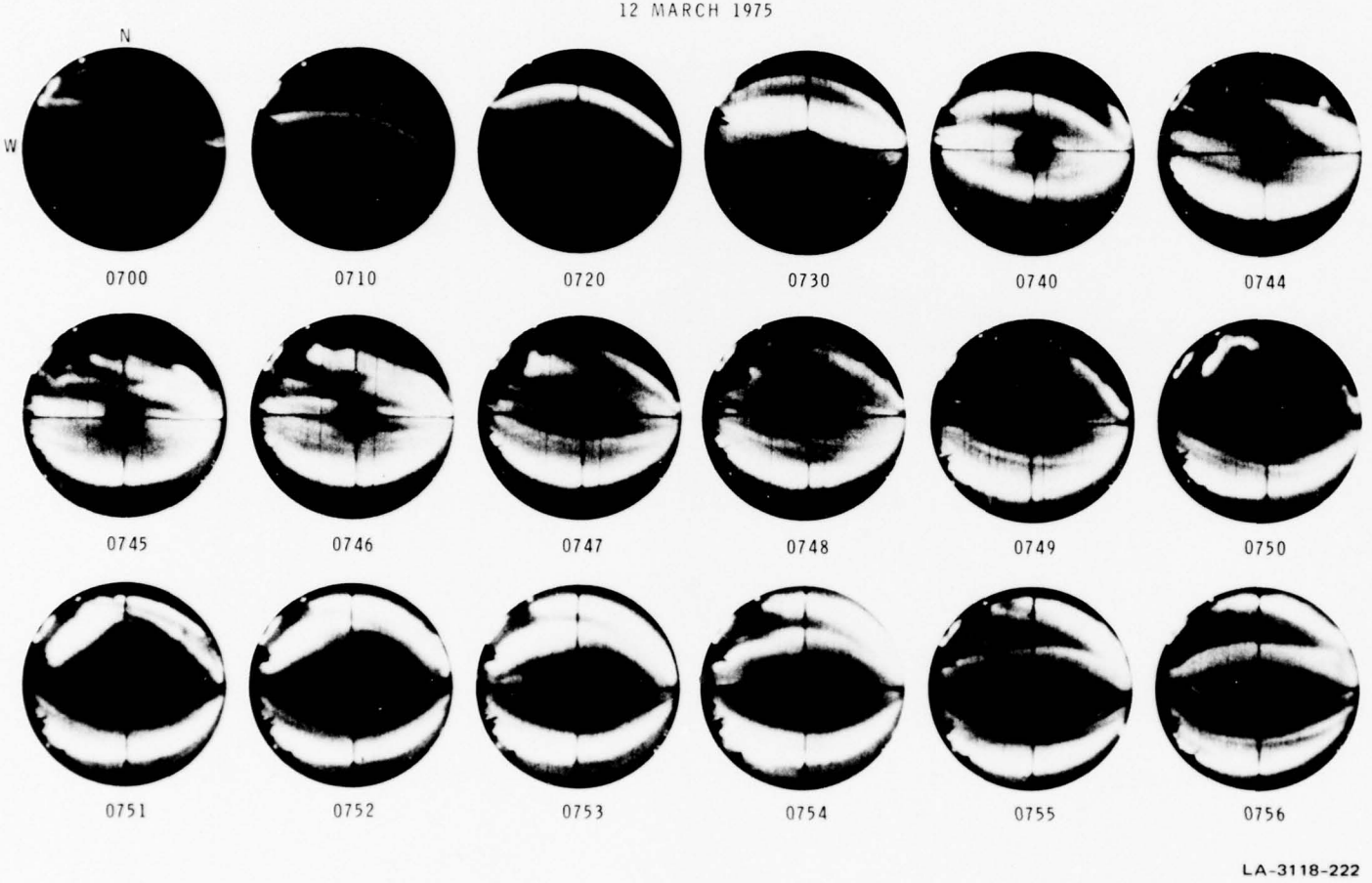

FIGURE 80 ALL-SKY PHOTOGRAPHS FROM FORT YUKON FOR THE PERIOD 0700-0756 UT, 12 MARCH 1975

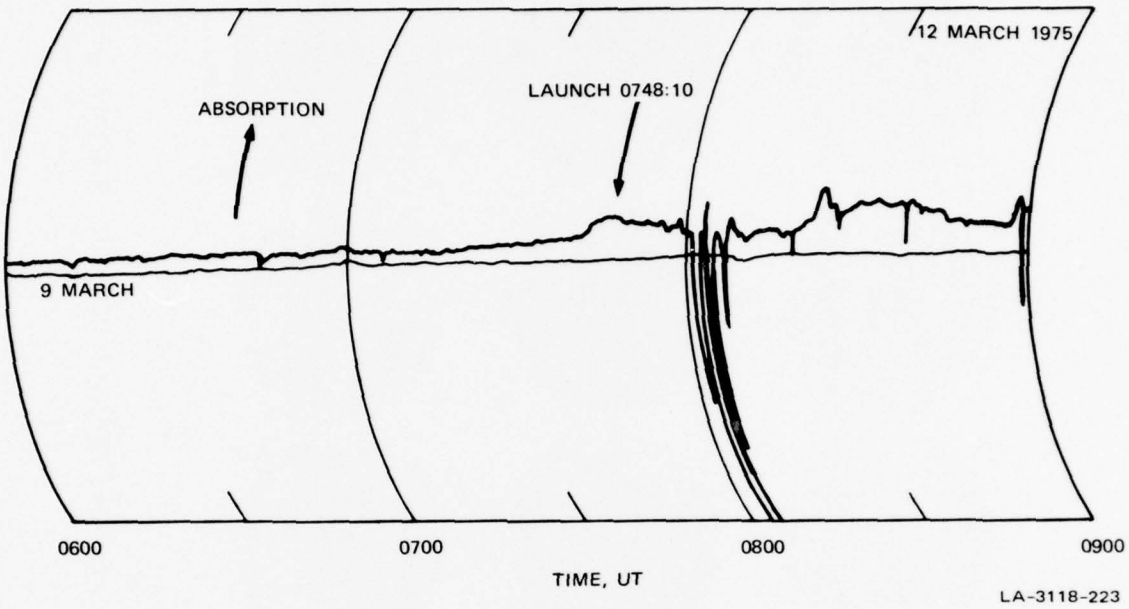

FIGURE 81 COLLEGE RIOMETER RECORD FOR 12 MARCH 1975. The record for 9 March 1975 is representative of a quiet day.

The variation of the height-integrated Hall and Pedersen conductivities is shown in Figure 83. The conductivities were computed from electron density data sampled during the 6 minutes required for each full scan in azimuth. The increase in conductivity before launch is another indication of the increased auroral precipitation.

e. Electric Field and Current

The ionospheric electric field during the two hours before the MULTI launch is indicated in Figure 84. Both the geomagnetic north and the geomagnetic east components are shown. It can be seen that the electric field was always northward with a magnitude of about 20 mV/m in the hour before launch. The east-west component was smaller, and primarily directed eastward.

The height-integrated electric current flowing horizontally in the ionosphere before launch is plotted in Figure 85. The components

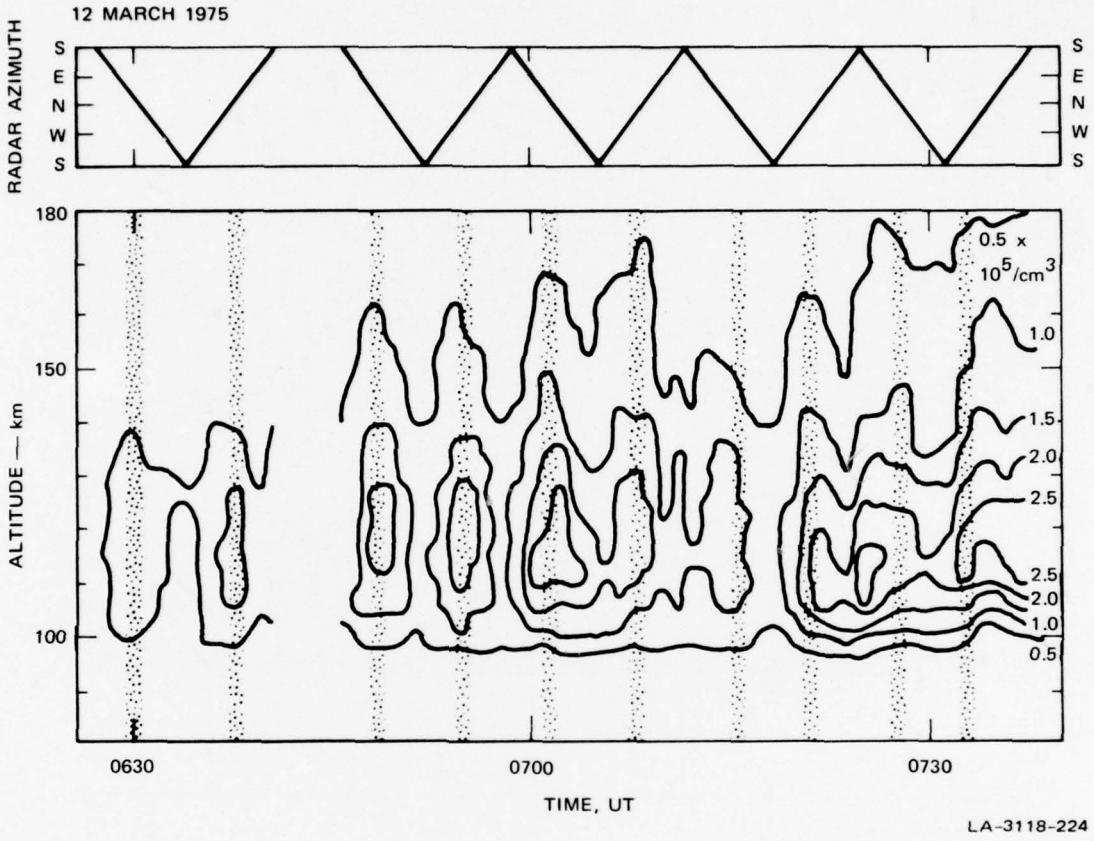

FIGURE 82 BACKGROUND CONTOURS (6-Minute Averages) OF ELECTRON DENSITY FOR THE EXPERIMENT ON 12 MARCH 1975

are computed from the radar measurements of electric fields and conductivities from each azimuthal scan. As a result they are representative of current flow in the ionosphere overhead at Chatanika.

It can be seen that the electrojet current was predominantly eastward, with a magnitude between 10 and 20 A/m, in the period before the MULTI launch. This is consistent with the College H-component magnetic records (Figure 78), which indicated a positive bay at that time.

f. Neutral Wind

The neutral wind determined from the radar measurements in the period before launch is shown in Figure 86. The large variable

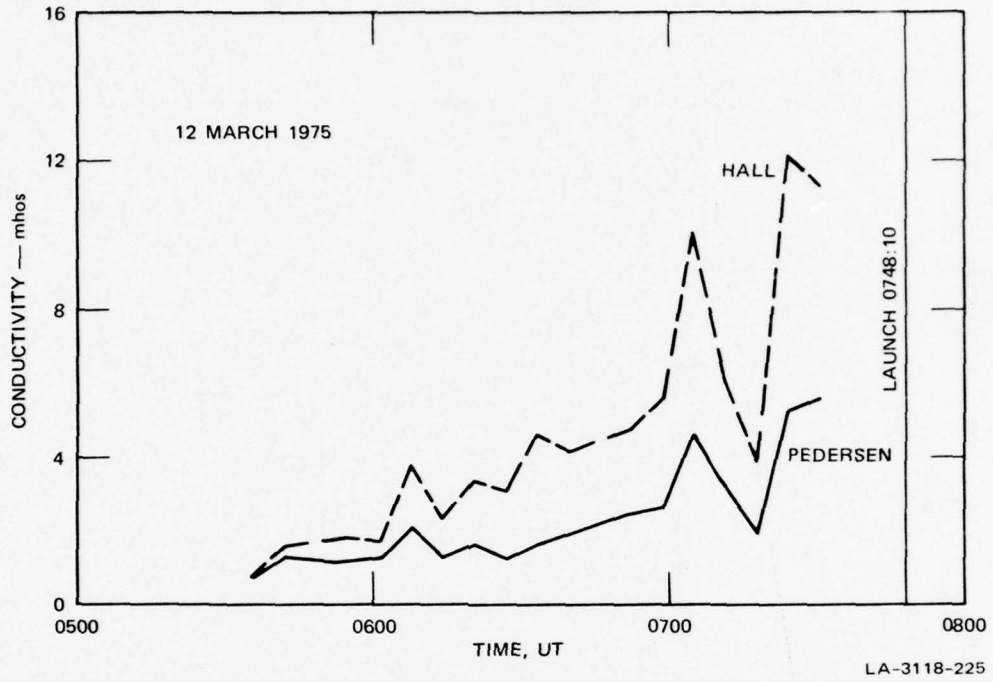

FIGURE 83 HEIGHT-INTEGRATED CONDUCTIVITIES FOR THE EXPERIMENT ON 12 MARCH 1975

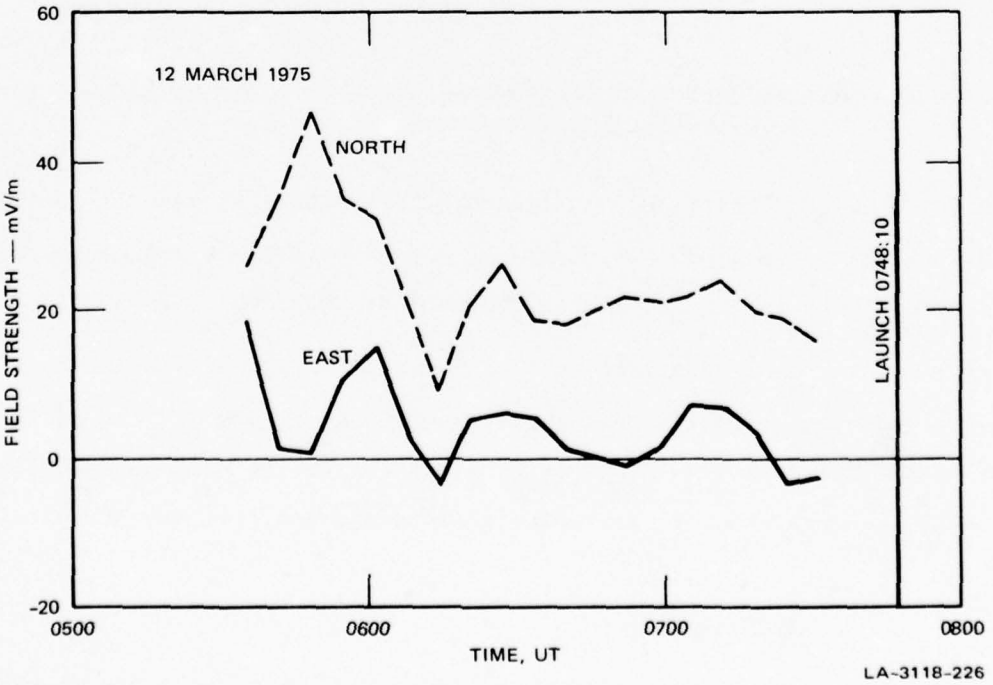

FIGURE 84 ELECTRIC FIELD FOR THE EXPERIMENT ON 12 MARCH 1975

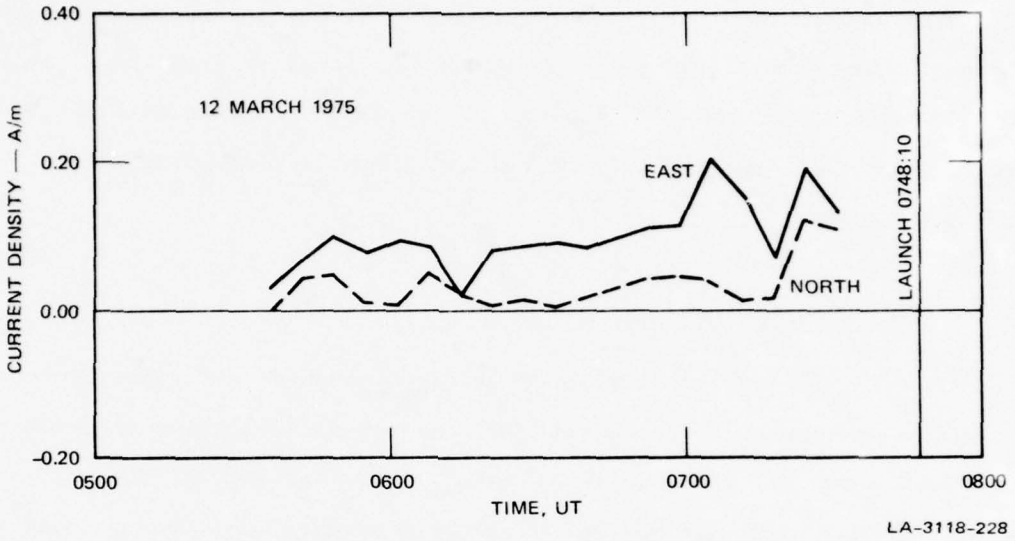

FIGURE 85 HEIGHT-INTEGRATED CURRENT DENSITY FOR THE EXPERIMENT ON 12 MARCH 1975

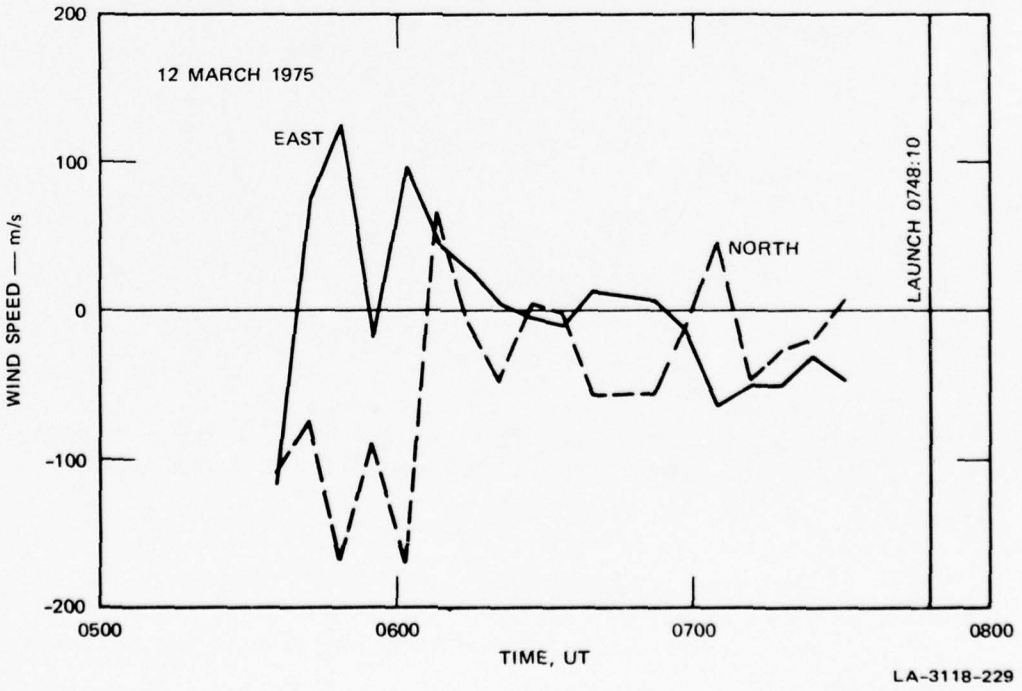

FIGURE 86 HEIGHT-AVERAGED E-REGION NEUTRAL WIND FOR THE EXPERIMENT ON 12 MARCH 1975

wind indicated in the time period before 0730 UT may be due to measurement uncertainty because of the low ionospheric densities at that time. In the half-hour before the MULTI launch the wind had a consistently westward component of approximately 50 m/s and a smaller, more variable northward component.

g. *Energy Deposition*

The energy dissipated in the ionosphere and upper atmosphere by the two sources of joule heating and auroral particle precipitation is shown in Figure 87. Early in the evening, joule heating was the major energy source. Later, as auroral activity increased, the energy input by auroral particles became more important.

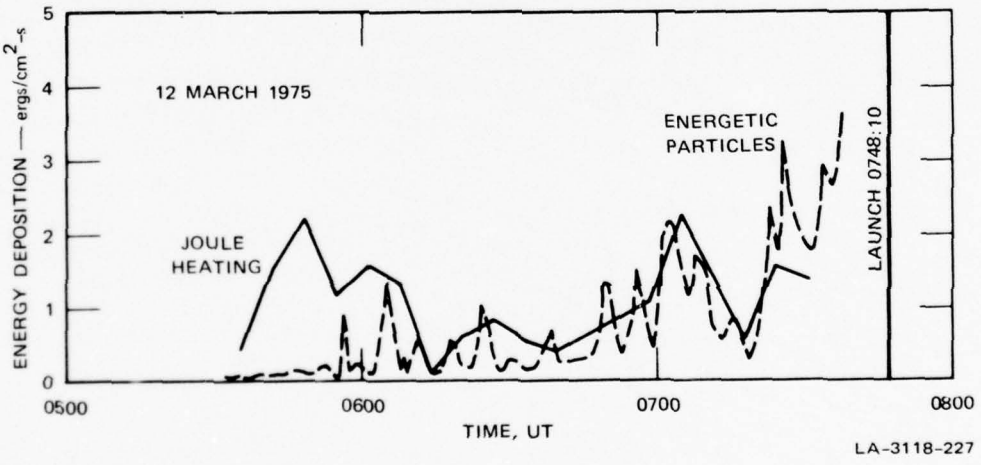

FIGURE 87 JOULE HEATING AND ENERGETIC PARTICLE CONTRIBUTIONS TO TOTAL ENERGY DEPOSITION FOR THE EXPERIMENT ON 12 MARCH 1975

h. Homer Auroral Radar Observations

The DNA-609 auroral radar at Homer, Alaska was operated during the MULTI launch period (0741 to 0803 UT). Selected auroral clutter maps are presented in Figure 88 in an all-sky format as if observed from Chatanika.

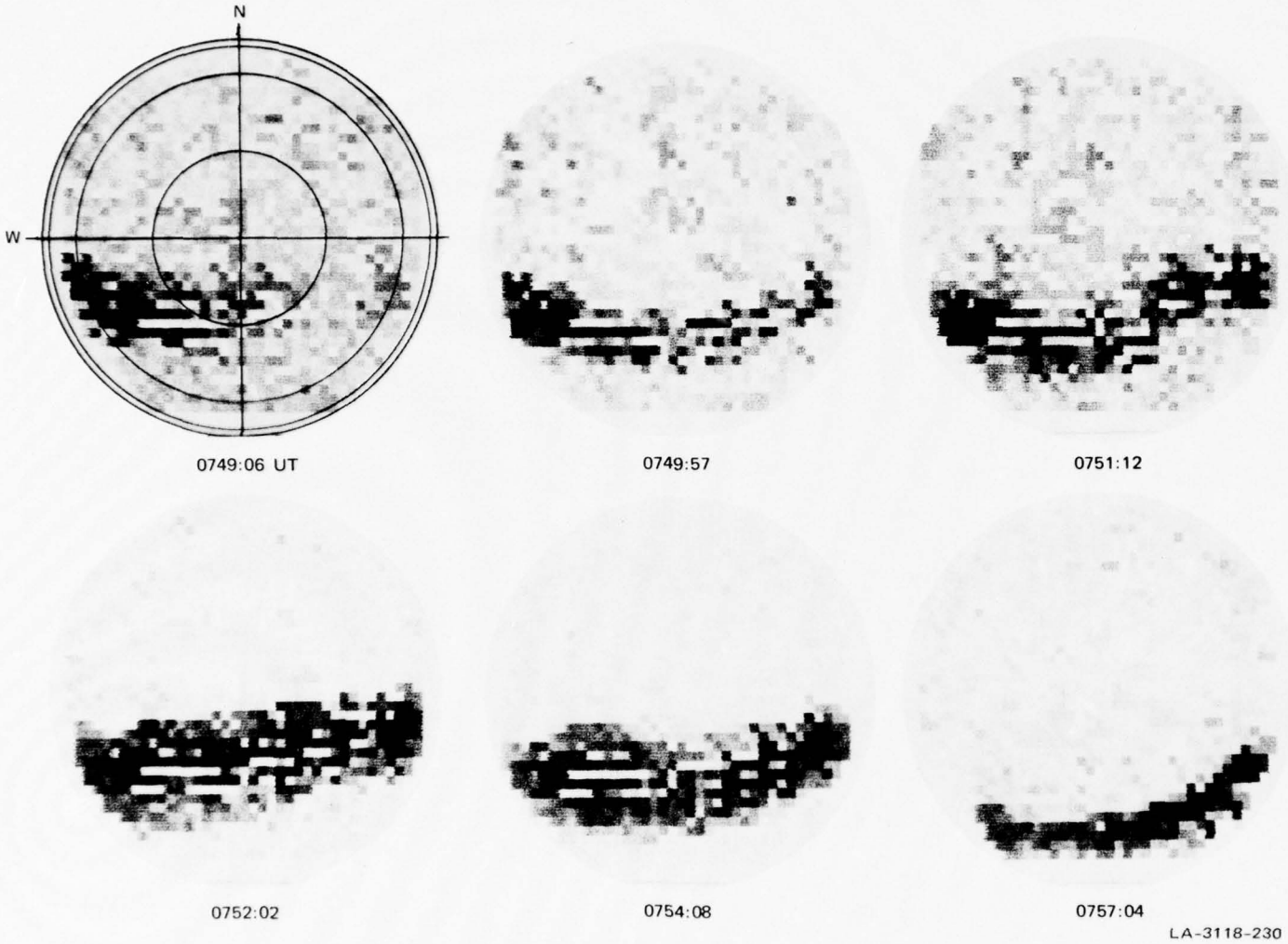

FIGURE 88 AURORAL-CLUTTER MAPS FROM THE HOMER RADAR DURING THE MULTI-ROCKET FLIGHT, 12 MARCH 1975

The region of auroral clutter echoes is typically associated with a high electric field strength (>30 mV/m) and an eastward electrojet. A comparison of the Homer radar data with the Chatanika all-sky photographs (Figure 79) shows that the radar echoes lie just south of the equatorward edge of the discrete visual aurora. Equatorward movement of the visual aurora is accompanied by a similar movement of the radar aurora. These data confirm the interpretation of the prelaunch ionosphere as a region of eastward current equatorward of the discrete aurora.

3. Correlated Measurements

When the decision was made to commit the MULTI rocket for a launch, the operation of the radar was changed to an automatic elevation scan mode. This was the first time such an operating mode was used at Chatanika. Improvements made to the radar system during the winter of 1974-75 included a computer control that enables automatic rapid scans in elevation at a fixed azimuth. When the radar azimuth lies along the geomagnetic meridian, a mechanical scan in elevation produces a two-dimensional (altitude, latitude) cross-sectional map of the auroral ionosphere (see Figure 89).

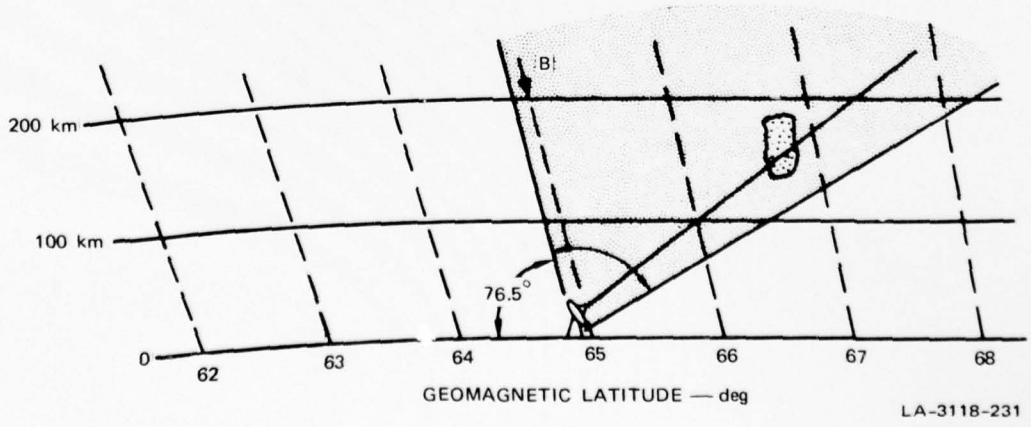

FIGURE 89 SCHEMATIC REPRESENTATION OF MERIDIAN-PLANE MAP OF THE IONOSPHERE OBTAINED BY THE CHATANIKA RADAR ON 12 MARCH 1975. Shaded area indicates region probed by the radar.

Starting at 0746:19 UT, the radar scanned between elevations of 30° and 103.5° in order to survey the region to be traversed by the rocket. Each scan was made at a rate of 0.33°/s and required approximately 3 m 40 s. The scan began before the MULTI launch, as shown in Figure 90. The radar beam moved southward during this scan. Electron density measurements are presented in a geographic format with isodensity contours in units of $10^5/cm^3$ at intervals of 1, 2, 3, 4, 5, 6, and 8. Data were averaged over 5-s intervals, corresponding to about 4 km of horizontal distance. Density measurements were available for every 4.5 km of range along the radar line of sight; completely independent measurements were made every 10 km. The trajectory of the MULTI rocket is also indicated. It can be seen that the maximum ionization occurred over a region extending to about 100 km north of Chatanika and including the trajectory upleg. This is consistent with the morphology visible in the simultaneous all-sky camera photographs.

In Figures 90 to 93 are shown the scan data obtained during and immediately after the MULTI flight. The regions of each scan that are potentially contaminated by rocket echoes are indicated by shading in Figures 90 to 92. The rocket echoes significantly distort the density contours only when detected by the main beam of the radar. This apparently occurred in the southernmost part of Figure 90, near the rocket apogee in Figure 91, and near the rocket reentry point in Figure 92.

It is evident from the ionization plots that the rocket penetrated the brightest part of the auroral form on its upleg and that the rocket descended through a region of less ionization. However, by comparing Figures 90 and 91 we see that the downleg region had been "predosed" by particle precipitations before launch. We also note that the ionization (and auroral precipitation) was relatively uniform before launch, and that greater spatial variation and structure are apparent in the following scans. Data taken immediately following the MULTI apogee

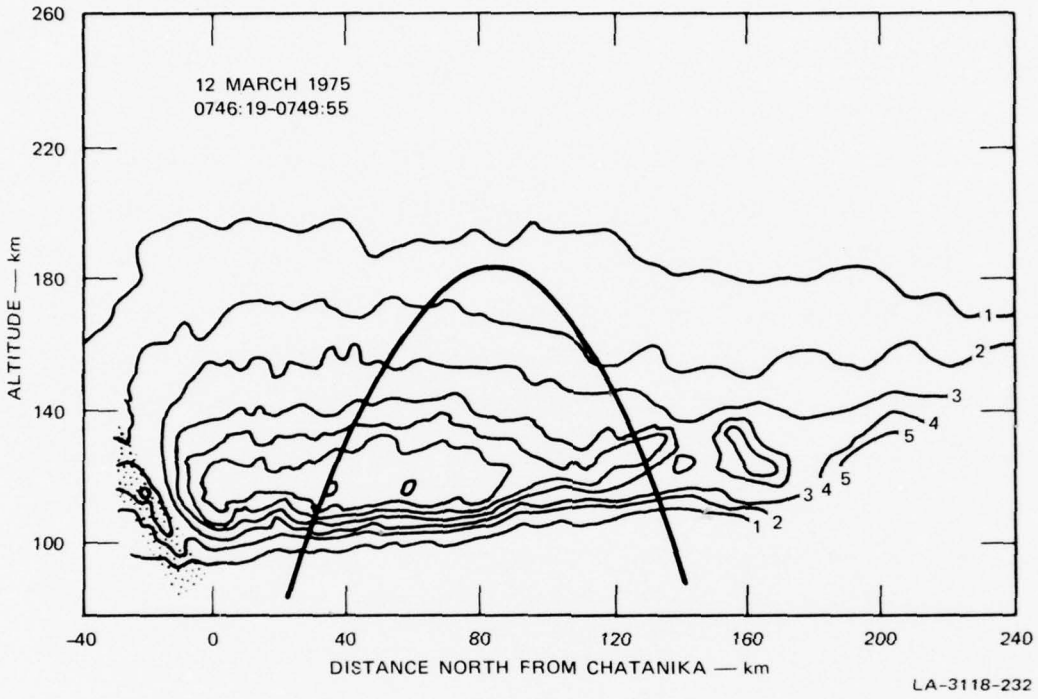

FIGURE 90 CONTOURS OF ELECTRON DENSITY IN A MERIDIAN-PLANE MAP BASED ON RADAR OBSERVATIONS FROM 0746:19 TO 0749:55 UT, 12 MARCH 1975. Isodensity contours are in units of $10^5/cm^3$ at intervals of 1, 2, 3, 4, 5, 6, and 8. Also indicated are a meridian-plane projection of the MULTI-rocket trajectory (solid line), and area of potential contamination from rocket echoes (shaded area).

time are a prime data set for "input-output" evaluations. In Figure 94 the rocket location at 30-s intervals is indicated by the letters B through K. The radar look direction at corresponding times lay along the line connecting the lettered bars. From 0752 to 0753:30 UT the radar and rocket were measuring ionospheric parameters along the same geomagnetic field lines. A comparison of the simultaneous rocket and radar data is expected to be very fruitful as tests of the UNTANGLE technique and optical emissions codes, and possibly as a determination of the effective recombination coefficient in the E-region.

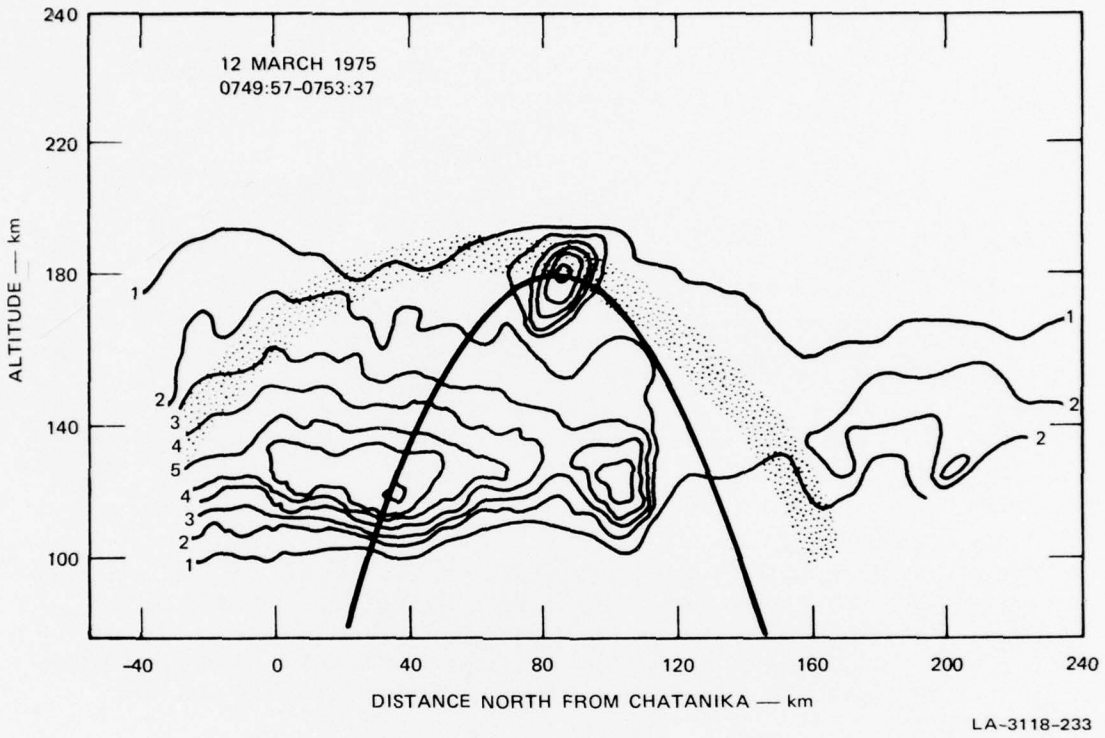

FIGURE 91 CONTOURS OF ELECTRON DENSITY IN A MERIDIAN-PLANE MAP BASED ON RADAR OBSERVATIONS FROM 0749:57 TO 0753:37 UT, 12 MARCH 1975. Isodensity contours are in units of $10^5/cm^3$ at Intervals of 1, 2, 3, 4, 5, 6, and 8. Also indicated are a meridian-plane projection of the MULTI-rocket trajectory (solid line), and area of potential contamination from rocket echoes (shaded area).

The above discussion shows the use of electron density measurements made during an elevation scan to indicate ionization and precipitation morphology. In addition, these data can be used to define the spatial variation of energy deposition and conductivity, as well as the latitudinal variation of the energy distribution of incident electrons. For example, in Figure 90 the broad, uniform region of ionization with maximum density near 120-km altitude is due to a "soft" incoming electron distribution with mean energy near 4 keV and little latitudinal variation. In order to quantitatively compute these parameters it is necessary to transform the density profiles to field-aligned profiles, since the incident electrons penetrate the atmosphere in a direction parallel to

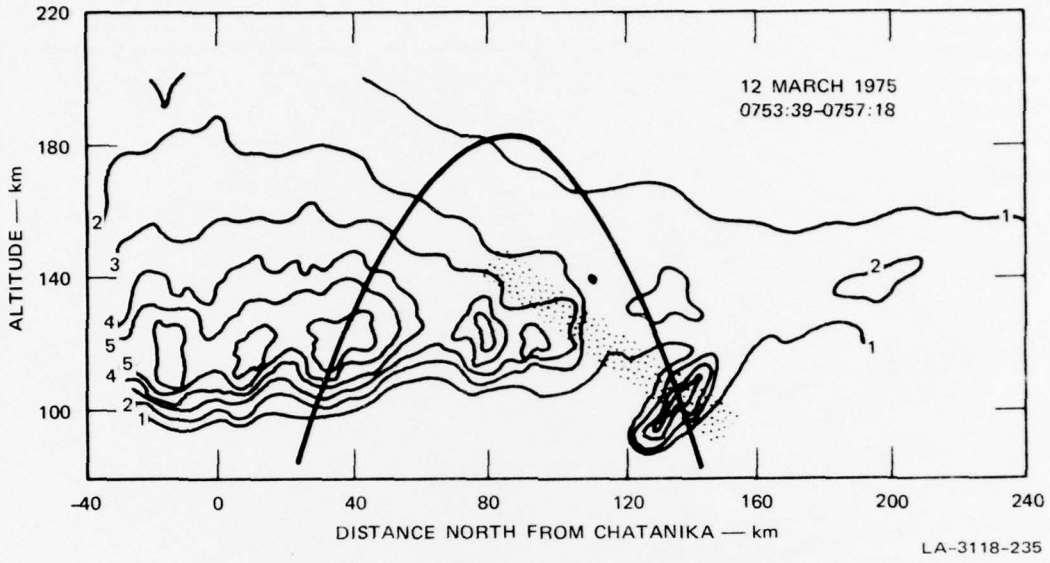

FIGURE 92 CONTOURS OF ELECTRON DENSITY IN A MERIDIAN-PLANE MAP BASED ON RADAR OBSERVATIONS FROM 0753:39 TO 0757:18 UT, 12 MARCH 1975. Isodensity contours are in units of $10^5/cm^3$ at intervals of 1, 2, 3, 4, 5, and 6. Also indicated are a meridian-plane projection of the MULTI-rocket trajectory (solid line), and area of potential contamination from rocket echoes (shaded area).

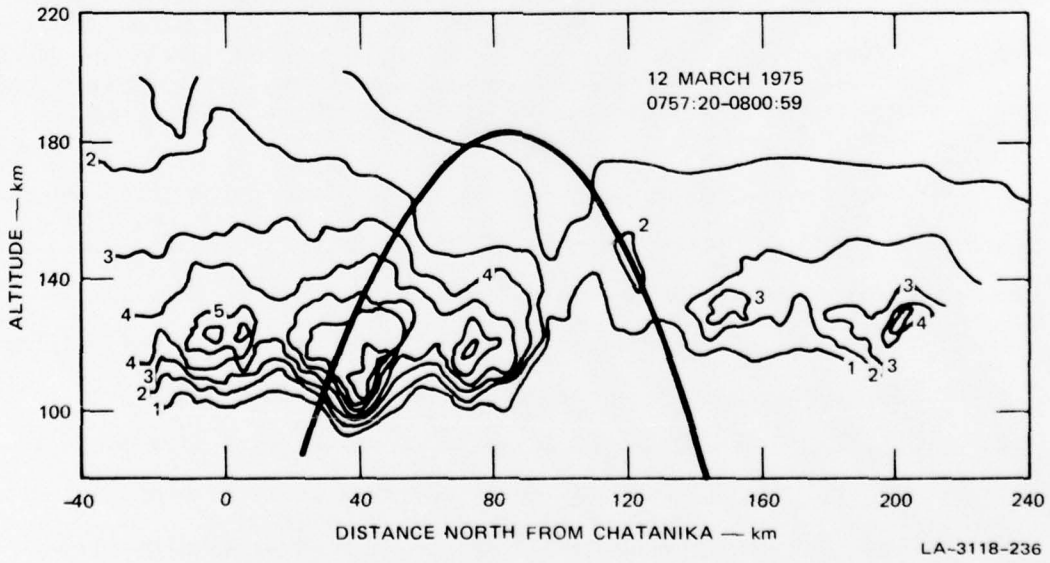

FIGURE 93 CONTOURS OF ELECTRON DENSITY IN A MERIDIAN-PLANE MAP BASED ON RADAR OBSERVATIONS FROM 0757:20 TO 0800:59 UT, 12 MARCH 1975 Isodensity contours are in units of $10^5/cm^3$ at intervals of 1, 2, 3, 4, 5, 6, and 8. Also indicated is a meridian-plane projection of the MULTI-rocket trajectory (solid line).

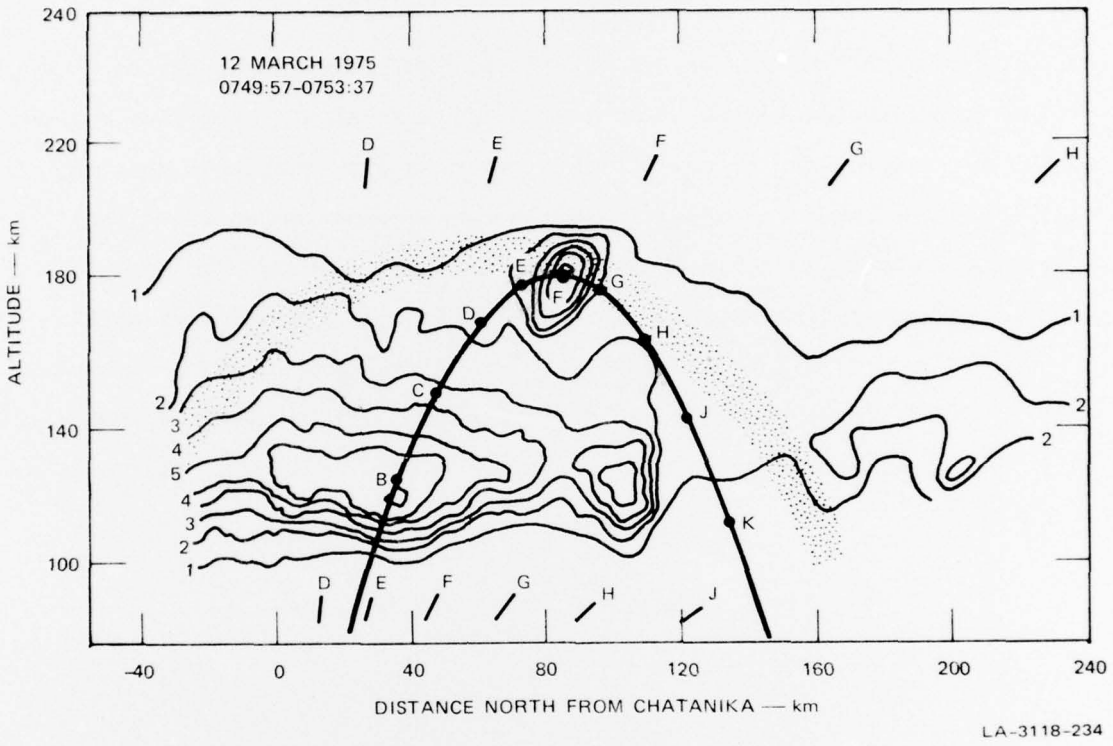

FIGURE 94 CONTOURS OF ELECTRON DENSITY IN A MERIDIAN-PLANE MAP AND A MERIDIAN-PLANE PROJECTION OF THE MULTI-ROCKET TRAJECTORY FOR THE TIME PERIOD 0749:57 TO 0753:37 UT, 12 MARCH 1975. Isodensity contours are in units of $10^5/cm^3$ at Intervals of 1, 2, 3, 4, 5, 6, and 8. Also indicated (by the letters B to K) are the rocket locations and radar look angles at 30-s intervals. The shaded area indicates region of potential contamination from rocket echoes.

the geomagnetic field lines. The software to accomplish this transformation is being developed, and it is expected that a complete analysis and interpretation of these meridian scans will be made available in a separate HAES report.

4. Summary

During the hour prior to the MULTI launch the auroral activity was to the north of Chatanika. The ionosphere above Chatanika was moderately disturbed with peak E-region electron densities near $2 \times 10^5/cm^3$, a northward electric field of about 20 mV/m, and an eastward electrojet of

10 to 20 A/m. Within 20 minutes before the MULTI launch the aurora rapidly moved southward and brightened. The Auroral structure was accompanied by a westward electrojet that produced a 200-γ negative bay. A westward-traveling surge appeared on the eastern horizon at about the time of the rocket launch. On the upleg of its trajectory the rocket penetrated a bright auroral form with peak electron densities of about $8 \times 10^5/cm^3$ near 120 km. The downleg of the trajectory appears to have been poleward of the most intense precipitation. It is expected that a detailed comparison of the simultaneous rocket and radar data will be very fruitful.

VI CONCLUSIONS

Background observations and Chatanika DNA 617 incoherent-scatter radar data obtained during the ICECAP '75 operation are collected and interpreted for rocket launches occurring during 26 February and 1, 4, 6, 10, 11, and 12 March 1975.

Observations made during the daytime launches (26 February, 1 March, and 6 March) are summarized in Table 6. Typically, little or no E-layer was present and electron densities at these altitudes were less than $8 \times 10^4/cm^3$. However, in the D-region, densities were less than $10^4/cm^3$. Associated with these low densities were low height-integrated conductivities--about 3 and 7 mhos for the Pedersen and Hall components. Since the radar made single-position observations during the launch period on 26 February, no vector quantities were obtained. However, for the launch on 1 March and at 0343 UT on 6 March, vector measurements were made. Joule dissipation during these launch periods was very low, typically less than 0.1 ergs/cm^2-s. Energy deposited by precipating electrons was estimated to be less than 1 erg/cm^2-s. It is estimated that the contribution due to photoionization is only of the order of 10% of the measured electron density profile.

Observations made during the evening launch periods on 6, 10, 11, and 12 March 1975 are summarized in Table 7. Because the radar malfunctioned, data were not obtained during the 4 March launch. The evening launches generally occurred during periods of enhanced geomagnetic activity.

By the time of the evening launch on 6 March 1975 the eastward ionospheric current system had become moderately intense and extended at

Table 6

COMPARISON OF PARAMETERS OBSERVED
DURING THE DAYTIME ICECAP '75 LAUNCHES

Conditions	26 February 2250 UT IC 503.22-1	1 March 0100 UT IC 503.14-3	6 March 0343 UT IC 507.11-1
Solar zenith angle (deg)	74.3	80.0	93.5
College ΔH	$\pm 5\ \gamma$	$\pm 10\ \gamma$	$+10\ \gamma$
Peak electron density	$8 \times 10^4/cm^3$	$8.7 \times 10^4/cm^3$	$2.5 \times 10^4/cm^3$
Integrated Pedersen conductivity (mhos)	2.7	2.3	0.63
Integrated Hall conductivity (mhos)	7.3	6.6	2.2
Electric field strength (mV/m)	Not measured	3.5 east 1.4 north	1.6 0.4
Current density (A/m)	Not measured	0.025 east -0.003 north	-0.002 -0.003
Joule heating ($ergs/cm^2$-s)	Not measured	0.08	>0.01
Particle energy deposition ($ergs/cm^2$-s)	1.5*	1.2*	0.16*
Neutral wind speed (m/s)	Not measured	30 east 41 north	-25.8 11.8
Time of measurement, UT	2251 to 2252	0100 to 0107	0344 to 0349

*Contaminated by UV photoionization.

least between College and Barrow. Electron density measurements, obtained as a function of azimuth, showed that electron precipitation had increased sharply to the north of Chatanika, giving rise to large density gradients across geomagnetic L-shells. Radar electric field measurements indicated that a northward field of 26 mV/m predominated during the launch interval, with an eastward component of 6 mV/m. This, coupled with a small eastward

Table 7

COMPARISON OF PARAMETERS OBSERVED DURING THE NIGHTTIME ICECAP '75 LAUNCHES

Conditions	6 March 0616:30 UT IC 507.11-3	10 March 0912:20 UT IC 507.11-2A	11 March 0633:09 UT IC 511.21-1A	12 March 0748:10 UT IC 519.07-1B
Solar zenith angle (deg)	109.0	118.6	108.8	114.1
College ΔH	+45 γ	-500 γ	+10 γ (just prior to a large substorm)	Recovery phase of -200 γ bay
Peak electron density	$>10^5/cm^3$	$13.1 \times 10^5/cm^3$	$3.8 \times 10^5/cm^3$	$2.5 \times 10^5/cm^3$
Integrated Pedersen conductivity (mhos)	4.2	21.6	19	7.8
Integrated Hall conductivity (mhos)	6.6	84.6	30	11.4
Electric field strength (mV/m)	5.8 east 25.5 north	-2.1 -15.4	3.7 54.3	-2.7 15.7
Current density (A/m)	0.12 east 0.03 north	-1.2 +0.5	1.15 0.36	0.13 0.11
Joule heating ($ergs/cm^2$-s)	1.4	-5.2	23.7	1.4
Particle energy deposition ($ergs/cm^2$-s)	0.81	+57.4	23.2	3.2
Neutral wind speed (m/s)	37 east -51 north	-10 219	-12 -166	-44 7.2
Time of measurement, UT	0613 to 0620	0909 to 0921	0633 to 0639	0723 to 0730

current, resulted in a low joule dissipation rate of 1.4 ergs/cm^2-s. Energy deposited by precipitating electrons reached 0.8 ergs/cm^2-s.

During the launch on 10 March, geomagnetic activity was high. A large westward current system had developed and was associated with brilliant and dynamic auroral displays. Electron densities at about 100-km altitude exceeded 10^6/cm^3 during most of the rocket flight. Associated with these high densities was an energy deposition rate of more than 15 ergs/cm^2-s. Although a very strong northward electric field was observed prior to launch, it rotated sharply to the south and decreased in intensity to 20 to 30 mV/m during the launch interval.

The joule heating rate associated with this electric field and a calculated westward current density of 1.8 A/m reached to more than 10 ergs/cm^2-s. Thus the total energy input rate during the launch period was more than 25 ergs/cm^2-s. The mean energy of the precipitating electrons was calculated to be 11.3 keV during the interval 0914 to 0921 UT.

The launch on 11 March occurred just prior to an intense auroral and geomagnetic substorm. Although a strong northward electric field of about 50 mV/m was observed by the radar, the magnetometer indicated that an intense westward electrojet developed. Joule dissipation, calculated using the radar-derived eastward current density of 1.2 A/m, was greater than 20 ergs/cm^2-s. Associated with this activity was enhanced electron precipitation (8×10^5/cm^3), observed when the radar beam probed an auroral form. The energy deposition rate, due to these electrons was about 10 ergs/cm^2-s. The differential energy distribution of these electrons is characterized by high fluxes with a fairly soft mean energy (3.5 keV).

The disagreement between the radar-derived current direction and that deduced from magnetometer data is associated with the arrival of a westward-traveling auroral surge in the northern sky and thus is most

likely due to large spatial inhomogeneities in parameters observed by the radar.

The launch on 12 March was supported by a new mode of radar operation--observations made while scanning in elevation along the geomagnetic meridian. This facilitated measurement of the latitudinal variation of auroral ionization and related parameters. Conditions during this evening launch were characterized by very active aurora and a large negative bay that reached maximum extent about 3 minutes before launch. Homer DNA-609 auroral radar observations indicated that a region of intense northward electric field (>30 mV/m) existed equatorward of Chatanika, with discrete auroral arcs lying poleward of this region. Electron precipitation was intense within the auroral forms and resulted in a peak density of $8 \times 10^5/cm^3$ at 120 km. A complete analysis of these elevation scans is being made and will be available in a separate HAES report.

REFERENCES

1. M. J. Baron, O. De la Beaujardiere, and B. Craig, "Project 617 Radar Readiness Achievement Program, Data Processing and Analysis," Final Report, Part A, Contract DASA01-67-C-0019, SRI Project 6291, Stanford Research Institute, Menlo Park, California (May 1970).

2. M. J. Baron, T. Watt, C. Rino, and J. Petriceks, "DNA Project 617 Radar: First Auroral-Zone Results," Final Report, Contract DASA01-70-C-0124, SRI Project 8661, Stanford Research Institute, Menlo Park, California (December 1971).

3. M. J. Baron, W. Chesnut, O. De la Beaujardiere, J. Petriceks, C. Rino, G. Smith, R. Tsunoda, and T. Watt, "DNA Project 617 Radar: Auroral Ionospheric Measurements," Final Report, Contract DNA001-72-C-0076, SRI Project 1703, Stanford Research Institute, Menlo Park, California (December 1972).

4. M. J. Baron, "DNA Project 617 Radar: Auroral Ionospheric Measurements," Final Report, Contract DNA001-72-C-0076, SRI Project 1703, Stanford Research Institute, Menlo Park, California (January 1974).

5. J. V. Evans, "Theory and Practice of Ionosphere Study by Thomson Scatter Radar," Proc. IEEE, Vol. 57, pp. 496-530 (1969).

6. T. M. Watt, "Effective Recombination Coefficient of the Polar D-Region Under Conditions of Intense Ionizing Radiation," Report DNA 3663T, Defense Nuclear Agency, Washington, D.C. (15 July 1975).

7. M. J. Baron and N. Chang, "ICECAP 73A, Chatanika Radar Results," Technical Report 4, Contract DNA001-74-C-0167, SRI Project 3118, Stanford Research Institute, Menlo Park, California (September 1974).

8. A. Brekke, J. R. Doupnik, and P. M. Banks, "A Preliminary Study of the Neutral Wind in the Auroral E-Region," J. Geophys. Res., Vol. 78, pp. 8235-8250 (1973).

9. C. L. Rino, L. A. Brekke, and M. J. Baron, "High Resolution Auroral-Zone Neutral Wind Measurements by Incoherent Scatter Radar," submitted to J. Geophys. Res. (1976).

10. A. Brekke, J. R. Doupnik, and P. M. Banks, "Incoherent Scatter Measurements of E-Region Conductivities and Currents in the Auroral Zone," J. Geophys. Res., Vol. 79, p. 3773 (1974).

11. P. D. Perrault and M. J. Baron, "ICECAP '74--Chatanika Radar Results," Technical Report 6, Contract DNA 001-74-C-0167, SRI Project 3118, Stanford Research Institute, Menlo Park, California (October 1975).

12. V. B. Wickwar, M. J. Baron, and R. D. Sears, "Auroral Energy Input from Energetic Electrons and Joule Heating at Chatanika," J. Geophys. Res., Vol. 80, p. 4364 (1975).

13. R. R. Vondrak, private communication (1976).

14. E. V. Thrane, "On the Diurnal and Seasonal Variations of the D- and E-Regions above Kjeller," in Magnetosphere-Ionosphere Interactions (Scandinavian University Books, Oslo, Norway, 1972).

15. V. B. Wickwar, private communication (1976).

16. U.S. Standard Atmosphere Supplements, 1966, U.S. Government Printing Office, Washington, D.C. (1966).

17. T. M. Watt, L. L. Newkirk, and E. G. Skelley, "Joint Radar/Satellite Determination of Effective Recombination Coefficient in the Auroral E-Region," J. Geophys. Res., Vol. 79, p. 4725 (1974).

18. J. B. Reagan and T. M. Watt, "Simultaneous Satellite and Radar Studies of the D-Region Ionosphere During the Intense Solar Particle Events of August 1972," J. Geophys. Res. (in press, 1976).

19. R. R. Vondrak and M. J. Baron, "A Method of Obtaining the Energy Distribution of Auroral Electrons from Incoherent Scatter Radar Measurements," Proceedings EISCAT Summer School, A. Brekke, Ed., [Tromso (Norway) University Press (in press), 1976].

DISTRIBUTION LIST

DEPARTMENT OF DEFENSE

Director
Command Control Technical Center
ATTN: C-312, R. Mason

Director
Defense Advanced Rsch. Proj. Agency
ATTN: Major Gregory Canavan
ATTN: Lieutenant Colonel W. A. Whitaker
ATTN: Nuclear Monitoring Research
ATTN: STO, Captain J. Justice
ATTN: Strategic Tech. Office

Defense Communication Engineer Center
ATTN: Code R410, James W. McLean

Director
Defense Communications Agency
ATTN: Code 480

Defense Documentation Center
12 cy ATTN: TC

Director
Defense Nuclear Agency
ATTN: STSI, Archives
ATTN: RAAE, Harold C. Fitz, Jr.
ATTN: DDST
ATTN: RAAE, Major John Clark
3 cy ATTN: STTL, Tech. Library
3 cy ATTN: RAAE
3 cy ATTN: RAAE, Charles A. Blank

Dir. of Defense Rsch. & Engineering
ATTN: AD/DS
ATTN: DDS&SS, Richard S. Ruffine
ATTN: DD/S&SS, Daniel Brockway
ATTN: DD/S&SS, John B. Walsh

Commander
Field Command
ATTN: FCPR

Director
Interservice Nuclear Weapons School
ATTN: Document Control

Chief
Livermore Division, Fld. Command, DNA
ATTN: FCPRL

OJCS/J-3
ATTN: WWMCCS, Eval. Ofc., Mr. Toma

Director
Telecommunications & Comd. & Con. Sys.
ATTN: Asst. Dir., (Sys)
ATTN: Scientific Advisor

DEPARTMENT OF THE ARMY

Commander/Director
Atmospheric Sciences Laboratory
ATTN: DRSEL-BL-D, H. Holt
ATTN: DRSEL-BL-SY-S, F. E. Niles
ATTN: DRSEL-BL-SY-R, E. Butterfield

DEPARTMENT OF THE ARMY (Continued)

Director
BMD Advanced Tech. Ctr.
ATTN: ATC-T, Melvin T. Capps
ATTN: ATC-O, W. Davies

Program Manager
BMD Program Office
ATTN: DACS-BMT, John Shea
ATTN: DACS-BMZ-D, Julian Davidson

Commander
Harry Diamond Laboratories
ATTN: Mildred H. Weiner, DRXDO-TI
ATTN: DRXDO-NP, Francis N. Wimenitz
2 cy ATTN: DRXDO-NP

Commander
Trasana
ATTN: EAB

Commander
U.S. Army Electronics Command
ATTN: DRSEL-NL-RD, H. S. Bennet

Commander
U.S. Army Foreign Science & Tech. Ctr.
ATTN: P. A. Crowley
ATTN: R. Jones

Commander
U.S. Army Materiel Dev. & Readiness Cmd.
ATTN: DRCLDC, J. A. Bender
ATTN: DRCDE-D, Lawrence Flynn

Commander
U.S. Army Missile Command
ATTN: Chief, Doc. Section
ATTN: DRSMI-XS, Chief Scientist

Commander
U.S. Army Nuclear Agency
ATTN: ATCA-NAW, J. Berberet

DEPARTMENT OF THE NAVY

Chief of Naval Research
ATTN: Code 464, Jacob L. Warner
ATTN: Code 427, CDR Ronald J. Oberle
ATTN: Code 464, Thomas P. Quinn

Commander
Naval Air Systems Command
ATTN: AIR 5381

Commander
Naval Electronics Laboratory Center
ATTN: Code 2200, Ilan Rothmuller
ATTN: Code 2200, Verne E. Hildebrand
3 cy ATTN: Code 2200

Director
Naval Surface Weapons Center
ATTN: Code WX21, Tech. Lib.
ATTN: Code WA501, Navy Nuc. Prgms. Off.

DEPARTMENT OF THE NAVY (Continued)

Director
Naval Research Laboratory
ATTN: Code 7730, Edgar A. McClean
ATTN: Code 7750, Darrell F. Strobel
ATTN: Code 7750, Paul Juluenne
ATTN: Code 7700, Timothy P. Coffey
ATTN: Code 7701, Jack D. Brown
ATTN: Code 7127, Charles Y. Johnson
ATTN: Code 2027, Tech. Lib.
ATTN: Douglas P. McNutt

Director
Strategic Systems Project Office
ATTN: NSP-2141
ATTN: NSP-2722, Marcus Meserole

DEPARTMENT OF THE AIR FORCE

Commander
ADC/DC
ATTN: DC, Mr. Long

Commander
ADCOM/XPD
ATTN: XPQDQ

AF Geophysics Laboratory, AFSC
ATTN: LKB, Kenneth S. W. Champion
ATTN: OPR, James C. Ulwick
ATTN: OP, John S. Garing
ATTN: OPR, Alva T. Stair
ATTN: SUOL, ARCRL Research Lib.

AF Weapons Laboratory, AFSC
ATTN: DYT, Lt Col Don Mitchell
ATTN: CA, Arthur H. Guenther
ATTN: DYT, Capt David W. Goetz
ATTN: SUL
ATTN: SAS, John M. Kamm
ATTN: DYT, Capt L. Wittwer

AFTAC
ATTN: TN
ATTN: TF, Maj Wiley

Commander
ASD
ATTN: ASD-YH-EX, Lt Col Robert Leverette

HQ USAF/RD
ATTN: RDQ

Commander
Rome Air Development Center, AFSC
ATTN: V. Coyne
ATTN: EMTLD, Doc. Library

SAMSO/MN
ATTN: MNX

SAMSO/SZ
ATTN: SZJ, Maj Lawrence Doan

Commander in Chief
Strategic Air Command
ATTN: XPFS, Maj Brian G. Stephan

ENERGY RESEARCH AND DEVELOPMENT ADMINISTRATION

Division of Military Application
U.S. Energy Rsch. & Dev. Admin.
ATTN: Doc. Con. for Major D. A. Haycock

EG&G, Inc.
Los Alamos Division
ATTN: James R. Breedlove
ATTN: James L. Walker
ATTN: J. H. M. Fu

University of California
Lawrence Livermore Laboratory
ATTN: Terry R. Donich, L-96

Los Alamos Scientific Laboratory
ATTN: Doc. Con. for Herman Hoerlin
ATTN: Doc. Con. for Eric Jones
ATTN: Doc. Con. for R. F. Taschek
ATTN: Doc. Con. for R. A. Jeffries
ATTN: Doc. Con. for John S. Malik

Sandia Laboratories
ATTN: Doc. Con. for A. Dean Thornbrough
ATTN: Doc. Con. for 3141, Sandia Rpt. Coll.
ATTN: Doc. Con. for J. C. Eckhardt, Org. 1250
ATTN: Doc. Con. for Clarence R. Mehl, Org. 5230
ATTN: Doc. Con. for Charles Williams
ATTN: Doc. Con. for W. D. Brown

OTHER GOVERNMENT AGENCIES

Department of Commerce
Office of Telecommunications
ATTN: Glenn Falcon
ATTN: William F. Utlaut

National Oceanic & Atmospheric Admin.
Environmental Research Laboratories
ATTN: R43, Donald J. Williams

DEPARTMENT OF DEFENSE CONTRACTORS

Aerodyne Research, Inc.
ATTN: M. Camac
ATTN: F. Bien

Aeronomy Corporation
ATTN: S. A. Bowhill

Aerospace Corporation
ATTN: G. W. Anderson
ATTN: Harris Mayer
ATTN: Irving M. Garfunkel
ATTN: R. D. Rawcliffe
ATTN: T. Taylor
ATTN: R. Grove
ATTN: V. Josephson
ATTN: Wallis Grabowsky

Analytical Systems Engineering Corp.
ATTN: Radio Sciences

The Boeing Company
ATTN: Glen Keister

Brown Engineering Company, Inc.
ATTN: N. Passino

DEPARTMENT OF DEFENSE CONTRACTORS (Continued)

Calspan Corporation
ATTN: Romeo A. Deliberis

University of Denver
Colorado Seminary
Denver Research Institute
ATTN: Sec. Officer for Mr. Van Zyl
ATTN: Sec. Officer for David Murcray

ESL, Inc.
ATTN: James Marshall

General Electric Company
Space Division
ATTN: M. H. Bortner, Space Sci. Lab.
ATTN: Robert H. Edsall

General Electric Company
TEMPO-Center for Advanced Studies
ATTN: Warren S. Knapp
ATTN: DASIAC
5 cy ATTN: DASIAC, Art Feryok

General Electric Company
ATTN: George H. Millman

General Research Corporation
ATTN: John Ise, Jr.
ATTN: John Boys
ATTN: Peter Redmond

Geophysical Institute
ATTN: T. N. Davis
ATTN: Neal Brown
ATTN: Technical Library

Honeywell Incorporated
ATTN: W. Williamson

HSS, Inc.
ATTN: Donald Hansen

Information Science, Inc.
ATTN: Walter F. Dudziak

Institute for Defense Analyses
ATTN: Ernest Bauer
ATTN: Hans Wolfhard
ATTN: Joel Bengston

IRT Corporation
ATTN: E. de Plomb

Johns Hopkins University
ATTN: Document Librarian

Kaman Sciences Corporation
ATTN: B. J. Bittner
ATTN: F. G. Foxwell

Lockheed Missiles and Space Company
ATTN: Billy M. McCormac, Dept. 52-54
ATTN: Tom James
ATTN: John Kumer
ATTN: John B. Cladis, Dept. 52-12
ATTN: Robert H. Au
ATTN: Martin Walt, Dept 52-10
ATTN: Richard G. Johnson, Dept. 52-12
ATTN: Robert D. Sears, Dept. 52-14
ATTN: J. B. Reagan, D/52-12

DEPARTMENT OF DEFENSE CONTRACTORS (Continued)

M.I.T. Lincoln Laboratory
ATTN: J. V. Evans
ATTN: Lib. A-082 for David M. Towle

Martin Marietta Aerospace
Orlando Division
ATTN: Roy W. Heffner

McDonnell Douglas Corporation
ATTN: Robert W. Halprin

Mission Research Corporation
ATTN: M. Scheibe
ATTN: Conrad L. Longmire
ATTN: D. Archer
ATTN: P. Fischer
ATTN: Dave Sowle
ATTN: Ralph Kilb

North Carolina State Univ. at Raleigh
ATTN: Sec. Officer for Walter A. Flood

Photometrics, Inc.
ATTN: Irving L. Kofsky

Physical Dynamics, Inc.
ATTN: Joseph B. Workman
ATTN: A. Thompson

Physical Sciences, Inc.
ATTN: Kurt Wray

The Trustees of Princeton Univ.
ATTN: F. W. Perkins, Plasma Physics Lab.

R & D Associates
ATTN: H. A. Ory
ATTN: Forrest Gilmore
ATTN: R. P. Turco
ATTN: Robert E. Lelevier
ATTN: Richard Latter

R & D Associates
ATTN: Herbert J. Mitchell

The Rand Corporation
ATTN: James Oakley
ATTN: Cullen Crain

Raytheon Company
ATTN: G. D. Thome

Riverside Research Institute
ATTN: R. Popolow

Science Applications, Inc.
ATTN: Lewis M. Linson
ATTN: D. Sachs
ATTN: Daniel A. Hamlin

Science Applications, Inc.
ATTN: Dale H. Divis

Space Data Corporation
ATTN: Edward F. Allen

DEPARTMENT OF DEFENSE CONTRACTORS (Continued)

Stanford Research Institute
ATTN: Walter G. Chesnut
ATTN: Robert S. Leonard
ATTN: J. G. Depp
ATTN: E. J. Fremouw
ATTN: Ray L. Leadabrand
ATTN: M. Baron
ATTN: L. L. Cobb
100 cy ATTN: Library
ATTN: Paul D. Perreault
ATTN: Richard R. Vondrak
ATTN: Theodore M. Watt

Stanford Research Institute
ATTN: Warren W. Berning

Technology International Corporation
ATTN: W. P. Boquist

DEPARTMENT OF DEFENSE CONTRACTORS (Continued)

Thiokol Chemical Corp. Astro. Met. Site
ATTN: G. C. Alford

Utah State University
ATTN: Doran Baker
ATTN: C. Wyatt
ATTN: Kay Baker
ATTN: D. Burt

Visidyne, Inc.
ATTN: William Reidy
ATTN: T. C. Degges
ATTN: J. W. Carpenter